TMRC-04-02

MDOT Research Report RC-1444

Preliminary Investigation of the Role of Bacteria in Concrete Degradation

Final Report

Submitted to the
Michigan Department of Transportation

By

Meghan Housewright
Thomas Van Dam
Lawrence Sutter
Karl Peterson
Michigan Technological University
Transportation Materials Research Center
1400 Townsend Drive
Houghton, MI 49931

April 2004

1. Report No. Research Report RC-1444	2. Government Accession No.	3. MDOT Project Manager Robert Muethel
4. Title and Subtitle Preliminary Investigation of the Role of Bacteria in Concrete Degradation		5. Report Date March 2004
7. Author(s) M.E. Housewright, K.R. Peterson, T.J. Van Dam, and L.L. Sutter		6. Performing Organization Code
9. Performing Organization Name and Address Michigan Technological University 1400 Townsend Drive Houghton, Michigan 49931		8. Performing Org Report No.
12. Sponsoring Agency Name and Address Michigan Department of Transportation Construction and Technology Division P.O. Box 30049 Lansing, MI 48909		10. Work Unit No. (TRAIS) 11. Contract Number: 11(a). Authorization Number:
15. Supplementary Notes		13. Type of Report & Period Covered 14. Sponsoring Agency Code

16. Abstract
This report describes work to expand the current knowledge of microbiological activity on the mineralogical properties of concrete. It was hypothesized that perhaps certain strains of bacteria might find the unique environment within concrete suitable habitation, and through metabolic activity, damage the concrete either directly or indirectly. Three types of coarse aggregate (carbonate, natural gravel, and blast furnace slag) were mixed with ordinary portland cement and were subjected to various media and inoculated with microorganisms to compare the extent of microbiological deterioration produced in each aggregate type. The concrete incubated in the glucose media was petrographically similar to concrete weathered by acid (having zones leached of calcium hydroxide), possibly as a result of the organic material on the concrete surface concentrating organic acids (and CO_2). Also, the extra-cellular polysaccharide material, as well as other constituents of biological membranes and cell walls, could have contributed to the calcium hydroxide leaching. Aggregate type did not play a role in the observed deterioration. The results detailed here lay the groundwork for future studies to isolate specific biodegradation mechanisms that may occur in the field.

17. Key Words Concrete deterioration, biodegradation	18. Distribution Statement No restrictions. This document is available to the public through the Michigan Department of Transportation.		
19. Security Classification (report) Unclassified	20. Security Classification (Page) Unclassified	21. No of Pages 54	22. Price

TABLE OF CONTENTS

1. Report No. Research Report RC-1444	2. Government Accession No.	3. MDOT Project Manager Robert Muethel
4. Title and Subtitle Preliminary Investigation of the Role of Bacteria in Concrete Degradation		5. Report Date March 2004
7. Author(s) M.E. Housewright, K.R. Peterson, T.J. Van Dam, and L.L. Sutter		6. Performing Organization Code
9. Performing Organization Name and Address Michigan Technological University 1400 Townsend Drive Houghton, Michigan 49931		8. Performing Org Report No.
12. Sponsoring Agency Name and Address Michigan Department of Transportation Construction and Technology Division P.O. Box 30049 Lansing, MI 48909		10. Work Unit No. (TRAIS) 11. Contract Number: 11(a). Authorization Number:
15. Supplementary Notes		13. Type of Report & Period Covered 14. Sponsoring Agency Code

16. Abstract
This report describes work to expand the current knowledge of microbiological activity on the mineralogical properties of concrete. It was hypothesized that perhaps certain strains of bacteria might find the unique environment within concrete suitable habitation, and through metabolic activity, damage the concrete either directly or indirectly. Three types of coarse aggregate (carbonate, natural gravel, and blast furnace slag) were mixed with ordinary portland cement and were subjected to various media and inoculated with microorganisms to compare the extent of microbiological deterioration produced in each aggregate type. The concrete incubated in the glucose media was petrographically similar to concrete weathered by acid (having zones leached of calcium hydroxide), possibly as a result of the organic material on the concrete surface concentrating organic acids (and CO_2). Also, the extra-cellular polysaccharide material, as well as other constituents of biological membranes and cell walls, could have contributed to the calcium hydroxide leaching. Aggregate type did not play a role in the observed deterioration. The results detailed here lay the groundwork for future studies to isolate specific biodegradation mechanisms that may occur in the field.

17. Key Words Concrete deterioration, biodegradation	18. Distribution Statement No restrictions. This document is available to the public through the Michigan Department of Transportation.		
19. Security Classification (report) Unclassified	20. Security Classification (Page) Unclassified	21. No of Pages 54	22. Price

TABLE OF CONTENTS

LIST OF FIGURES

LIST OF TABLES

CHAPTER 1 – INTRODUCTION

The purpose of this work was to expand the current knowledge of microbiological activity on the mineralogical properties of concrete. It was hypothesized that perhaps certain strains of bacteria might find the unique environment within concrete suitable habitation, and through metabolic activity, damage the concrete either directly or indirectly. Three types of coarse aggregate (carbonate, natural gravel, and blast furnace slag) were mixed with ordinary portland cement in order to compare the extent of microbiological deterioration produced in each aggregate type. Of specific interest was whether microbiological activity creates any particular unsoundness in concrete made with blast furnace slag coarse aggregate, as slag is known to contain both iron and sulfur, which are used in the metabolic cycle of some bacteria, producing acids. Organic and mineral acids, as well as other organic molecules, are known to interfere with the chemistry of both cement and natural minerals, like silicates and carbonates. The goal of this study is to expand the knowledge regarding the petrographic evidence of microbiological activity in concrete from two bacteria cultures: an alkali-tolerant culture isolated from soil and a culture of *Acidithiobacillus ferrooxidans*.

Microbiological activity at the surface of concrete could influence its weathering and deterioration. The lime in cement can be very reactive in the presence of acids. Protective reaction products may form on the surface, but if the acid is continually regenerated, the protective layer may dissolve. And, as seen in the corrosion of concrete sewer pipes, biological activity may take place behind the reaction product, continuing as long as nutrients and an electron acceptor (e.g., O_2) are available. Silicate and carbonate minerals show susceptibility to microbial activity; these same materials are in cement and concrete aggregate. This study is specifically interested in the effects of biological activity on concrete made with blast furnace slag. However, since the geomicrobiology literature on concrete is relatively narrow, all petrographic evidence of microbial activity on cement is of interest. The background literature does not address the effects of continually generated organic acids on concrete microstructure. Additionally, exopolysaccharides, and ligands could attack both the calcareous and noncalcareous parts of concrete.

In this study, optical and the environmental scanning electron microscopy (ESEM) was used to examine fractured surfaces of concrete made with three different aggregate types that was exposed to microbial activity. Four-inch cylinders were split and placed in either glucose or acetate media, and inoculated with microorganisms cultured from soil at an alkaline pH (around 10). Since pavement joints have more surface area exposed than the road surface, and are in contact with fluids for longer durations of time, deterioration usually starts at the joints. Therefore this study was designed to mimic joints in concrete pavement. The tensile split cylinders were tied together to have less than an inch of space between the two halves at the top surface. After approximately 12 weeks, representative petrographic thin sections were made of the fracture surfaces from the cylinders. The hypothesis for this experiment is that the concrete would show signs of calcium and silica removal due to biological activity and that these effects would be more pronounced in those concrete cylinders incubated in the glucose media, versus the acetate media.

In another experiment concrete made from the same mixture was subject to the activity of Fe(II) oxidizing bacteria, *Acidithiobacillus ferrooxidans*. Blast furnace slag contains calcium sulfide (CaS) and sulfides can be oxidized by Fe(III). Thus it was hypothesized that the oxidation of Fe(II) to Fe(III) by *A. ferrooxidans* would oxidize the CaS found in slag to sulfate, which would be detrimental to the concrete. In a natural environment, the oxidation of the CaS by the Fe(III) would regenerate Fe(II) for the bacteria. Thus, this action could continue cyclically in the presence of CaS and oxygen.

The organization of this report is as follows. Although research regarding microbial action on concrete is limited, certain literature from cement chemistry and geomicrobiology is relevant. Chapter 2 reviews literature and reference material on cement mineralogy and the effects of aggressive chemicals on the mineralogy, as well as the literature concerning silicate and carbonate geomicrobiology. Chapter 3 covers the methods and materials employed for this study. Chapters 4 and 5 detail the results of the experiments performed here, with the fourth chapter focusing on the glucose and acetate media concrete incubations and the fifth chapter providing the results of the concrete incubations with *A. thiobacillus*. Chapter 6 presents a discussion of both sets of results. And finally, Chapter 7 provides conclusions and offers recommendations for future research.

CHAPTER 2 – LITERATURE REVIEW

2.1 CONCRETE CONSTITUENTS

Concrete is a mixture of aggregate, cement, air, water, and often chemical admixtures. Portland cement, like the type used in this study, is formed from calcareous and siliceous argillaceous material fused by heat to make clinker composed of the following four principal minerals: tricalcium silicate, dicalcium silicate, tricalcium aluminate, and tetracalcium aluminoferrite. The clinker is ground and blended with gypsum ($CaO{\cdot}SO_4{\cdot}(H_2O)_2$) to prevent flash setting (these phases are impure in practice). With the addition of water, these minerals hydrate, forming calcium silicate hydrate (approximate stochiometry: $((CaO)_3{\cdot}(SiO_2)_2{\cdot}(H_2O)_8)$, calcium hydroxide ($Ca(OH)_2$), ettringite ($((CaO)_6{\cdot}(Al_2O_3){\cdot}(SO_3)_3{\cdot}(H_2O)_{32})$, and monosulfate ($((CaO)_4{\cdot}(Al_2O_3){\cdot}(SO_3){\cdot}(H_2O)_{12})$. Chemical agents, as well as physical ones, can attack these constituents. Often seen as inert filler, the mineralogy of the aggregate can also play a role in the chemical stability of hydrated cement paste, which ultimately will lead to failure (Mindess et al. 2003).

2.2. EFFECTS OF ORGANIC AND MINERAL ACIDS ON CONCRETE

Organic and mineral acids can attack the hydrated cement paste in concrete. Many natural waters contain carbonic acids from the breakdown of organic matter. Pure water is capable of dissolving 1.2 g/L of CaO, and this effect can be greatly enhanced in the presence of dissolved carbon dioxide (CO_2). CO_2 follows the equilibrium equation shown below in water:

$$CO_2\ (\text{dissolved}) + H_2O \leftrightarrow H_2CO_3 + H^+ \leftrightarrow HCO_3^- + H^+ + CO_3^{2-}$$

Below a pH of 5 the equilibrium favors CO_2 whereas between pH 7 and 9 it favors bicarbonate. The solubility of CO_2 is only slightly influenced by pH and salt concentrations, but since HCO_3^- is soluble in water, pH and salt concentrations can greatly effect the CO_2 concentration in water. The presence of $CaCO_3$ can enhance the solubility of CO_2, and CO_2 can also increase the solubility of $CaCO_3$. From the cement chemist's perspective, CO_2 can be present in water as either "free" or "aggressive" CO_2. Free CO_2 is the amount required to stabilize Ca^{2+} ions in accordance with the following equilibrium:

$$CaCO_3 + H_2CO_3 \rightarrow Ca(HCO_3)_2$$

The quantity of free CO_2 increases as more calcium bicarbonate ($Ca(HCO_3)_2$) is formed. Aggressive CO_2 is that amount of CO_2 in excess of the existing equilibrium. Because of the presence of calcium in the cement, CO_2 reacts to form a thin layer of $CaCO_3$ on the surface of the concrete. $CaCO_3$ is generally highly insoluble in water, except when it reacts with the CO_2 in the water, forming highly soluble calcium bicarbonate. Thus pure water alone, or water with carbonate and bicarbonate in equilibrium, poses little risk of concrete deterioration. It is only when CO_2 fluxes through the system that there is significant calcium dissolution from the cement, with the leaching CaO leaving a layer of hydrous silicon dioxide (Lea 1970).

In cases of acid attack, the extent of damage often depends on the development of a protective layer of reaction product between the cement and the acid. The thickness and characteristics of this layer depend on the attacking fluid, as some products are more insoluble than others. In one study, cement mortar cubes were stored in carbonic acid (pH 4.4) for varying periods of time. A protective layer formed on the cube surface from the lime and carbonic acid reaction product. Over the course of time this layer increased in thickness, further blocking the diffusion of dissolved CaO. When the protective layer was mechanically destroyed, the rate of material removal increased (Koelliker 1965).

Acid attack leaves distinctive petrographic evidence. In the case of nitric acid attack, a layer of corrosion products covers the undamaged cement paste. H^+ ions diffuse across this boundary to a corrosion zone beneath the corrosion product. This reaction zone is a fairly thin layer compared to the much thicker zone of corrosion products. Under plane polarized light the corrosion front appears divided into two layers, the outer white layer, formed from SiO_2, and an inner brown layer, formed from hydrate oxides of aluminum and iron; the thickness of the two layers is pH dependent, as iron solubility increases as pH decreases (Pavlik 1994).

In *Concrete Petrography; a Handbook of Investigative Techniques*, St. John et al. (1998) describe the general petrographic appearance of hydrated cement paste exposed to soft acidic waters (figure 1.1). The outer zone of gelatinous silica is the completion of the reaction. This zone is isotropic, owing to its poor crystallinity. The carbonation zone can block the leaching of the calcium hydroxide. It is that outer corrosion zone which can be divided into the white and brown layers. Pavlik (1994) found that the boundary between these two layers becomes more diffuse over time.

The type of acid affects the corrosion rate. Low molecular weight acids like lactic, butyric, acetic and tartaric acids react with cement in a similar manner as the nitric acid explained above (Lea 1970). Some of these acids act faster than others. Acetic acid, for one, partially ionizes, thus buffering the solution exposed to the corroded layer and slowing its growth (Pavlik 1994). Humic acids react with concrete to form calcium humate, which is virtually insoluble. Similarly, insoluble calcium oxalate forms when cement reacts with that acid (Lea 1970).

Due to their high ionization strength, mineral acids, such as hydrochloric, deserve special attention. Portland cement mortar prisms kept in 15 percent HCl for 5 days showed leaching of the cement material, increasing the porosity of the mortar. The leached calcium quickly buffers the acid, though, allowing for the formation of silica, alumina, and iron gels, which form protective layers over the undamaged concrete (Chandra 1988).

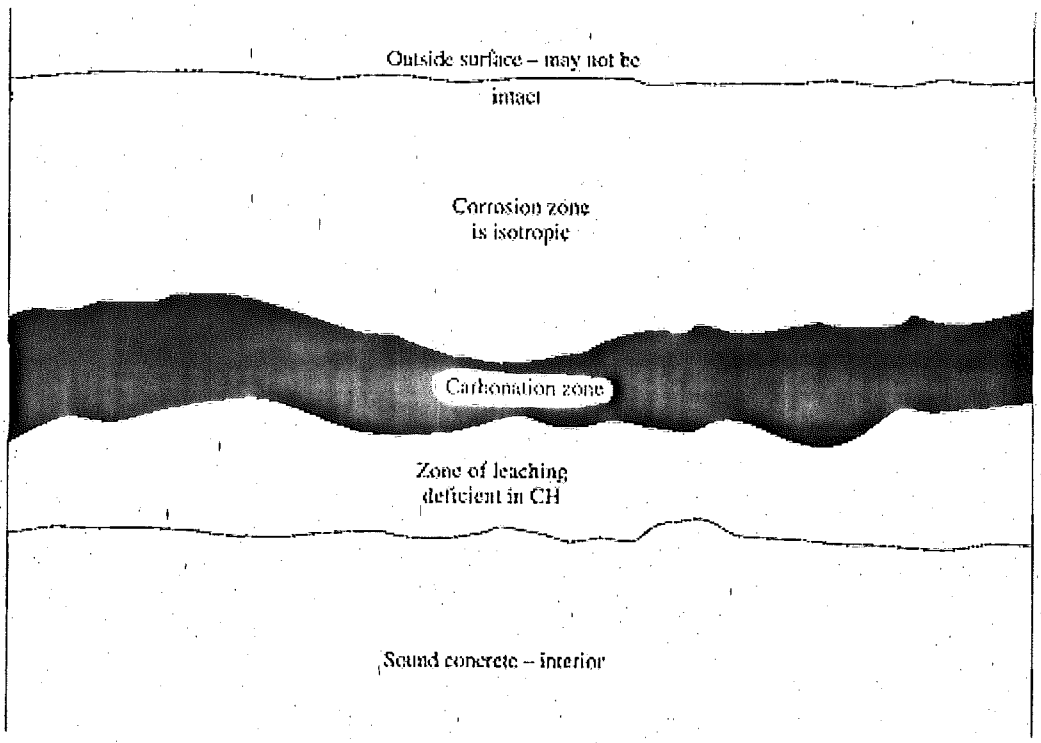

Figure 1.1. Diagram of typical petrographic appearance of acid attacked concrete. Concrete acted upon by soft acidic waters shows these characteristic layers (figure from St. John et al. 1998, pg. 273).

2.3. BLAST FURNACE SLAG COARSE AGGREGATE

Once considered just a waste product, blast furnace slag is now widely used as a construction material. One common use is as an aggregate in portland cement concrete. Slag, the by-product of the metal smelting industry, consists of gangue from metal ore, flux material, and unburned fuel components. Blast furnace slag is leftover from the pig iron making process. Ninety-five percent of slag consists of CaO, SiO_2, Al_2O_3, and MgO. The remaining 5 percent consists of sulfur, manganese, iron, titanium, fluorine, sodium, and potassium. The mineralogical composition of slag varies with the rate of cooling. However, the most prevalent mineral is melilite, which is a solid solution between the isomorphous minerals gehlenite ($2CaO{\cdot}MgO{\cdot}2SiO_2$) and akermanite ($2CaO{\cdot}Al_2O_3{\cdot}SiO_2$). Also present is the mineral form of calcium sulfide that it referred to as oldhamite (Hammerling 1999).

Gutt et al. (1967) found slag to be an adequate coarse aggregate for concrete. In strength tests and tests of sulfate attack resistance, the blast furnace slag concrete performed comparably to that made with natural gravel or limestone. In another study, Everett and Gutt (1967) concluded that blast furnace slag could be satisfactorily used for reinforced concrete without fear that the increased sulfide content of the slag inhibited passivation of the steel. In contrast, Parker (1960) documented unsoundness in slag aggregate concrete caused by the oxidation of the sulfide in slag. Hammerling (1999) also reports the dissolution of calcium sulfide from slag aggregate. Petrographic thin sections and SEM images revealed empty voids within the assembly of calcium sulfide inclusions close to the cement matrix, and the presence of secondary

minerals containing sulfur and/or calcium in the air voids in the matrix adjacent to the slag aggregate concrete. Furthermore, calcium sulfide is not thermodynamically stable, especially under highly alkaline conditions. Sulfate ions can attack the minerals of hydrated cement paste; the formation of new minerals (e.g. ettringite, gypsum, brucite) can create enough pressure to disrupt the microstructure of the concrete. The oxidation and hydration of sulfides in aggregate can cause expansive reactions affecting the durability of the concrete (Casanova et al., 1996).

2.4 CROWN CORROSION

Concrete sewer pipes are susceptible to the effects of microbiological attack, referred to as crown corrosion. The alteration of concrete microstructure by sulfuric acid producing bacteria can severely damage pipes in a relatively short period of time. Parker (1945) was the first to cite the role of bacteria in this process. Subsequently much research has been done on this topic, and the corrosion of concrete sewer pipes is now very well characterized. The mechanism by which this happens (figure 1.2) is the result of the synergistic actions of two populations of metabolically distinct microbes, the sulfide oxidizers and the sulfate reducers. Sulfur oxidizing bacteria (SOB) oxidize elemental sulfur to sulfuric acid. The source of the sulfur is hydrogen sulfide, which is mainly produced by sulfate reducing bacteria (SRB) that reduce SO_4^{2-} containing compounds to H_2S. In sewer pipes, these anaerobic organisms live in the sewage, the mud layer at the bottom of pipes, and in the slime layer (the biofilm coating) of pipelines above and below the water level. These microorganisms thrive in environments where their end product, H_2S, can easily diffuse out or be converted back to sulfate (Vincke, et al., 2000). The destruction of the concrete pipes is from the biogenic sulfuric acid production. When the dissolved H_2S volatilizes, it can accumulate in the sewer atmosphere, and re-dissolve in the moisture present on the pipe crown or it can be absorbed directly into the pores of the concrete. On the concrete it reacts with O_2 to form sulfur. The sulfur oxidizing bacteria oxidize the sulfur to sulfuric acid at the crown or the walls of the pipe (Islander et al, 1991).

Most of these sulfur-or sulfide- oxidizing bacteria are acidophilic organisms of the genus *Acidthiobacillus*. These organisms are autotrophs that gain energy from the oxidation of sulfur and fix CO_2 (Islander et al., 1991). Since the pH of un-corroded concrete is alkaline (10 to 12), these organisms cannot initially inhabit the surface, but the pH of the surface decreases with carbonation. Additionally, H_2S is an acidic gas, and its diffusion contributes to the neutralization of the concrete of the pipe wall. Species from the *Acidthiobacillus* genus can colonize the surface at neutral pH, beginning a succession of species from this genus. Species like *A. neapolitanus*, *A. intermedius*, and *A. novellus* can grow at circumneutral pH levels, producing sulfuric acid, which further acidifies their environment. *A. thiooxidans* grows at the lowest pH levels. Coexisting with these bacteria is an acid-resistant, H_2S oxidizing (to thiosulfate) fungus (Milde, et al., 1983; Sand, 1987). Maeda et al. (1999) reported that *A. ferrooxidans* is also involved in crown corrosion. This autotroph oxidizes Fe(II) to Fe(III) to fix CO_2. In addition to concrete pipes, *Acidthiobacillus* have also been implicated in the corrosion of concrete potable water storage tanks, which were storing eutrophic water with a high H_2S content (Coleman and Gaudet, 1993). In addition to the sulfide-oxidizing bacteria, heterotrophic and nitrifying bacteria have also been implemented in concrete corrosion. However, the biogenic sulfuric acid production receives the most attention in the literature (Rogers et al., 1993).

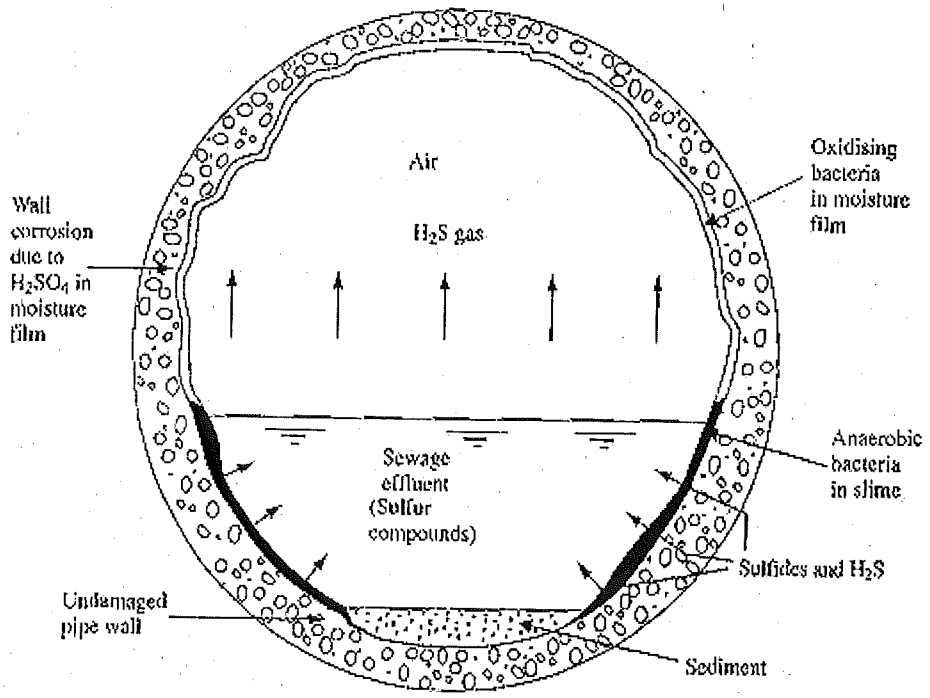

Figure 1.2. Diagram of crown corrosion showing the conditions that promote the microbial attack of concrete sewer pipes by the actions of sulfide oxidizing acidophilic bacteria. (figure from St. John et al., 1998)

Only about 5 percent of the pores in new concrete are large enough for bacteria to habitate (greater than 1 μm). However, small, interconnected voids allow for the diffuse transfer of dissolved compounds, establishing chemical gradients. The acid dissolution increases the concrete porosity, leaving bigger voids for the bacteria. As in other case of acid attack, biological sulfuric acid (BSA) attack leaves a corrosion product of sand particles, un-reacted cement particles, and various sulfates, produced by re-precipitation of ions dissolved from the cement. Its main mineral constituent is gypsum ($CaSO_4 \cdot 2H_2O$), which severely weakens the concrete. Ettringite can also form from the $CaSO_4$ and calcium aluminate in an expansive reaction, which can cause microcracking. At surface pH levels below 3, gypsum formation is favored, while greater pH values favor ettringite formation. The corrosion layer can also serve to protect the organisms living in and under it by holding water, thus reducing the effects of dry periods (Vincke et al., 2000).

In a study comparing BSA attack to that of purely chemical sulfuric acid corrosion, the authors found that the BSA attack proceeded at a faster rate. During the chemical attack, an impervious corrosion layer forms, preventing further corrosion until brushed off. However, in the microbiological attack, the bacteria are in the transition zone between the corroded and the non-corroded layers, thus the impervious layer does not stop the corrosion. If the impervious layer becomes sufficiently thick so as to become anaerobic, then the sulfur oxidizing bacteria will cease to function. Regardless of the treatment, though, the corrosion rate increases toward the end of the tests, as all of the pore space for crystal expansion became filled with the continued gypsum crystal growth, creating more microcracking (Beeldens et al., 2001).

Biogenic sulfuric acid production is a unique phenomenon, specific to geochemical environments with an exogenous sulfur source. Although the bulk of the literature on the microbial corrosion of concrete covers sewer pipes and SOB, a small number of other studies have isolated bacteria from concrete in environments without an exogenous sulfur source. In a study of concrete structures of a hydraulic facility, Zherebyateva et al. (1991) claimed that microbial activity caused the loss of hydrosilicates from the cement paste. As no exogenous sulfur source was present, nitrifying and heterotrophic bacteria mainly caused the corrosion. Accordingly, the bacterial activity starts in microzones where the lower pH of the neutral aggregate comes into contact with the alkaline cement. Heterotrophic bacteria metabolize complex organic compounds, from the air or pore water, to simpler organics. Cyanobacteria contribute to the supply of organic material. Nitrifying bacteria oxidize ammonium salts to nitrous and nitric acids, which can then be used by denitrifier bacteria. Because of the overall alkalinity of the environment, there are no mycelial fungi.

2.5 OTHER RESEARCH OF THE EFFECTS OF BACTERIA ON CONCRETE

Alkaliphilic microorganisms, which thrive in high pH environments, receive comparatively less attention within the concrete/cement literature than the mechanisms involved in crown corrosion. One study isolated a species of *Clostridium* from a bio-deteriorated casein-containing concrete (Karlsson et al., 1988); the authors do not go into detail on the specific effects of the bacteria on the concrete microstructure.

Certain alkaliphiles precipitate $CaCO_3$, which could possibly be used to repair cracks in concrete surfaces. The bacterial cell serves as a nucleation point for the calcium carbonate. *Bacillus pasteurii* uses urea as an energy source, producing ammonia and raising the pH of its external milieu. The rise in pH causes the precipitation of calcium carbonate, with the cell surface serving as a nucleation site for mineral dissolution (Stocks-Fischer et al., 1999). This biomineralization process has been evaluated for repairing cracks in cement mortar beams. Compressive strength increased in cracked beams treated with *B. pasteurii* and urea-chloride media compared to untreated beams. The same study also reports that calcite precipitation by *B. pasteurii* ameliorated the effects of sulfate attack, alkaline exposure, deicing chemical exposure, and freeze-thaw action (Ramakrishnan et al., 2002).

2.6. MICROBIAL INTERACTIONS WITH SILICATE MINERALS

Cement and most aggregates contain silicate minerals. Geomicrobiologists have found that microbial activity can enhance the weathering of geologically important minerals like feldspar and quartz. The bio-attack on silica can be mediated by four general mechanisms:

- Microbially produced ligands of cations
- Microbially produced organic or inorganic acids, which are sources of protons
- Microbially produced alkalis (ammonia or amines)
- Microbially produced extra-cellular polysaccharides (EPS) acting at acid pH.

These chemicals attack Si-O-Si bonds (siloxans) or Al-O bonds; or the chemicals can remove cations from the crystal lattice structure, causing it to collapse. Additionally, since many of these

organisms attach themselves to mineral surfaces, their metabolites are concentrated in a localized area (Ehrlich, 2002).

Microbially produced ligands of divalent cations can dissolve calcium containing silicates. Webley et al. (1960) demonstrated that a soil strain of *Pseudomonas*, which produced 2-ketogluconic acid from glucose, could dissolve natural and synthetic silicates. The complex between the cationic bonds of the silicates by the 2-ketogluconate were more stable than the silicates (Duff et al., 1963). Vandevivere et al. (1994) suggests that the silicate mineral solubilizing activity of gluconic acid is due to the chelation, rather than protonation, since the process took place at circumneutral pH. Bennett et al. (1988) supported these findings. Their study reported the dissolution of quartz by organic acids (citric, oxalic, pyruvic, and humic acids) was greatest in the pH range of 3 to 7. Acetate, fumarate and tartrate were ineffective in dissolving silica as a complex.

Weak organic acids and carbonic acid can solubilize silica acting as acids, too. Welch and Ullman (1993) found that plagioclase (Ca-Na feldspars) weathered fastest at a pH of 3. The weathering rate was slower as the pH increased. Polyfunctional organic acids like oxalate, citrate, succinate, pyruvate, and 2-ketogluterate, were the most effective, while acetate and propionate were less effective than HCl and HNO_3. The polyfunctional acids acted mainly as acidulents at low pH and as chelators at neutral pH. This combined effect raised the silica dissolution rate from that which would be expected by protonation alone. The organic acids that preferentially chelated aluminum were the most effective in enhancing plagioclase dissolution (Ullman, et al., 1996).

Extra-cellular polysaccharides can also remove silica from minerals. In a TEM study on lichen weathering, Barker and Banfield (1996) found that active weathering was occurring in the lower thallus region (below the photosynthesizing portion of the organism, where it comes in contact with the rock substrate). They noted mineral fragments coated with organic polymers and secondary minerals in this portion of the thallus. In other instances, the silicate minerals were converted to siliceous relics following the removal of structural cations, suggesting a chelation mechanism (Jones et al., 1981). Microbial mats growing on rock surfaces in radioactive hot springs enhanced silica dissolution, creating a gelatinous layer of glycocalyx and siliceous gel (Heinen and Lauwers, 1988).

2.7. GEOMICROBIOLOGY OF CARBONATES

Microorganisms can be involved in both the precipitation and dissolution of carbonate minerals. There are five mechanisms by which carbonate can be precipitated biologically (Ehrlich, 2002):

- Aerobic or anaerobic oxidation of carbon compounds
- Aerobic or anaerobic oxidation of nitrogen compounds with the release of NH_3 and CO_2 in unbuffered environments containing sufficient amounts of appropriate cations
- The reduction of $CaSCO_4$ to CaS by sulfate reducing bacteria
- The hydrolysis of urea leading to the formation of ammonium carbonate
- Removal of CO_2 from a bicarbonate containing solution.

When oxidation of carbon containing organic matter takes place in neutral to alkaline environments, some of the resulting CO_2 will precipitate as carbonate, since:

$$CO_2 + H_2O \leftrightarrow H_2CO_3$$
$$H_2CO_3 + OH^- \leftrightarrow HCO_3^- + H_2O$$
$$HCO_3^- + OH^- \leftrightarrow CO_3^{2-} + H_2O$$

If phosphate is above a critical concentration, its mineral precipitation by certain soil bacteria will interfere with the calcium carbonate deposition (Rivadeneyra et al., 1985).

The metabolism of NH_3 containing substances, like amino acids, purines, and pyrimidines, and any other nitrogen containing compounds, can raise the pH of the external environment. In water, NH_3 hydrates to NH_4OH, which partially dissociates to NH_4^+ and OH^-. This rise in pH induces carbonate deposition. The precipitation of carbonate via anaerobic sulfate reduction takes place via the following reactions:

$$CaSO_4 + 2(CH_2O) \rightarrow CaS + 2CO_2 + 2H_2O$$
$$CaS + 2H_2O \rightarrow Ca(OH)_2 + H_2S$$
$$CO_2 + H_2O \rightarrow H_2CO_3$$
$$Ca(OH)_2 + H_2CO_3 \rightarrow CaCO_3 + 2H_2O$$

where CH_2O is organic matter.

The hydrolysis of urea, as described above, leads to the formation of ammonium carbonate, which will precipitate in the presence of appropriate cations. The removal of CO_2 from a solution by autotrophic microorganisms (assimilated as HCO_3^-), increases the carbonate concentration of the solution, in accordance with:

$$2HCO_3^- \leftrightarrow CO_2 + H_2O + CO_3^{2-}$$

Thus, in the presence of adequate Ca^{2+}, $CaCO_3$ forms (Ehrlich, 2002).

Preservationists have studied the nature of microbial activity in contact with stone monuments. Often these surfaces are covered with geomicrobial patinas that help protect the monument. The patinas are layered, divided into calcite and gypsum layers, and an outer layer where biological activity takes place (by algae, fungi, bacteria, and cyanobacteria). Of the different microorganisms in this layer, only the bacteria precipitate calcite. Inoculation of rock slabs led to the formation of different mineral phases containing phosphate, which may be explained by the mineralization of organic matter, followed by the mobilization of phosphate to form mineral phases. There were layers of calcite and gypsum, and an outer layer where biological activity takes place (by algae, fungi, bacteria, and cyanobacteria) (Urzi et al., 1999).

In acidic conditions carbonates are readily dissolved. This is shown by:

$$CaCO_3 + H^+ \rightarrow Ca^{2+} + HCO_3^-$$
$$HCO_3^- + H^+ \rightarrow H_2CO_3$$
$$H_2CO_3 \rightarrow H_2O + CO_2$$

$Ca(HCO_3)_2$ is very soluble compared to the $CaCO_3$; thus $CaCO_3$ dissolves in even weak acids. Urzi et al. (1991) also did a study on a *Micrococcus* strain isolated from stone surfaces to investigate its ability to adhere to marble surfaces and produce extra-cellular polysaccharides. They measured biodeterioration activity in terms of pH drop, organic acid production, and weight loss of marble slabs. For those slabs treated with media and the *Micrococcus* strain the pH went down within the first 5 days of incubation (from 7 to 5), but rose to alkaline levels (8) over the course of the experiment (90 days). Weight loss was highest during this period of acid production.

2.8. ALKALIPHILES

Alkaline solutions are marginal environments for biological activity, but certain microorganisms have physiological adaptations that make life at high pH possible. The surface of concrete and concrete pore waters tend toward these alkaline levels due to the abundance of lime. Thus, in natural environments, alkaliphiles may be associated with concrete. These microbes vary in their tolerance toward pH. Some species are viable at neutral and high pH levels (facultative), while other species can only exist at the high end of the pH range (obligate). Generally, the term alkaliphile is reserved for bacteria that grow optimally at pH values above 9, but cannot grow, or grow only slowly, at circumneutral pH. Microorganisms capable of growth at these pH levels are found everywhere, but often in fewer numbers than those confined to neutral pH environments (alkaliphiles to neutriphiles found in soil ranges from 1/100 to 1/1000) (Horikoshi, 1998).

Alkaliphiles have solved two main problems created for them by the high pH environment. The first problem overcome is the maintenance of a cytoplasmic pH that is, by necessity, lower than the surrounding pH. This leads to the second problem. If the cytoplasmic pH is lower than the external pH, the organisms cannot utilize the conventional chemiosmotic gradient to drive ion-coupled solute uptake, oxidative phosphorylation, or motility. Cells operating at neutral pH make use of a proton-motive force, the net effect of which is to maintain the inside of the cell negative and alkaline relative to its external environment. The charge differential across the cell membrane, which drives essential cell processes, is created by the excretion and re-uptake of hydrogen ions. Alkaliphiles employ a Na^+/H^+ antiport system to keep their cytoplasmic pH lower than the external pH and to generate a sodium-motive force, which co-transports substrates and sodium (Kitada et al., 1994). Na^+/H^+ antiporters re-uptake the protons extruded from respiration, which acidifies the internal pH relative to the outside, while maintaining a conventional electrochemical gradient (positive out). Symporters are involved in sodium re-uptake, transporting sodium and other solutes into the cell (Ivey et al., 1993).

Alkaliphiles also have adapted cell walls to their high pH surroundings. Compared to neutraphilic *Bacillus* species, alkaliphilic *Bacillus* species have acidic compounds in the their cell walls (Aono and Horikoshi, 1983). These compounds include galacturonic acid, glucuronic acid, glutamic acid, aspartic acid, and phosphoric acid. The peptidoglycan of the alkaliphilic *Bacillus* was found to have high pH adaptations: the peptidoglycan was characterized by an excess of hexosamines, muramic acid, D- and L- alanine, D-glutamic acid, meso-diaminopimelic acid, and acetic acid were also found (Aono *et al*, 1984). Additionally, the cross-linkage rate of peptidoglycan was higher in the cells grown at alkaline pH versus those grown at neutral pH (Aono and Sanada, 1994).

2.9. ACIDITHIOBACILLUS FERROOXIDANS

The iron oxidizing acidiphile was used for one experiment in this study. It is a well-characterized gram-negative rod that derives energy and reducing power from the oxidation of ferrous iron, reduced forms of sulfur, metal sulfides, H_2, and formate. The organism fixes CO_2 via the Calvin-Benson cycle, and uses inorganic forms of nitrogen. These microbes can metabolize in the pH range of 1-4.5, but do so optimally at 2.5. The ferric iron produced by this organism will precipitate above pH 1.9. Its temperature growth range is from 15-42°C, with the optimum from 30-35°C. Ferrous iron oxidation yields relatively little energy for biological activity. Precise quantities have yet to be determined, but a generally accepted estimate is 90.1 mol Fe^{2+} oxidized for every 1 mol of carbon assimilated (Ehlrich, 2002).

CHAPTER 3 – MATERIALS AND METHODS

3.1. CONCRETE MIXTURE PREPARATION

All concrete used for this study consisted of coarse aggregate, fine aggregate, cement, air entrainer, and water. The cement used was Lafarge (Alpena) Type I portland cement. All mix water was Houghton City tap water. Each cylinder was made using either carbonate rock (from the Rockwood Quarry), natural gravel (from Superior Sand and Gravel), or blast-furnace slag (from Levy Slag) as coarse aggregate. The aggregates were mechanically sieved into four fractions following the AASHTO 26A blend listed in table 3.1.

Table 3.1: Aggregate Gradation. The AASHTO 26A blend is listed in the second column. The gradation used for this study is listed in the third column.

Sieve size (mm)	Percent Passing sieve by weight	Percent Retained on sieve by weight
19.1	100	0
12.5	95-100	4
9.5	60-90	75
4.75	5-30	18
2.36	0-12	3

Sand from Superior Sand & Gravel was used for the fine aggregate. The three coarse aggregate types, as well as the sand, were tested (in accordance with ASTM C127 and C128) to determine their bulk specific gravity (BSG), apparent specific gravity (ASG), and percent absorption. The results of these tests are listed in table 3.2, which presents the average of three tests for each material. Appendix A contains the sample data for all tests.

Table 3.2. Material properties of aggregates. The procedure used to find these properties can be found in Appendix A.

Material	Bulk SPG	Apparent SPG	Percent Absorption
Natural Gravel	2.69	2.80	1.41
Carbonate	2.59	2.76	2.31
Slag	2.31	2.47	2.71
Sand	2.74	2.78	0.73

The mixtures were designed to yield $3.295*10^{-2}$ m^3 of concrete for each aggregate type, a volume that fills twenty 10 cm x 20 cm (4 x 8 inches) molds. The main objective of the mixture designs was to keep the volume of coarse aggregates roughly equal between the different mixtures, while maintaining the same water-to-cement (*w/c*) ratio and adequate workability. Table 3.3 lists the volume constituents used for all of the mixtures.

Table 3.3. Volume constituents of concrete mixtures.

Material	Volume (percentage)	Volume (m^3)
Coarse Aggregate	40	0.013179
Fine Aggregate	30	0.009884
Paste	25	0.008237
Air	5	0.001647
Total	100	0.032948

For each aggregate, at least one test batch was made to ensure the workability of the mix. If the mix was too harsh, or too watery, adjustments were made to the proportions of the final mix. Table 3.4 presents the batch weights used for the final mix of each aggregate type. The BSG values were used to determine the required weight of the coarse and fine aggregates: BSG*Volume (m3)*1000 (kg/m3). Appendix B contains the worksheet used to determine the required amount of water and cement for the mixtures, as well as the amount of air-entrainer to add. Table 3.5 lists the volume of air-entrainer used for each mix. All constituents were weighed on an Ohaus I-20W scale (150 kg capacity, reads to the hundredth of the kilogram).

Table 3.4. Batch weights of constituent materials.

	Natural Gravel (kg)	Carbonate (kg)	Slag (kg)
Coarse	35.45	34.13	30.44
Fine	27.08	27.08	27.08
Water (for hydration)	5.22	5.22	5.22
Cement	9.50	9.50	9.50
Water (for absorption)	0.70	0.99	1.02
Total water	5.92	6.21	6.25

Table 3.5. Volume of air-entrainer added to mixture.

Aggregate	Air-Entrainer (ml)
Natural Gravel	5.2
Limestone	6.64
Slag	7.4

The cylinder molds were coated with mineral oil prior to casting. A hole was drilled into the bottom and covered with duct-tape. This hole allowed for the cylinders to be easily removed from the molds with a compressed air hose. All concrete was mixed using a three-blade rotary drum mixer powered by a one horsepower electric motor with a 0.17m^3-capacity. The concrete was mixed in a buttered mixer, with the test batches serving this purpose. Constituents were added to the rotating mixer and mixed in the following manner: mixed 3 minutes, rested 3 minutes, mix 2 minutes. A slump test was performed on each final mixture, the results of which are listed in table 3.6.

Table 3.6. Slump test results for final mixture.

Aggregate	Slump (cm)
Natural Gravel	17.78
Limestone	15.24
Slag	6.35

Cylinders were cast in three layers, tamping each layer 15 times with a metal rod. After finishing they were placed in a moist curing room.

3.2. PREPARATION OF CYLINDERS FOR USE

The cylinders were kept in their molds in the moist curing room until needed (all in excess of 28 days). The 20 cm high cylinders were cut into 10 cm high cylinders using a block saw. These 10 cm high cylinders were then split in two using a split tensile strength test. The two halves of concrete, plus any additional sizable pieces that broke off during splitting, were weighed with an Ohaus digital balance (reads to the tenth of the gram).

3.3. CULTURING OF MICROORGANISMS

The culture used for this study was enriched from soil taken adjacent to a concrete pavement, brought up in one of two medias, one with acetate as a carbon source and the other with glucose (D-dextrose) as a carbon source. One gram of soil was added to 10 ml sterilized Milli-Q water, and then vortexed. Two ml of this solution were used to inoculate the two different media. Both enrichments tolerated an alkali pH of 11 to 12, and were isolated at 30°C. The cultures grown on acetate did not lower the pH of their media, whereas those grown on glucose brought the pH from alkaline levels down to 5 over the course of 2 to 3 days, at 30°C. The glucose media is published as Horikoshi media and consists of the following (L^{-1}): 10g D-dextrose; 5g peptone; 1g yeast extract; 1g KH_2PO_4; 0.2g $MgSO_4 \cdot 7H_2O$; 10g Na_2CO_3 (Horikoshi, 1971). The acetate media is an alkaline mineral base media consisting of the following (L^{-1}): 1g K_2HPO_4; 1g $(NH_4)H_2PO_4$; 0.1g $MgSO_4 \cdot 7H_2O$, 10g Na_2CO_3, with 20mM sodium-acetate. Both media were mixed in Milli-Q water. In both culture types the media turned turbid within 1 to 2 days; this was accompanied by the appearance of a sticky pinkish mass suspended in the liquid, presumed to be biomass. Both gram-negative and gram-positive organisms were in both cultures.

3.4. GLUCOSE AND ACETATE MEDIA EXPERIMENTS

The two halves of each split 10-cm diameter cylinder were tied loosely together with string. An attempt was made to re-assemble large pieces that had broken off from the two halves in the splitting process. The fit between halves was not perfect, due to the nature of the breaks, but the gap between the halves was no more than 1-inch. The tied-together cylinders were placed in 15-cm diameter plastic containers and submerged in 80 percent ethanol for 20 minutes to sterilize them. Immediately following sterilization, they were submerged in 1 liter of media (either the acetate media or the Horikoshi media) and incubated at 30°C. Each treatment was done in triplicate. No sodium carbonate was added to either media. NaCl was added to both types of media at 0.5 percent (12.7 g L^{-1}), since alkaliphiles require sodium at 0.5 to 2 percent to remain viable (Horikoshi, 1998). Those cylinders incubated in the glucose media are referred to as GC, and those incubated in the acetate media are referred to as AcC. The pH of the liquid in the containers was measured every several days throughout the course of the experiment (88 days for the Horikoshi media and 84 days for the acetate media). The media was changed 4 times during this period. This was done every 14 to 17 days, except in the case of the last media change for the glucose treatment. In this case the period between the third and fourth media change was extended to 28 days due to a lost order for the required chemicals.

At the end of this period the cylinders were dried in an oven at 50°C for 24 hours and then weighed on the same Ohaus balance previously used. Before being placed in the oven, the cylinders were photographed. Once dried, the surfaces of the cylinders were stabilized with epoxy. Prior to the epoxy stabilization, micrographs were taken (Philips XL40ESEM) of features on the concrete's fractured surface. Representative petrographic thin sections were made of these fracture surfaces, following the procedures outlined in Walker and Marshall (1979). These thin sections were observed using the stereomicroscope (Olympus SZH-10 stereo zoom optical microscope equipped for conventional and UV illumination), the petrographic light microscope (Olympus BX-60 petrographic microscope equipped for plane polarized, cross-polarized, and UV illumination), and the ESEM (Philips XL40 environmental scanning electron microscope equipped with an EDAX energy dispersive x-ray analyzer system (EDS)).

3.4.1 pH Measurements

The pH of the liquid media in which the cylinders were submerged was taken with an Orion pH probe. Five measurements were taken for each replicate. Without the addition of calcium carbonate, the pH of both medias is circumneutral. In the beginning of the incubation period, the pH for both of the medias rose to alkaline levels very quickly. Once alkaline levels were reached, the pH was taken with pH paper. At alkaline pH the paper turns blue-green to deep blue. If the pH paper returned a color within this range when exposed to the media, the pH was recorded as 10. The actual pH could have been higher or slightly lower.

3.4.2 Acetate Measurements

Acetic acid can be measured using several types of chromatography. Originally the microbial growth on the acetate media was to be monitored via gas chromatography. However, repeated attempts to do so failed, and ultimately, the acetate measurements were abandoned.

Most likely the failure of this method was due to the high concentration of salts in the analytical matrix; these salts could not be consistently rinsed from the injection-port liner. Partitioning the acetic acid into vinyl chloride did not achieve reproducibility.

3.4.3 Controls

In both the acetate media and the Horikoshi media an attempt was made to create abiotic controls using 250 μM $HgCl_2$ (simply autoclaving the media was not effective). Heavy metals inhibit biological activity (personal communication, Lueking 2003). When added to cultures, the 250 μM $HgCl_2$ inhibited biological growth; cultures without the $HgCl_2$ became turbid over the course of two days when incubated at 30°C, while the media containing the $HgCl_2$ remained clear for seven days. Thus, cylinders, in triplicate, were placed in the two types of media with the addition of 250 μM $HgCl_2$. Unfortunately, after several weeks the pH of the cylinders in the Horikoshi media dropped. This drop, accompanied by a foul odor and the change in color of the media (reddish at the high pH, versus a green color at the lower pH levels) indicated that the cylinders were contaminated in spite of the presence of $HgCl_2$. Possibly, the metal adsorbed into the concrete. There was no overt appearance of contamination amongst the acetate media cylinders dosed with 250 μM $HgCl_2$. Growth in this media is accompanied by the appearance of pink biomass; such growth does not cause a precipitous drop in pH, as it did in the Horikoshi media. However, given the lack of success in the Horikoshi case, these controls were also abandoned, as it was felt that the risk of handling concrete contaminated with mercury outweighed the benefits of studying it.

Representative thin sections were made from concrete unexposed to any media treatment. Cylinders of each aggregate type were taken from their molds and split as described above. After covering the surface with epoxy, thin sections were made as described previously.

3.5 IRON(II) OXIDATION EXPERIMENT

The iron oxidizing acidiphilic microorganism *Acidthiobacillus ferrooxidans* was used for one part of this study. The culture (ATCC 19859) was grown in the following media: 3.5g $(NH_4)_2SO_4$; 1.16g KCl; 0.58g K_2HPO_4; 0.58g $MgSO_4 \cdot 7H_2O$; 0.0168g $Ca(NO_3)_2 \cdot 4H_2O$ in 800 ml Milli-Q water, pH to 2 with 10N sulfuric acid. To this, 20g $FeSO_4 \cdot 7H_2O$ in 200 ml Milli-Q water was added. Both components were filter sterilized. The final pH of the media was near 2. This media is listed as ATCC Medium #2039 (Starkey's media), without the addition of Wolfe's Mineral Solution, which was deemed unnecessary (Lueking personal communication, 2003). The cultures were incubated at 30°C.

The 20-cm high concrete cylinders of each aggregate type were cut into 5-cm pieces with the block saw. These 5-cm circular pieces were then cut in half-circles, which were then weighed. Autoclaved Mason jars were used as containers for this experiment. The concrete pieces were placed in 80 percent ethanol for 20 minutes before beginning the experiment. Three pieces of each aggregate were then placed into 300 ml of one of the following solutions: Starkey's media without the iron (II) sulfate solution (referred to as A, for acid); Starkey's media with the iron (II) sulfate solution (referred to as AF for acid with Fe(II); Starkey's media with the

iron (II) sulfate solution inoculated with 1 ml of *A. ferrooxidans* from an active culture (referred to as AFB, for acid with Fe(II) and bacteria). All jars were kept at 30°C.

During the course of this three-week experiment, the pH was monitored with pH paper. If the pH rose above 2 (as indicated by orange paper, rather than red), 10 to 15 ml of 5 percent sulfuric acid was added. Initially, 0.5 percent sulfuric acid was used, but it was insufficient in keeping the pH below 3 for a 24-hour period. Thus, the higher concentration of acid was used in the interest of minimizing the volume of acid required. The media was changed every seven days. Generally, the pH rose to 3 in all treatments by 24 hours after acidifying. The last week of the experiment saw a decrease in the concrete's ability to donate alkalinity, and thus less sulfuric acid was added. Vigilant monitoring of the pH was required for two reasons: 1) as the pH moves toward neutral, Fe(II) becomes increasingly unstable in oxidizing environments, converting to Fe(III); 2) *A. ferrooxidans* optimum pH is around 2. At the end of three weeks, the pieces of concrete were removed from their solutions and vacuum impregnated with epoxy. Representative thin sections were made, as described previously.

CHAPTER 4 – RESULTS OF GLUCOSE AND ACETATE MEDIA INCUBATIONS

Biological growth occurred in both the acetate and glucose medias. An organic film appeared in both sets of media in which the concrete cylinders were submerged. The film was much more developed in the glucose media, where it attached to the surface of the concrete. The unpleasant odor emitted from the glucose media submerged concrete cylinders was further evidence of biological growth. Lastly, the pH of this glucose media dropped approximately 1 unit from near-neutral 24 hours after refreshing the media. Biological activity is the probable cause for this drop, as it did not occur in the acetate media, a poorer carbon source. This chapter shows these results in detail. All of the concrete subjected to the same treatment showed similar pathology. Therefore, the photographs and micrographs in this chapter only show one sample (randomly chosen) rather than the concrete of all three aggregate types. The corresponding photographs and micrographs showing the other two aggregate types are located in Appendix C.

The biological film on the GC, which can be seen in figure 4.1a, grew mostly on the cement paste, rather than the aggregate. Although no quantitative measurements were taken, there is qualitative evidence that less intense biological activity took place in the acetate media. A pink mat of biological material did form in the acetate media, but it stuck only sparingly to the concrete, and it emitted no odor. The cylinders in figure 4.1b are covered in very little organic matter compared to those in figure 4.1a. These cylinders did exhibit a white precipitate on the fracture surface of the cement paste. X-Ray diffraction revealed a spectrum that matches hydroxy apatite, as well as calcium carbonate.

Figure 4.2 shows the magnified images of the surface of GC AcC. These images are characteristic of the entire surface. Compared to the GC (4.2a), the AcC (4.2b) bore very little organic matter. Any mucopolysaccharide-like material appeared sparingly, in very small patches on the AcC surface. The delicate, cup-shaped calcite/apatite mineral deposits (4.2b) did not appear on the GC.

ESEM images (figure 4.3) of the GC surface resolve the fibrous material seen in figure 4.2a. This material is not seen on the surface of the AcC (figure 4.4). Instead, the ESEM images show the hollow, spheroid-shaped minerals, as well as some platey minerals. Possibly, the rounded deposits are organic in nature, but their origin cannot be definitively determined with these micrographs. These visual inspections did not reveal greater biological activity on a cylinder of a particular aggregate compared to any of the other aggregate types.

a.

b.

Figure 4.1. Fracture surfaces of cylinders immediately following incubation period. **a)** The photograph was taken shortly after the cylinder was removed from the glucose media at the end of 88 days. All of the cylinders in the glucose media emerged with a similar orange colored, slimy organic matter covering parts of the fracture surface. Generally, as can be seen in this photographs, this material tended to grow on the cement paste rather than the aggregate. In some parts, the cement paste appeared lighter than is typical (photo of blast furnace slag aggregate concrete). This is the slag aggregate concrete. **b)** The photographs were taken shortly after the cylinders were removed from the acetate media at the end of 84 days. The white precipitate, which was found mainly on the fracture surfaces, was common to all of the cylinders. The precipitate appeared in both long white lines, as well as tiny dots (photo of carbonate aggregate concrete). This is the carbonate aggregate concrete.

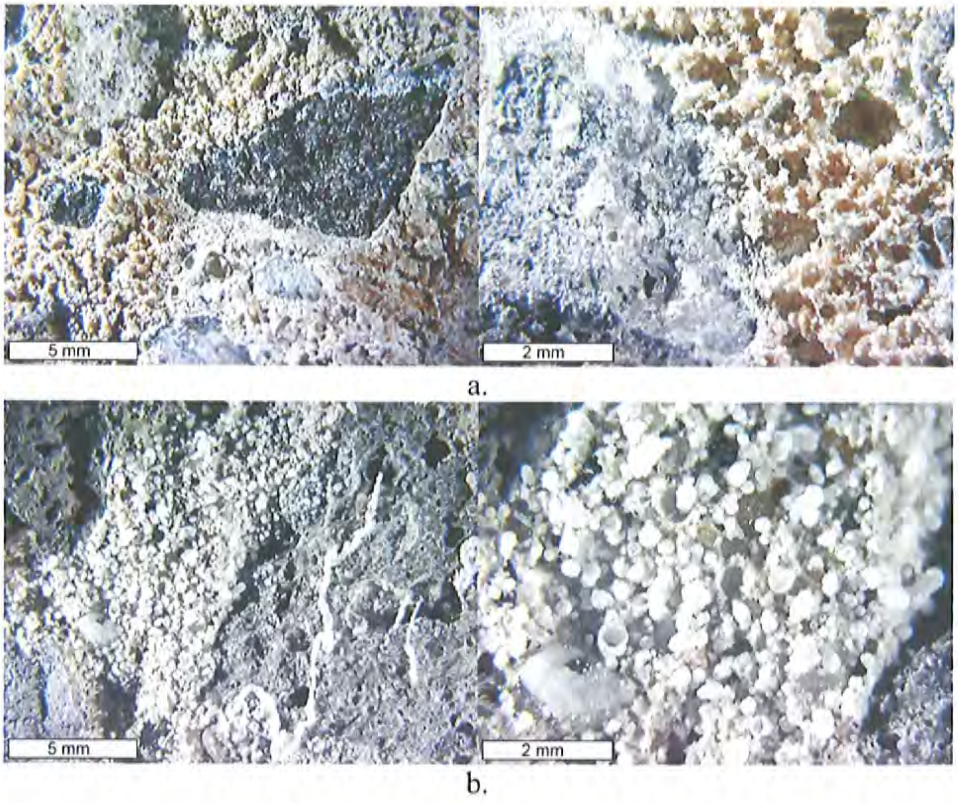

Figure 4.2. Magnified images of the surface of the cylinders. These micrographs were taken with a stereomicroscope approximately a half an hour after removing the concrete cylinders from the media at the end of their incubations. The left-hand micrographs of each set were taken using the 10x objective (5 mm scale bar), while the right-hand ones were taken using the 25x objective (2 mm scale bar). **a)** The micrographs show the pink colored film on the GC in more detail than figure 4.1.a. This film generally covers the paste rather than the aggregate. This is the natural gravel aggregate concrete. **b)** On all of the AcC the white, cup like mineral deposits can be seen very clearly. Generally these white deposits are on the cement paste, rather than the aggregate. This is the slag aggregate concrete.

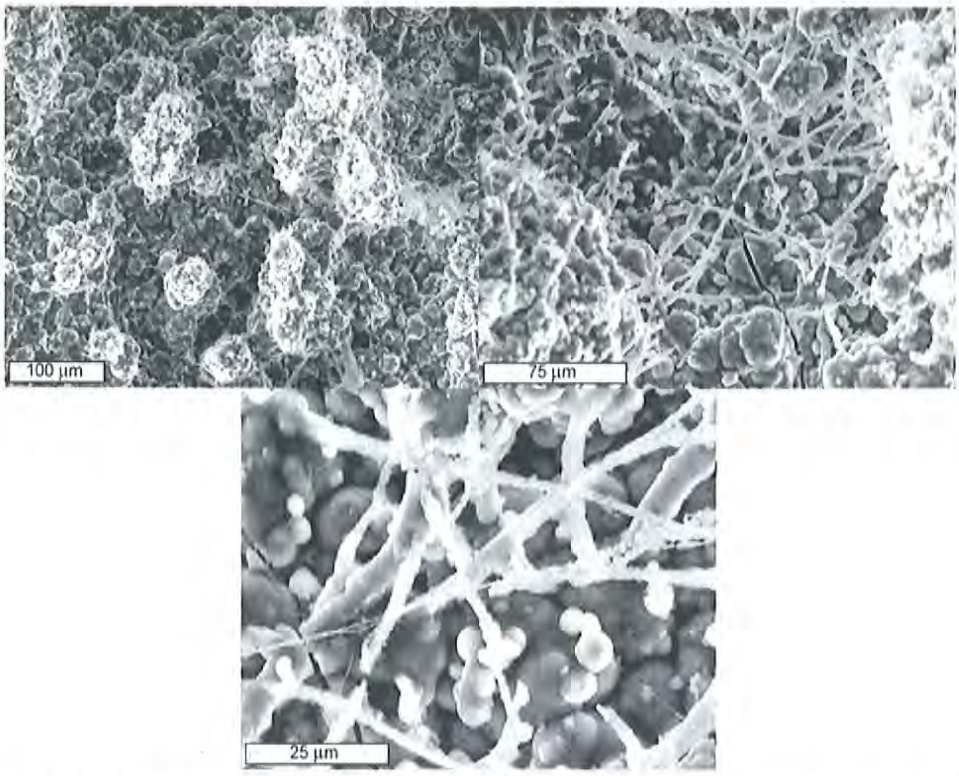

Figure 4.3. ESEM Images of the surface of the GC. This series of micrographs was taken with an ESEM of the organic material seen in figure 4.2. The material is very fibrous and appears biological in nature.

Petrographic examination revealed corrosion of the GC. The control cylinders that were subject to no treatment appear normal within thin-section (figure 4.5). Throughout the composite micrograph the cement paste has a uniform color. All of the thin section micrographs presented in the following figures are composite images of cross-sections showing the outer fracture surface (top of image), toward the inner, unexposed surface of the cylinders. These composites are shown in (from left to right): plane light, epiflourescent mode, and cross-polarized light. In the cross-polarized images the birefrigent areas (bright spots) show that calcium hydroxide has not leached calcium hydroxide from the paste. Since the surfaces of these control cylinders were epoxy stabilized very soon after they were split, the lack of a distinct carbonation zone, which appears as a band of highly birefringent minerals, is not unusual.

In contrast, the cement in the GC (figure 4.6) is leached of calcium hydroxide. This is most evident in the cross-polarized image, which shows a several millimeter zone at the surface depleted in the birefrigent calcium hydroxide mineral, compared to the sound paste beneath the zone. In the epifluorescent mode image the leached zone is darker; since it is more porous it can absorb more epoxy dye, thus appearing darker. The lack of a normal carbonated zone is unusual. The concrete also exhibits a poorly crystalline surficial crust best seen in the thin-sections in figure 4.7.

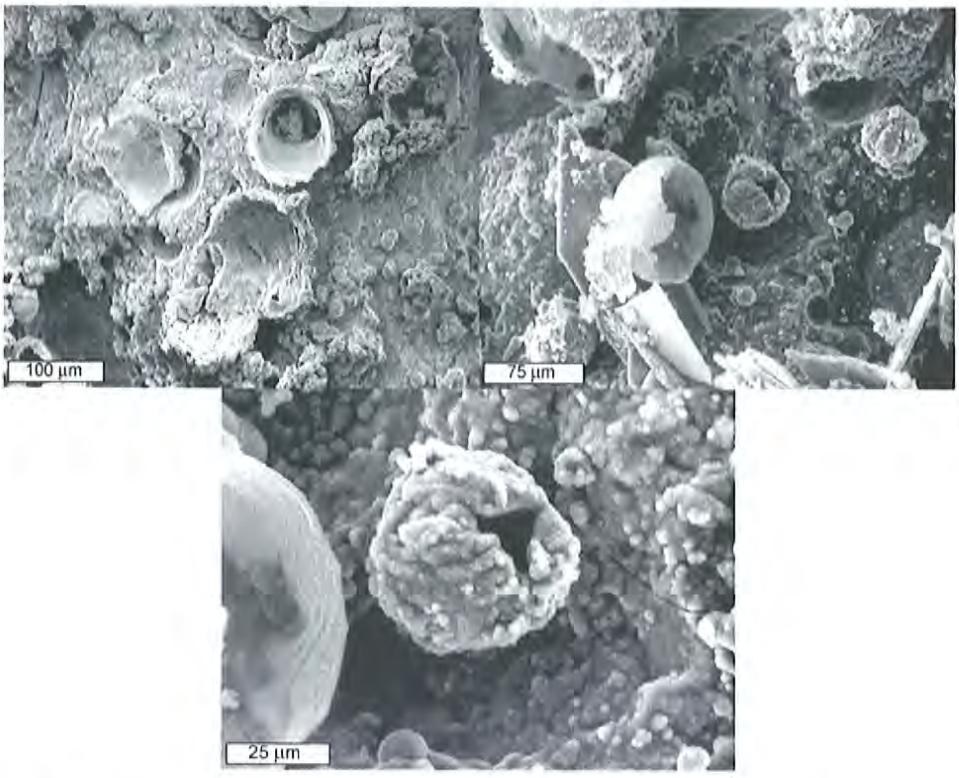

Figure 4.4. ESEM Images of the surface of the AcC. This series of micrographs was taken with an ESEM of the surficial deposits seen in figure 4.2. The morphology of these deposits is neither clearly biological nor abiological.

X-ray energy maps, shown in figure 4.8a, of these thin-sections show this crust is mainly composed of phosphorous. The most important aspect of these x-ray maps is the confirmation of the calcium hydroxide, as indicated by fewer red bright spots toward the fracture surface. Additionally, calcium hydroxide depletion around the aggregates in the leached zone is also visible. The corresponding electron backscatter image (4.8b) clearly shows the zones of sound and unsound cement paste. The unsound paste appears more porous, compared to the dense paste toward the bottom of the image. The elemental map in figure 4.8a also shows that the surficial crust is mainly phosphorous and calcium, which likely correspond to the minerals apatite and calcium carbonate.

Figure 4.9 focuses on the line between the zones of leached and unleached paste. The paste appears leached approximately 2 mm from the fracture surface. Some of the surficial apatite crusts had vaterite (a calcite polymorph) inclusions (figure 4.10).

The AcC does not show the same signs of leaching that the GC exhibits. Figure 4.11 shows that the cement paste is consistent throughout the composite images of the light micrographs. Also, unlike the GC thin-sections, the AcC has a thick carbonation zone (approximately 2-mm).

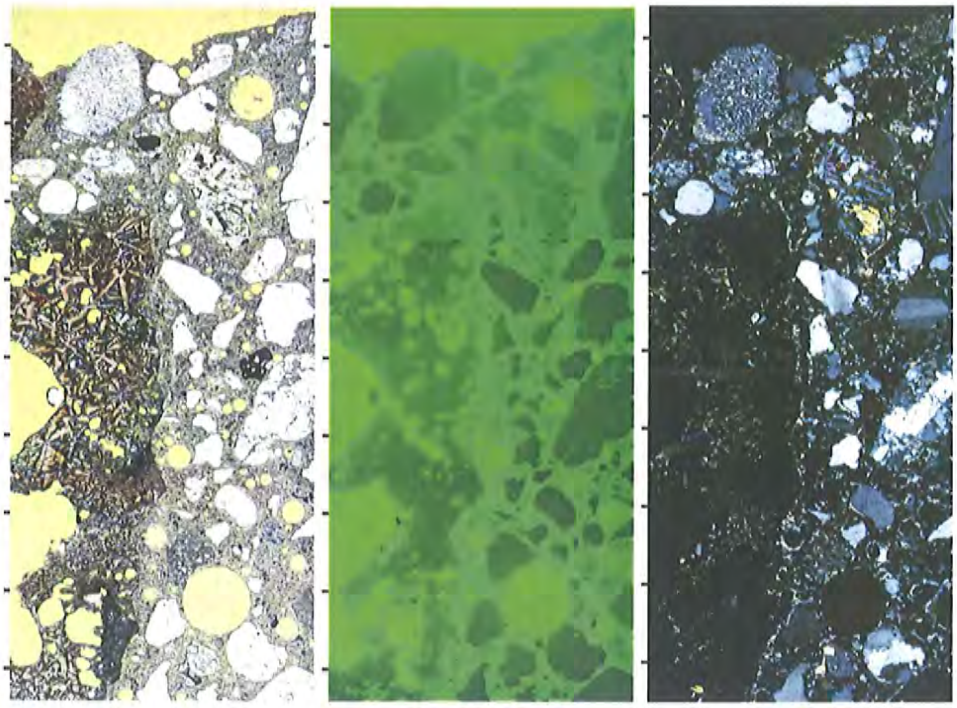

Figure 4.5. Thin-sections of the control cylinders. These petrographic thin-sections are from concrete cylinders unexposed to any biological agents. Note that the cement paste is a uniform color throughout the montage. The tick marks on the side are 0.5 mm apart. This is the slag aggregate concrete.

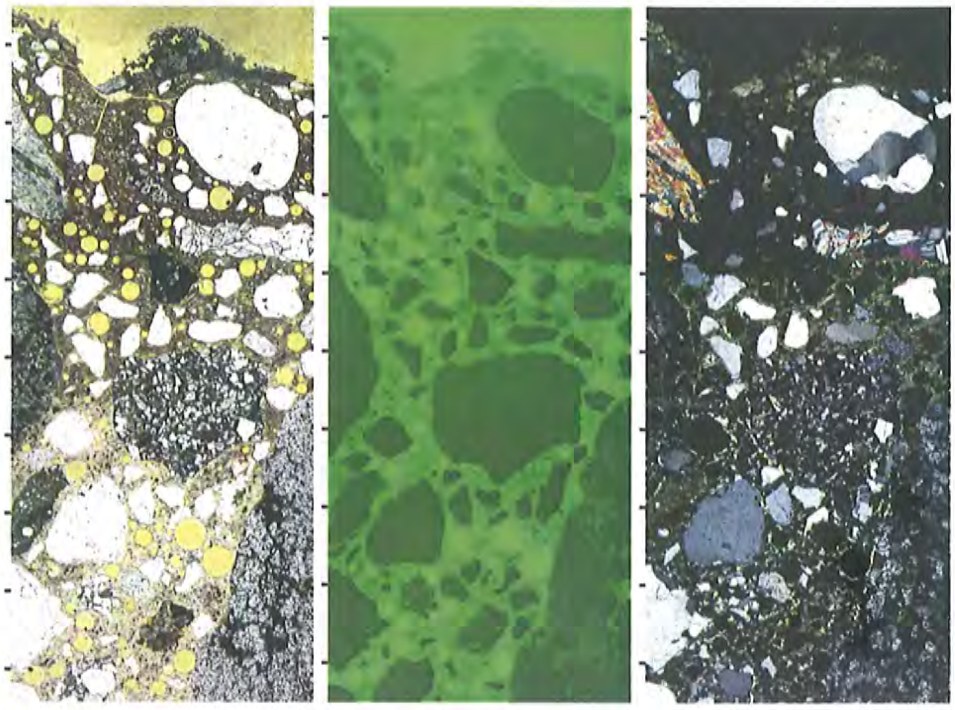

Figure 4.6. Petrographic thin-sections of the GC fracture surface. These petrographic thin-sections are from the GC. These thin-sections all show a poorly crystalline crust of varying thickness at the immediate surface (0.1 to 0.5 mm). Beneath the surficial crust is a zone of calcium hydroxide depleted cement paste (approximately 2 mm), beyond that is sound cement paste. The tick marks on the side are 0.5 mm apart. This is the carbonate aggregate concrete.

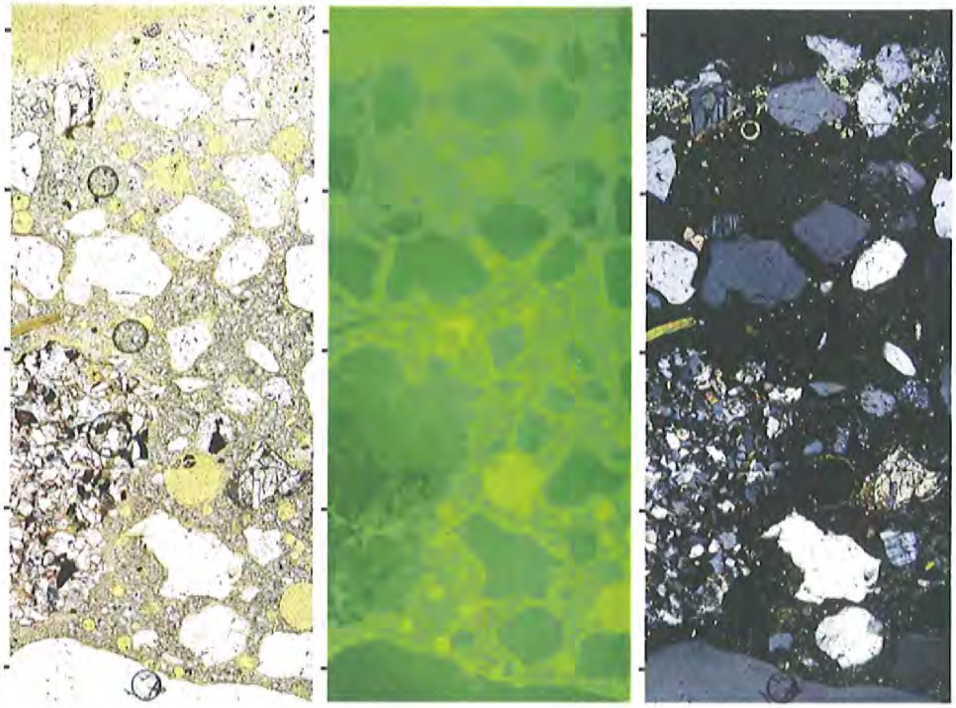

Figure 4.7. Detailed image of the GC. These petrographic thin show the surface of the GC in more detail (10x). The amorphous and highly porous nature of the surfical crust can be clearly seen. This is especially clear in the cross-polarized image, where the isotropic crust appears black. Material is absent from the interface between the aggregate and the paste in the crust area. The tick marks on the side are 0.5 mm apart. This is the carbonate aggregate concrete.

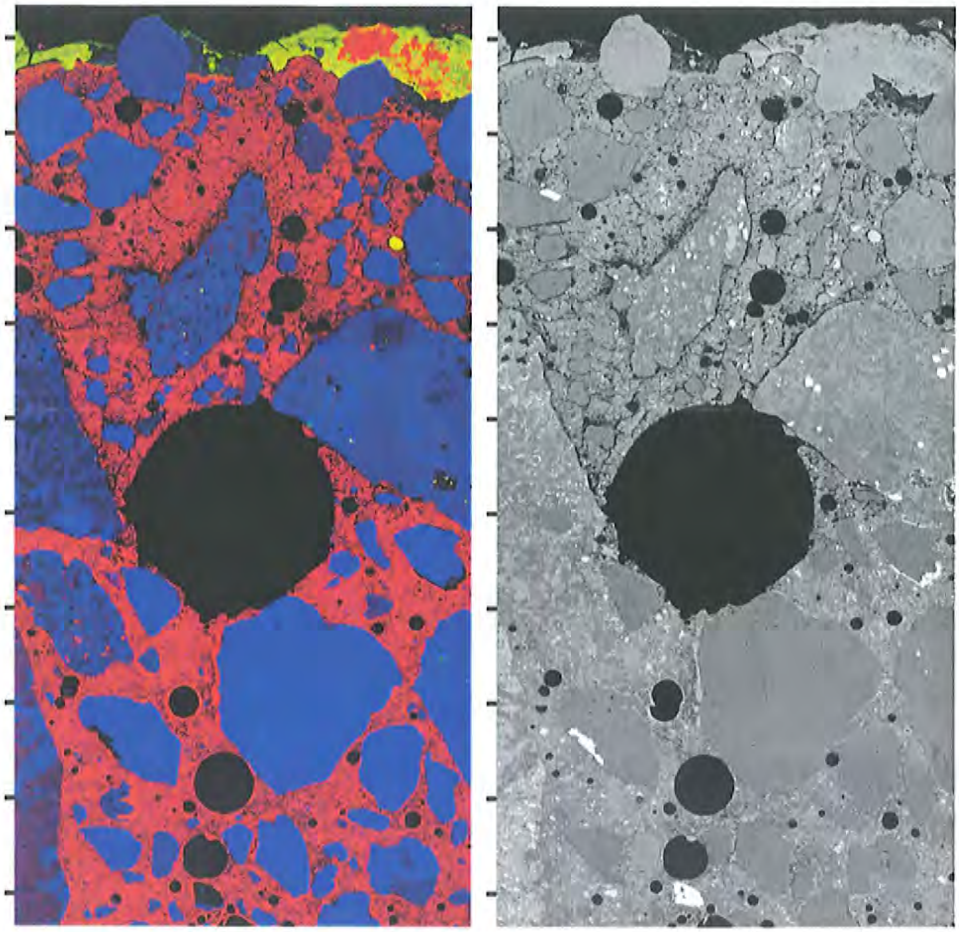

a. b.

Figure 4.8. X-ray energy map and backscatter image of the GC. a) This image is an X-ray energy maps made from the petrographic thin-sections of the blast furnace slag aggregate GC. The color-coding for these maps is: red = Ca, blue = Si, and green = P. This map confirms the leaching seen in the petrographic thin-section. The top of the image has fewer red bright spots, which correlates to fewer calcium counts. The elemental map shows that the surficial crust is composed mainly of phosphorous, with some calcium. The slag aggregate at the surface appears depleted in silica compared to aggregate in the unleached zone. b) In the corresponding back scatter images it is clear that the aggregates are undamaged (no evidence of microcracking). These composite images show the material removal from the interface between the aggregate and the cement paste in the leached zone. Also evident is the porous nature of the leached paste, as compared to the sound, dense paste toward the bottom of the image. This is the slag aggregate concrete. The tick marks on the side are 0.5 mm apart.

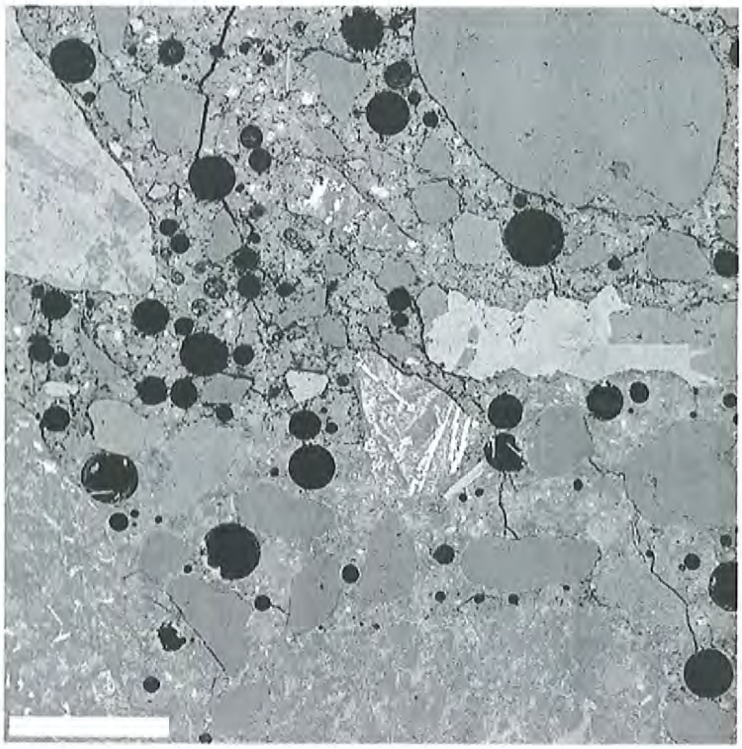

Figure 4.9. Back scatter image of GC. The top of this image is oriented toward the fracture surface. The cement paste toward the bottom of the image is clearly denser compared to the paste toward the surface. The scale bar is 1 mm in length. This the carbonate aggregate concrete.

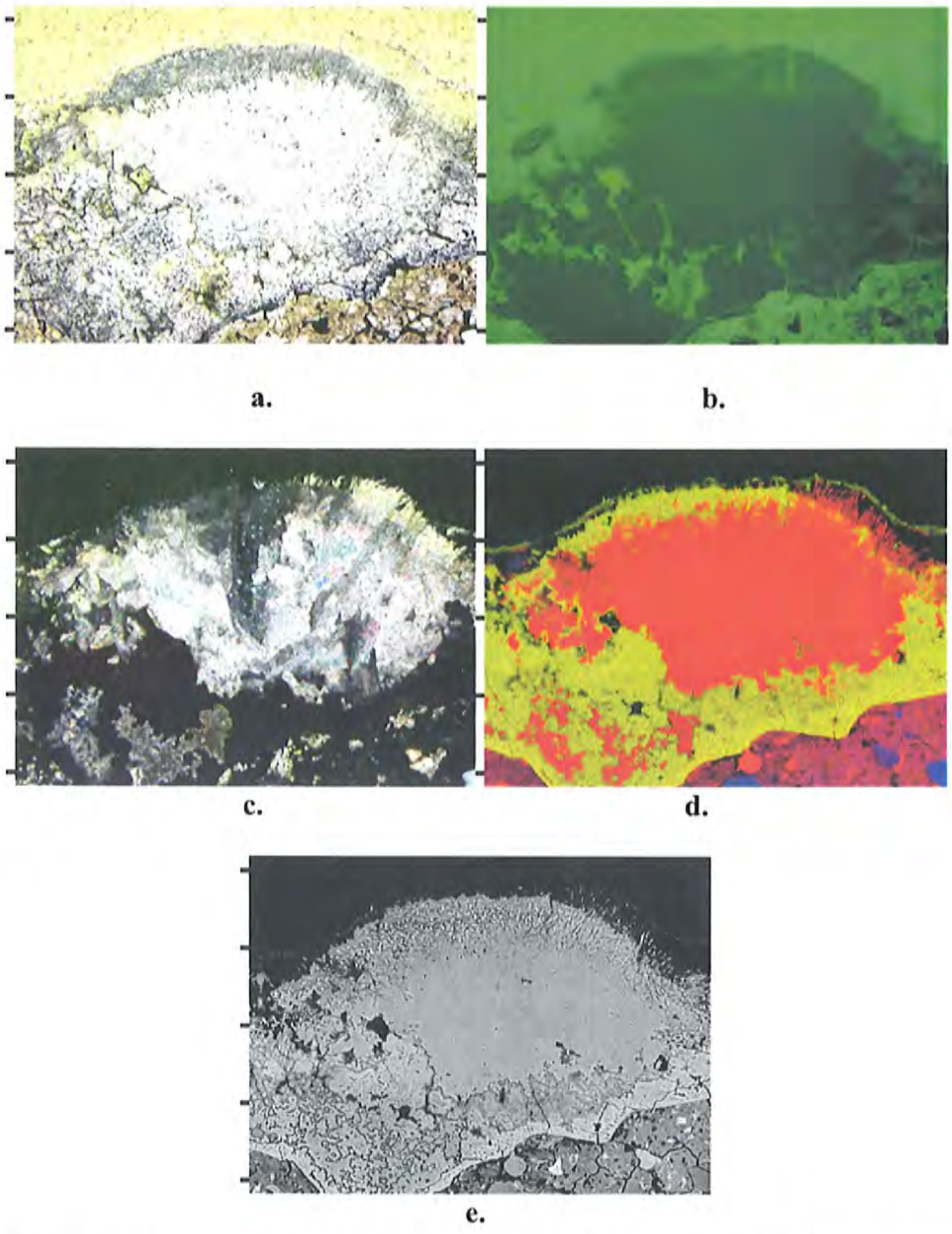

Figure 4.10. Vaterite deposit. These micrographs show the presence of the fibrous calcite polymorph vaterite in the apatite crust on the GC surface. a) plane-polarized light. b) epifluorescents. c) cross-polarized. d) energy x-ray map, red = Ca, blue = Si, yellow = P. e) back-scatter image. The tick marks on the side are 0.5 mm apart. This is the natural gravel aggregate concrete.

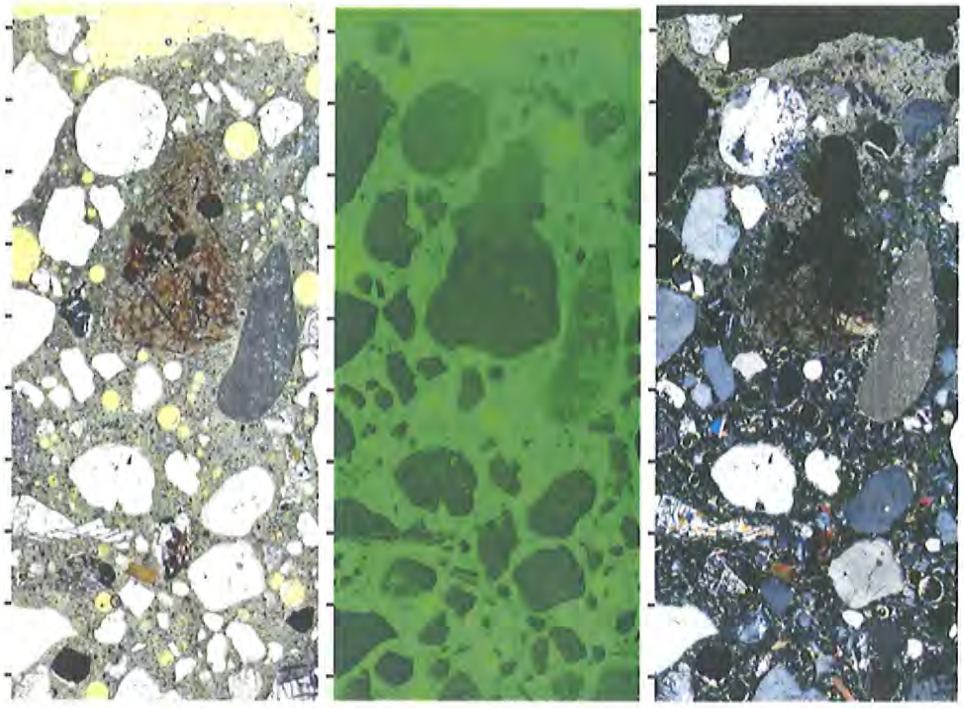

Figure 4.11. Thin-sections of the AcC. These petrographic thin-sections are from the slag aggregate AcC, and they do not show signs of calcium hydroxide leaching; the color of the paste is consistent throughout the composite. The carbonation zone, best seen at the surface of the cross-polarized image, is thick, but within normal limits. The aggregate and the cement-aggregate interface appears to be intact. The thin-sections show a thin, poorly crystalline crust at the surface. Generally these thin-sections are unremarkable. The tick marks on the side are 0.5 mm apart.

The delicate apatite crust can also be seen in the light micrographs of figure 4.11, but it is better seen in the energy x-ray maps in figure 4.12a. These images confirm that the small round mineral deposits indeed contain phosphorous, and are thus likely apatite (also seen in figure 4.13). Most importantly, these maps show that no appreciable leaching of the calcium hydroxide from the cement paste took place during the incubation. The cement-aggregate interface also appears intact. The backscatter images in figure 4.12b show that the cement paste is considerably less porous than the leached zones pictured in the backscatter images of the glucose concrete (figure 4.8b). The carbonation layer is similarly dense. According to the technique used here, no detrimental alteration occurred to the microstructure of the concrete in the acetate media.

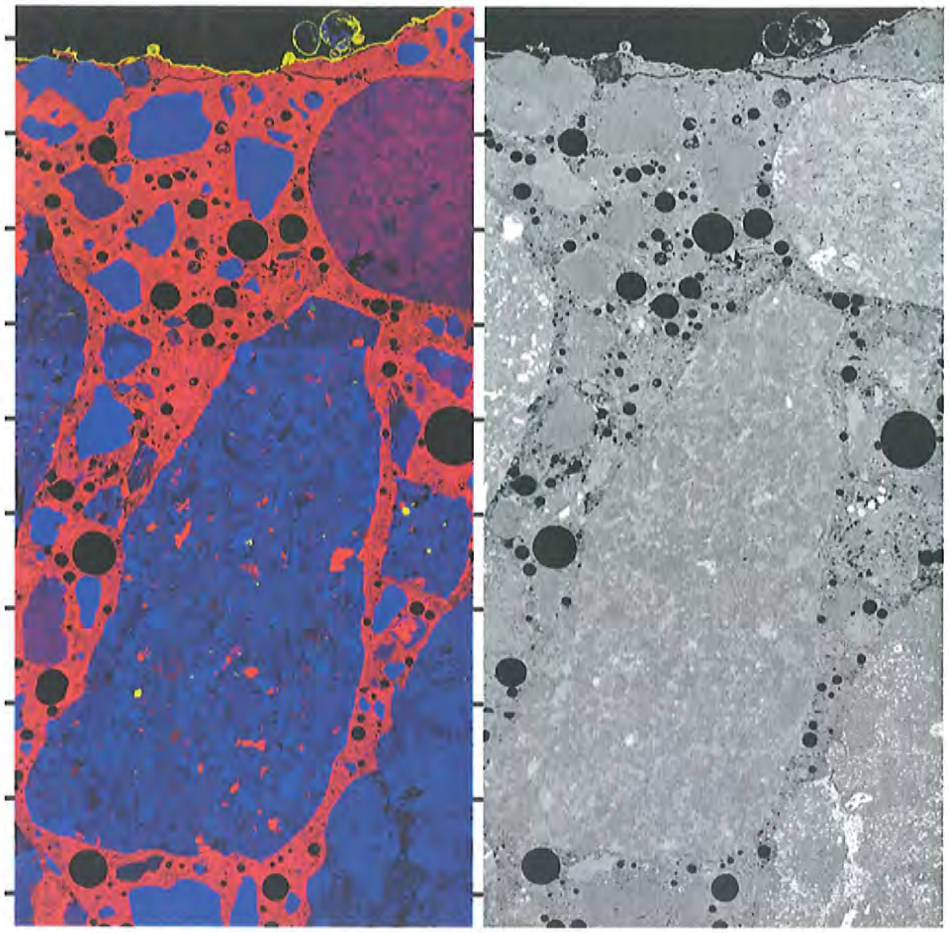

a. b.

Figure 4.12. X-ray energy map and electron back scatter image of the AcC. a) Shown here is the X-ray energy maps of the natural gravel aggregate type petrographic thin-sections of the AcC. The x-ray energy maps are coordinated as follows: red = Ca, blue = Si, and green = P. The paste aggregate interface is intact. The x-ray map shows no calcium leaching (the color is consistent throughout the composite). There is a thin crust of phosphorous on the surface. b) The corresponding backscatter image shows that the paste is uniformly dense, from the fracture surface inward. The scale bars in both images are 0.5 mm apart.

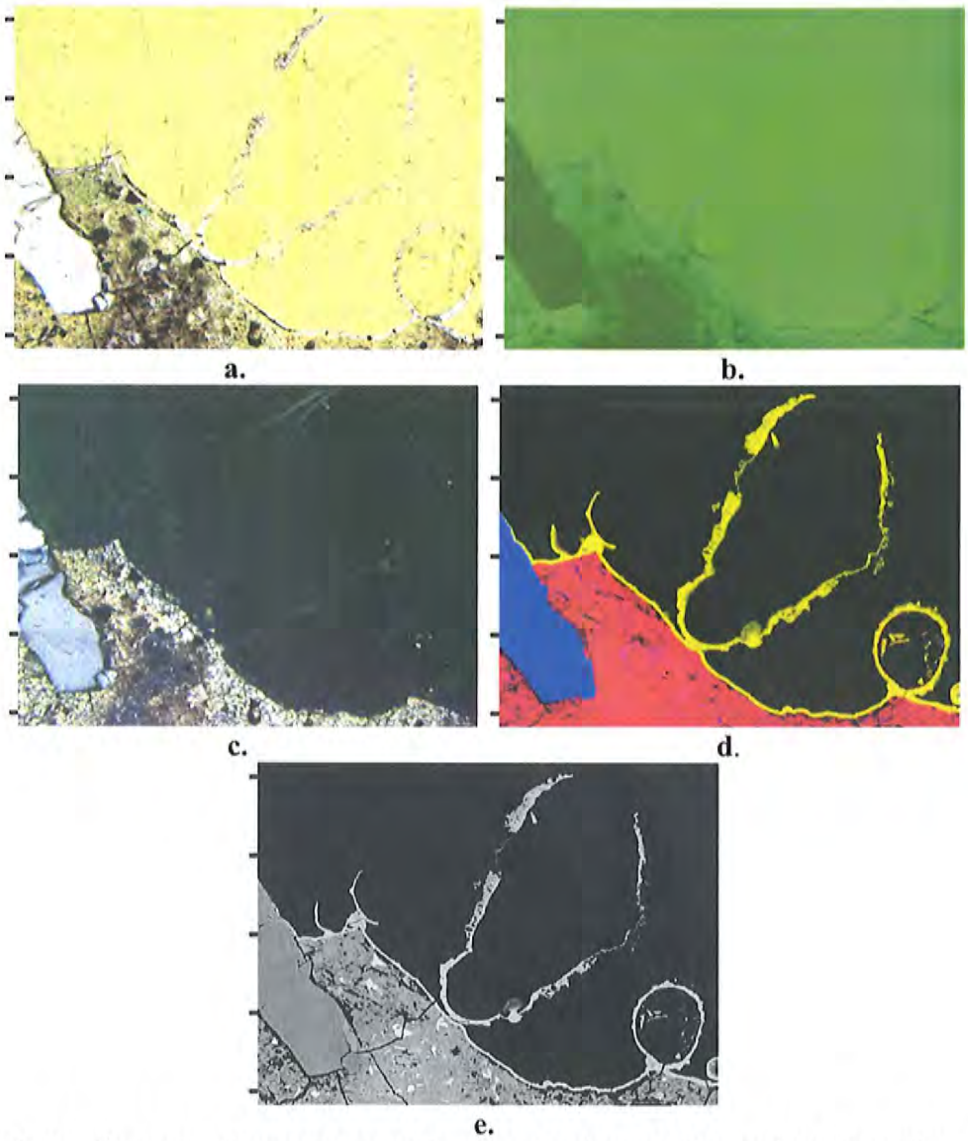

Figure 4.13. Apatite crust. These micrographs show the thin apatite crust on the surface of the carbonate aggregate AcC. The tick marks on the side are 1-mm apart. a) plane-polarized light. b) epifluorescent. c) cross-polarized. d) energy x-ray map, red = Ca, blue = Si, yellow = P. e) backscatter image.

All replicates followed a similar trend in pH, regardless of the aggregate type (figure 4.14): the pH of the neutral media rises until the media is replenished. The pH of the media starts at approximately 6.7 and rises to alkaline levels, remaining there until the media is replenished. For the glucose media, an exception to this general observation occurred in the first 20 days because of the large range in pH levels between the different replicates for each aggregate type (Appendix D shows this range).

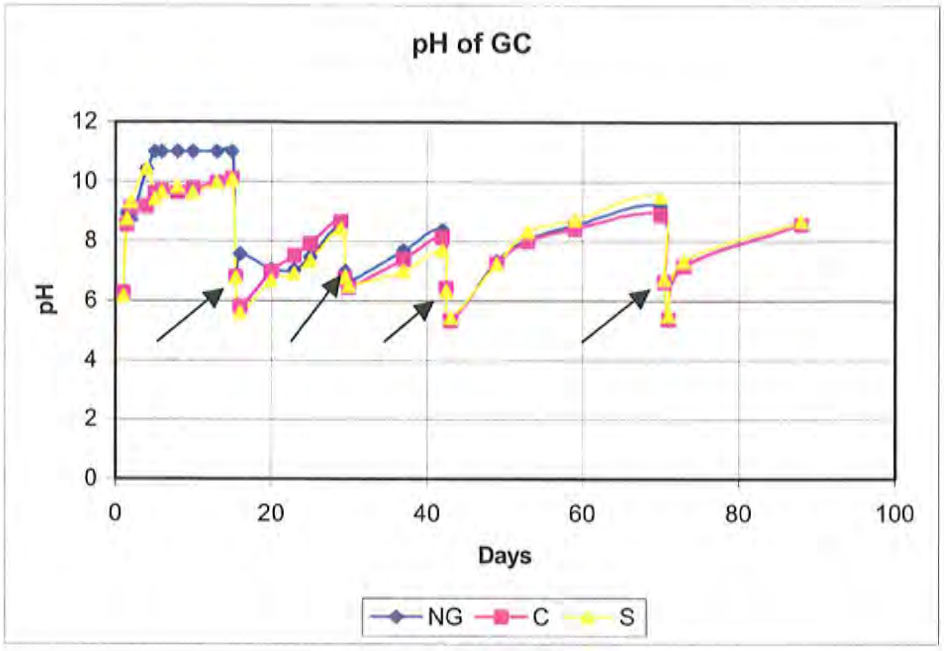

a.

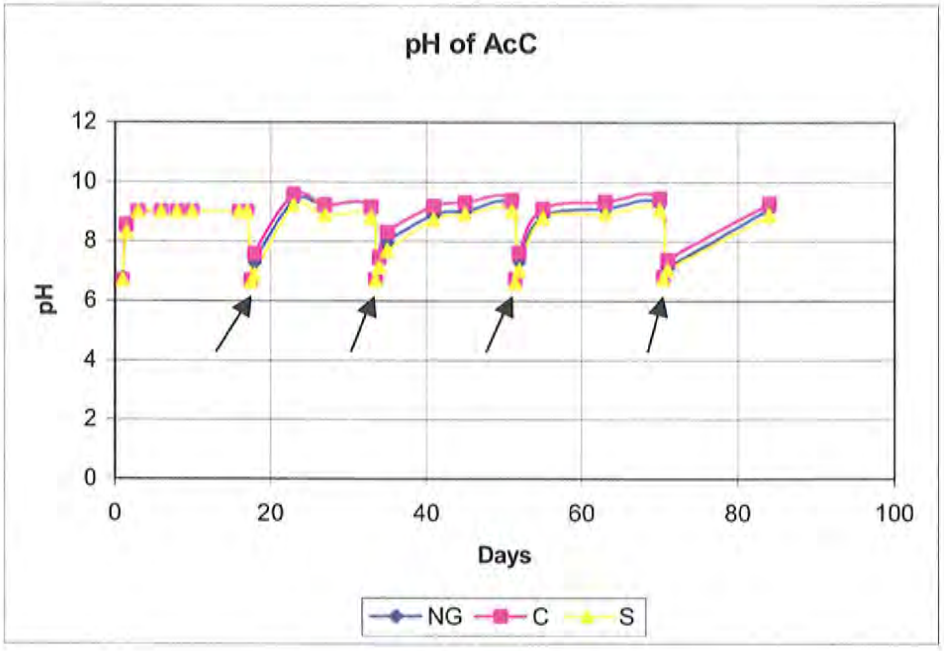

b.

Figure 4.14. pH Measurements. a) This graph shows the pH fluctuations in the GC. b) This graph shows the pH fluctuations in the AcC. In the GC system, the pH goes down following the media change (indicated by arrow), whereas in the AcC system, the pH goes up immediately following the media change.

A Student's-t test (assuming unequal variance) was performed between the average pH measurements of the replicates of cylinders of a given aggregate incubated in the AcC solution and those of the same aggregate in the GC media solution (table 4.1). In no case does the computed t-statistic for the data exceed t-critical value. Thus, either the difference in the range in the pH values between the glucose media and acetate media is insignificant, or the difference between the length of time required to raise the pH from neutral to alkaline is insignificant, or both. The slope of the line is generally flatter for the rise in pH in the GC system compared to the AcC system (figure 4.15). The data for the two systems (glucose and acetate) was not taken synchronously, and thus direct comparison is difficult, as is rigorous statistical analysis. The points shown on the plot represent the average pH of all of the replicates in the given media Instead of using all of the data, the points on the plot represent the pH of the media change, and then the first appearance of alkaline pH (or the pH value immediately before the subsequent media change). The histograms in figure 4.16 more clearly show that the rise in pH of the replicates in the GC media took place over a shorter period of time (4.16a) than did the rise in pH of the AcC media replicates (4.16b). These values were rounded to the nearest whole number, thus values greater than 8.5 are considered alkaline.

Table 4.1. Results from t-test (performed in Microsoft Excel).

	NG Glucose	NG Acetate	LS Glucose	LS Acetate	Glucose	S Acetate
Mean	8.24	8.31	7.89	8.43	7.90	8.18
Variance	3.14	1.02	1.99	1.06	2.32	1.02
Observations	30	27	30	27	30	27
Hypothesized Mean Difference	0		0		0	
Df	47		53		51	
t Stat	-0.1895		-1.6481		-0.8068	
P(T<=t) one-tail	0.4253		0.0526		0.2118	
t Critical one-tail	1.6779		1.6741		1.6753	
P(T<=t) two-tail	0.8505		0.1052		0.4235	
t Critical two-tail	2.0117		2.0057		2.0076	

It is clear from the data that the pH of the GC systems decreased immediately following the media change (figure 4.14a). This drop occurred after all transfers except for once with the natural gravel cylinders (following the transfer after the start of the experiment). Table 4.2 lists the average pH drop of the three replicates for each aggregate. This drop in pH occurred in a 12 to 24 hour period after transfer. This drop did not occur in the AcC media solution where the solution pH went up immediately following the transfer (figure 4.14b).

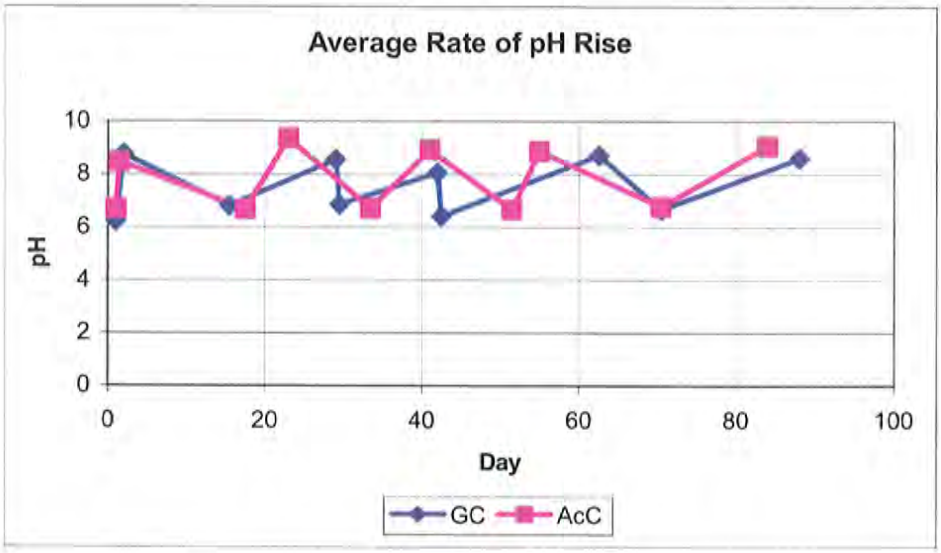

Figure 4.15. Rate of rise in pH. The data on this graph are the average of the three aggregate types for each treatment, either glucose media or acetate media. The lower points are at the media change, and the higher points indicate the first measurement of alkaline pH (9).

Table 4.2. The average drop in pH of the glucose media solution for the three replicates of each aggregate type.

NG	LS	S
0.50	0.92	0.90
0.91[1]		

[1] 0.91 is the average drop in pH if the first data point is left out, as the difference is negative.

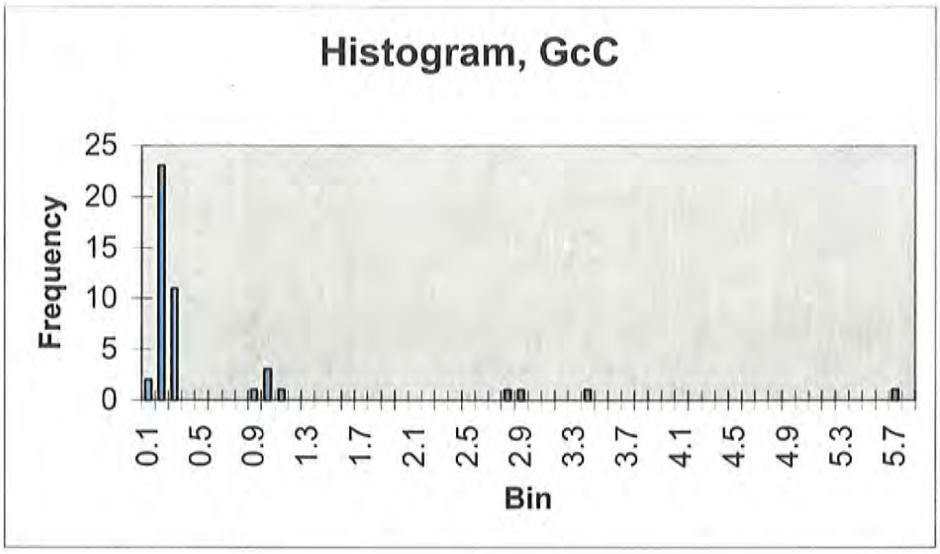

a.

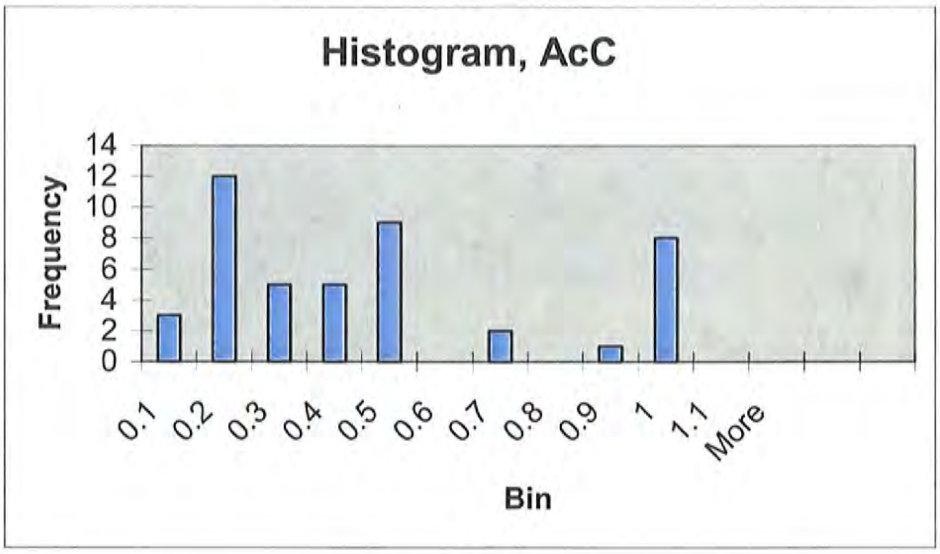

b.

Figure 4.16. These two histograms shows the frequency of the slopes from the lowest pH data point to pH 9 of the two different media. The data from all nine of the replicates for each media type were used to make these plots. Generally, these slopes were smaller for the glucose replicates (a) then for the acetate replicates (b); the more gradual slopes appear with greater frequency in the glucose media.

CHAPTER 5 – CONCRETE INCUBATED WITH *A. FERROOXIDANS*

The pH of the media in which the pieces of concrete were submerged was sufficiently maintained so that only the system containing the bacteria *A. ferrooxidans* showed any Fe(II) oxidation (figure 5.1). Removed from the media and rinsed lightly with distilled water, the AFB concrete was covered by rust colored material (figure 5.2). The concrete shown in figures 5.1 and 5.2 is the slag aggregate concrete, however the appearance of both the media and the concrete's surface after being removed from the media was typical of all the aggregate types, given the same type of treatment.

a.

b.

Figure 5.1. Photographs of the AF and FB medias. a) AF slag aggregate concrete incubated in acidic media, with Fe(II). **b)** AFB slag aggregate concrete. Without the bacteria the iron stayed as Fe(II) and did not oxidize, as evidenced by the greenish color of the abiotic system, versus the rust color of the biological system.

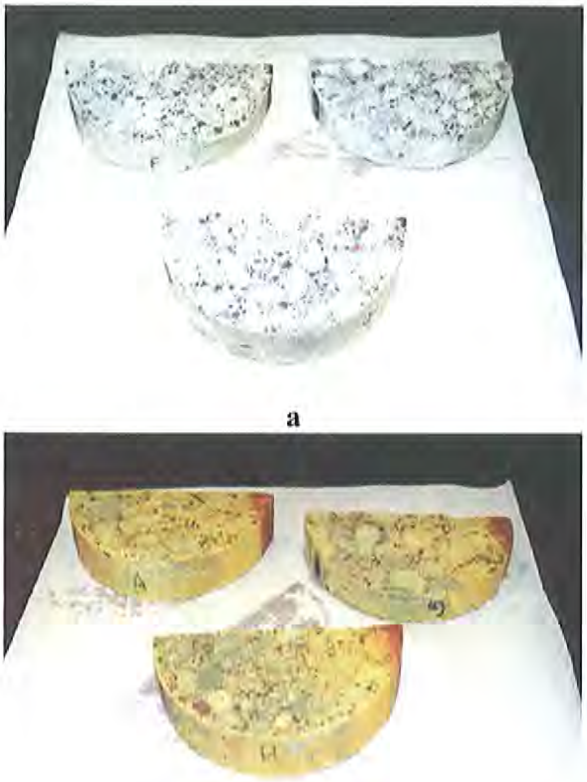

a

b.

Figure 5.2. Photograph of the AF and AFB concrete surfaces. a) AF slag aggregate concrete. b) AFB slag aggregate concrete. The Fe(II) oxidizing activity of the bacteria is evident by the rust colored appearance of the concrete surface.

The thin-sections from this part of the study are all similar regardless of the type of treatment they received. All of the thin-sections, including those exposed only to the acidic media, show a corrosion layer (approximately 5-mm thick) at the surface, behind which is a red-colored band. Some leaching of the CH is visible, but it is less than that of the GC incubated concrete. Micrographs of the complete suite of thin-sections are in Appendix E. Only the AFB concrete is discussed in this chapter. Additionally, since the concrete of all of the aggregate types had similar petrography, only one aggregate type is shown for each figure. The thin sections of the aggregate types not included in this chapter are also pictured in Appendix E.

The corrosion product layer is clearly visible in figures 5.3. Also visible is the rust-colored band below the corrosion product. The energy x-ray maps (figure 5.4a) of the fracture surface indicate that the surficial layer is a sulfur-containing mineral (most likely gypsum). The gypsum layer is continuous over the carbonate aggregate (figure 5.3). Due to its calcareous nature, it likely dissolved with the cement. Figure 5.4a also shows a continuous corrosion layer over the slag aggregate. In contrast, the silicate bearing aggregates shown in that image (5.4a) are not abreast with the cement paste. However, the interface of the gravel in the corrosion zone

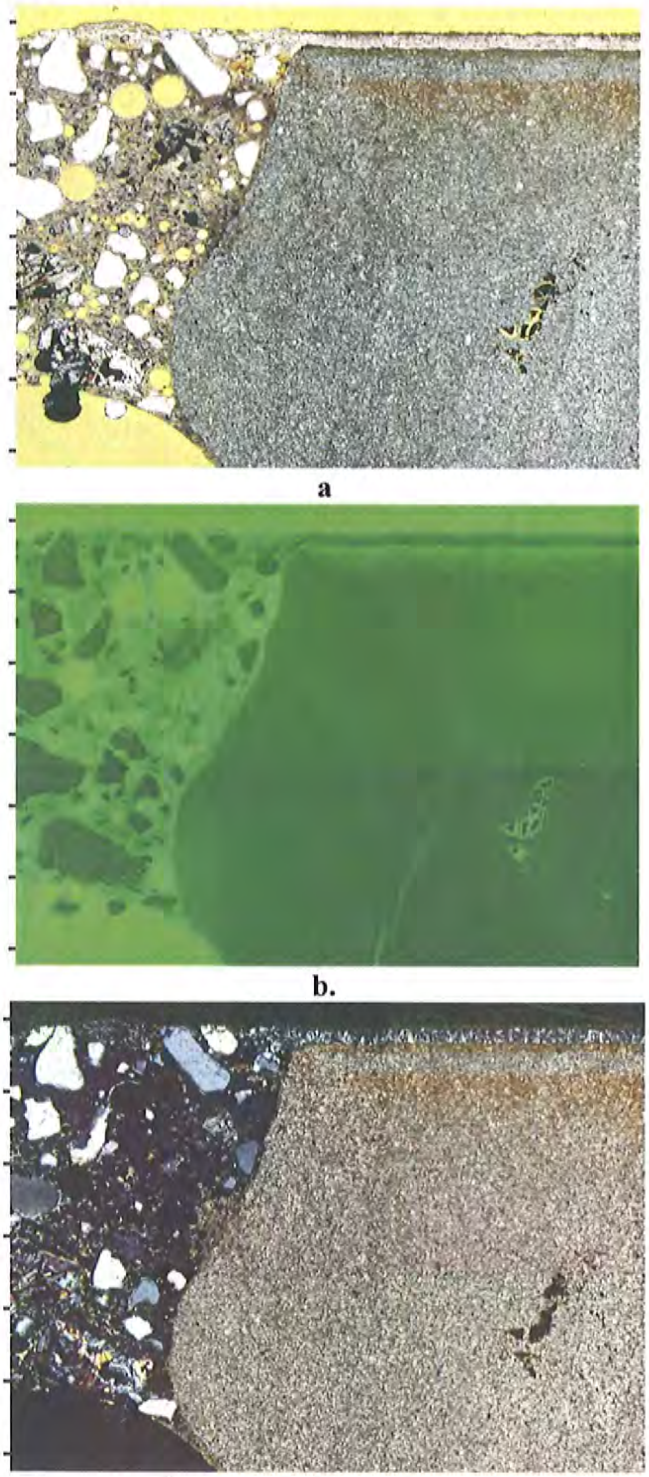

Figure 5.3: Petrographic thin-section of AFB. These petrographic thin-sections, at the surface of the carbonate aggregate AFB, are as follows: a) plane-polarized light, b) epifluorescents, c) cross-polarized. A thin layer of corrosion product lies flat along the exposed surface. The tick marks on the side are 0.5 mm apart.

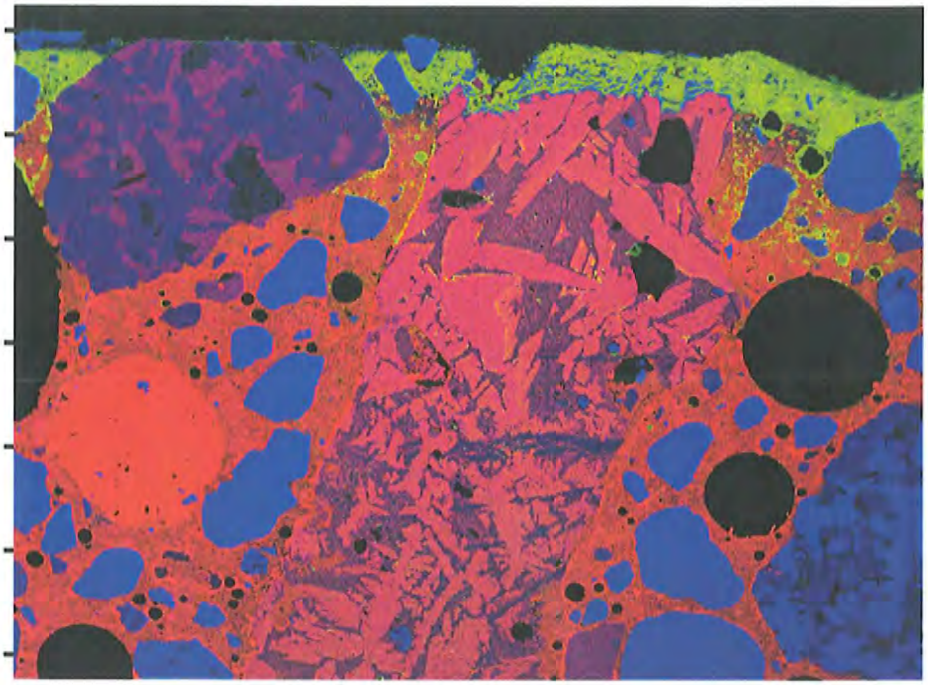

a.

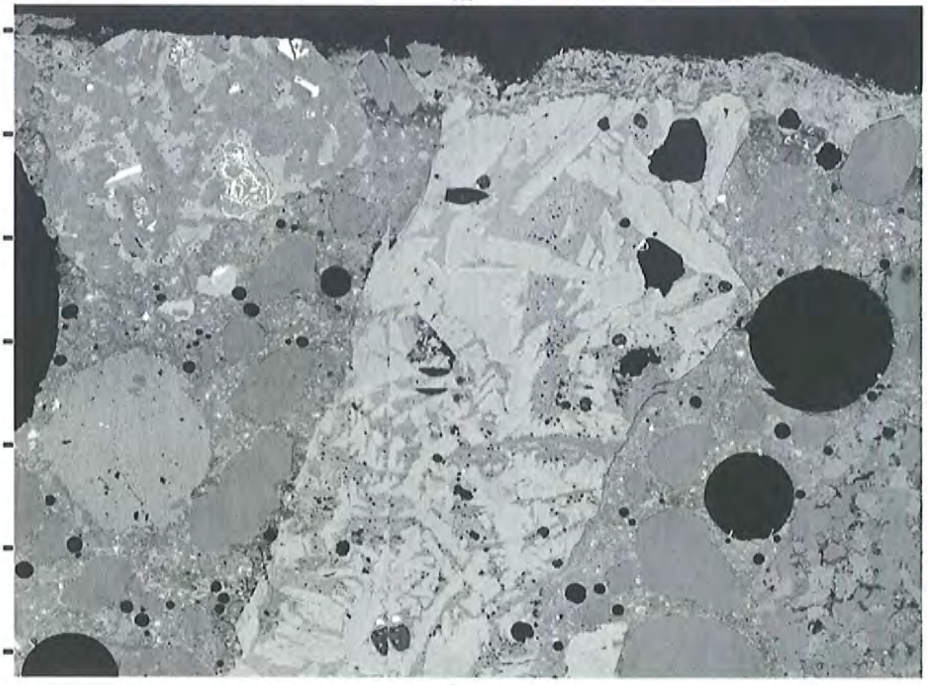

b.

Figure 5.4. X-ray energy maps and electron back scatter images of the AFB. a) In the map, yellow = S, blue = Si, red = Ca. This shows a gypsum layer on the surface of the slag aggregate concrete. The fact that the slag aggregate (center of image) is flush with the cement paste indicates it has been worn away by the sulfuric acid, as compared to the silicate bearing aggregates to its left and right. **b)** In the corresponding back scatter image the cement paste appears relatively dense and unleached. The tick marks on the side are 0.5 mm apart.

is consumed by gypsum. The cement paste behind the corrosion layer does not appear remarkably porous (figure 5.4b). From both the petrographic thin-sections and the x-ray maps it is evident that there is no appreciable zone of calcium hydroxide leaching. Also, the interface between the aggregate and the paste appears intact. The leach zone is relatively small and concentrated at the gypsum layer. Also, gypsum crystals were observed in the air voids.

CHAPTER 6 – DISCUSSION

St. John *et al.* (1998) note that concrete is a relatively inexpensive building material, and as such any discussion of it susceptibility to natural corrosive agents should take place within that context. However, results that may be of little interest to the engineer may be of broader interest to the geomicrobiologist, and thus the behavior of concrete acted upon by biological agents should be seen within both view points. The results of this study are consistent with many in the literature on the biological degradation of stone surfaces and of the organic and mineral acid degradation of concrete.

6.1. GLUCOSE AND ACETATE MEDIA INCUBATED CONCRETE

Acid corrosion of concrete leaves characteristic petrographic evidence, as shown in figure 6.1. Thin-sections from the cylinders in the richer glucose media (figures 4.6 and 4.7) bear some characteristics in common with the thin-sections pictured in figure 6.1; both showing calcium hydroxide leaching. All aggregate types appear equally affected; in no aggregate type is the leaching superlative. None of these thin-sections showed the red-colored band often associated with acid corrosion. Also, the carbonation zone is very thin, and almost undetectable in the glucose incubated concrete (figures 4.6 and 4.7) compared to figure 6.1. There is, however, an amorphous crust (figure 4.10). In figure 6.1 it is identified as amorphous silica, whereas in figure 4.10 this crust is clearly calcium and phosphorous.

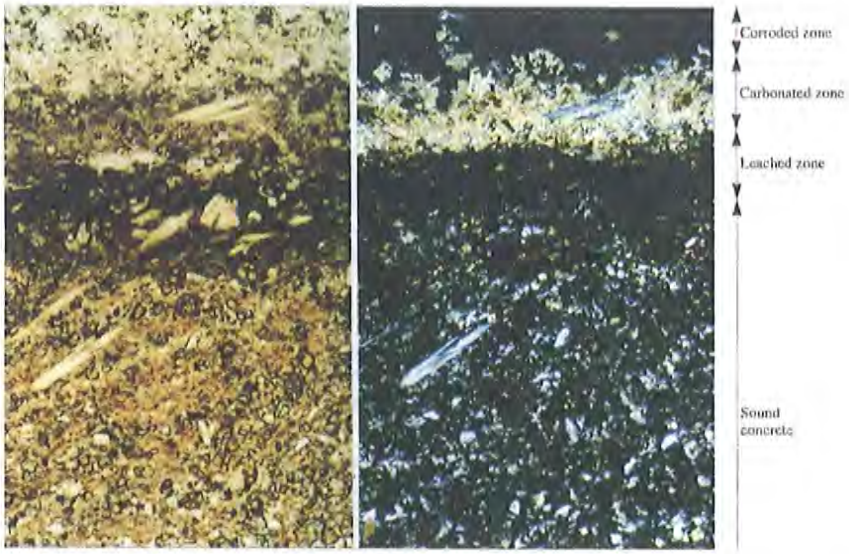

Figure 6.1. Petrographic evidence of acid corrosion. Above is a petrographic thin-section of corroded concrete pipe made with asbestos. (Plane light, L; Cross-polarized: R) The isotropic corrosion zone at the concrete's surface is amorphous silica and indistinct relics of miscellaneous material. The dark zone, behind the highly birefringent carbonation layer, has bee leached of calcium hydroxide. The unaltered concrete at the bottom of the thin-section still has bright patches of the calcium hydroxide mineral (St. John *et al.*, 1999).

The elemental maps (figure 4.8a) show that the aggregate exposed to the corrosion zone is slightly leached in silica, though it does not appear to have been re-precipitated in the amorphous zone. Other researchers report similar petrography. De Belie et al. (1997) soaked concrete made with carbonate and natural gravel aggregates in a mixture of lactic and acetic acids. At the surface, after 18 days, was an extremely porous isotropic corrosion zone. Below this was a brown-gray zone, also highly porous, that exhibited calcium hydroxide leaching. Behind the leaching zone was unaltered paste. These zones were also seen in cases of nitric acid attack and acetic acid attack alone. The acetic acid caused less corrosion, as it was neutralized more quickly (Pavlik, 1994). These studies did not mention the presence of apatite in the corrosion layer, which is identified as siliceous in nature.

Several researchers have examined the damage caused by microorganisms growing on concrete and stone surfaces, in many cases forming biofilms. The surface of the concrete incubated in the glucose media was well colonized (figure 4.1) with microorganisms. The magnified pictures of the surface in figure 4.2a show slimy, pink organic matter. Both figures show that the organic matter tends to be located on the cement rather than the aggregate. This distribution of microorganisms might be related to the highly porous nature of the cement compared to the aggregate. However, the slag aggregate is quite porous, but appears no more colonized than the other two types of aggregate. ESEM images (figure 4.4) of this material resemble biological structures in other published work (e.g., Krumbein, 1983). Microorganisms cannot be differentiated on the basis of appearance alone, however the structures in figure 6.2a resemble those seen on the surface of the concrete incubated in the glucose media (figures 4.3 and 6.2b).

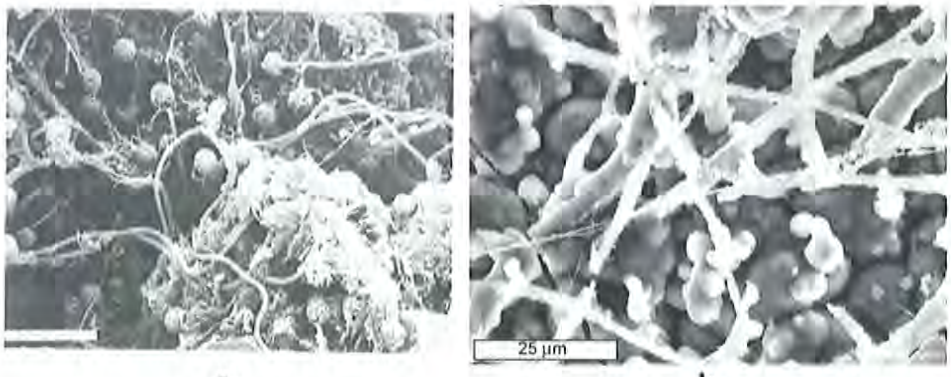

a. b.

Figure 6.2. SEM micrographs of biological material. a) Micrograph of coccoid cyanobacteria. Scale bar = 6 uM (taken from Krumbein, 1983; pg 37). b) Micrographs of biological material growing on the concrete in the glucose media. Both show fibrous material.

When examined under the light microscope (phase microscopy), the culture grown in the glucose media did not show any fungus hyphea or yeast, but they may have been present in the biofilm. Gram staining showed gram negative rods and gram positive cocci. This is a broad study, and thus it was not of interest to know the specific microorganisms within the culture. The micrographs, however, confirm the presence of microbial activity on the concrete surface.

Biofilms are of key importance to the survival of microorganisms on surfaces, especially surfaces in oligotrophic environments subject to desiccation, trapping nutrients and moisture. They also control the $CaCO_3$ dissolution from lime surfaces. Urzi et al. (1991) found that the biodeterioration activity of a strain of *Micrococcus*, isolated from rock surfaces, followed a five step mechanism: i) adhesion, (ii) exopolysachharide formation, (iii) acid production and marble dissolution, (iv) new formation of calcium carbonate deposits at the surface after equilibrium with the surrounding media, (v) patina development and possible intermediate stabilization of crusts with associated dissolution and precipitation of calcite. Marble slabs suspended in media lost 5 percent of their weight within the first 5 to 10 days of incubation. The weight loss stopped after this time, as re-precipitation balanced dissolution. The weight loss was attributable to the pH drop from 7 to 5.3, which dissolved the $CaCO_3$ during the first 5 to 10 days. After that, the pH rose as the organic acids were neutralized by the excess calcium ions from the marble.

In this study, the pH went down immediately within the first 24 hours, but then began to rise again (figure 4.14). It is unknown why there was no evidence of biological activity for the first 20 days of the GC incubation in two of the three replicates for each aggregate type. The initial drop in pH after the media change was most likely the result of biological activity. It is also likely that some sort of succession took place wherein organisms capable of different types of metabolism became dominant after the glucose was depleted (fermentation, nitrification, etc). Such organisms would continue to produce acidic by-products. However, eventually the calcium in solution would neutralize the metabolites, raising the pH. The calcium hydroxide leach front probably advanced most significantly within the first few days following repletion of the media. The thin carbonation zone could be an indicator that acid production, organic and from CO_2, continued as the pH reached more alkaline levels. Microbial adhesion is not sensitive to relatively alkaline pH (8.6) (Fletcher and Floodgate, 1973). Thus alkaline organisms could still inhabit the surface after a rise in pH.

Both the light micrographs (figures 4.6 and 4.7) and the backscatter images (figure 4.8b) of the GC show that the aggregate cement interface is not fully intact and is depleted in calcium (figure 4.8a). Paste has been removed from the interface. The aggregates' microstructure appears unaltered; there is no cracking, nor is there major leaching. Generally, the slag and carbonate interfaces are more heavily affected than the natural gravel's. The calcium hydroxide in the transition zone between the cement and aggregate is generally oriented in the same direction, making it more porous to attacking fluids (De Belie, et al., 1997).

Because of the protective corrosion layer, the rate of calcium ion removal by acid from concrete is inversely proportional to exposure time, following a rate of $1/t$. This layer blocks the diffusion of calcium hydroxide. If the corrosion product layer is removed, the rate of dissolution goes from parabolic to linear, and thus its removal can be more damaging than a stronger acid (Grube and Rechenberg, 1989). Unfortunately, this study provides no information as to the rate this layer grows, or at what depth microorganisms penetrate the surface. Bacteria can solubalize silicate and carbonate minerals. Organic acids could dissolve a layer of siliceous relic, or one of apatite. This layer could also be dissolved by exopolysachharide material, which is also necessary for microbes to attach to surfaces (Allison and Sutherland, 1987). EPS material has been implicated in the weathering of rock material by lichen, in investigations using transmission electron microscope (Barker and Banfield, 1996; Baker and Banfield, 1998). Similar weathering

was seen by microbial mats on rocks in and around a hot spring (Heinen and Lauwers, 1988), as well as in basaltic glass in deep-sea sediments (Staudigel et al, 1995).

The thin-sections made from the concrete in the acetate media are unremarkable compared to those that were in the glucose media (figure 4.11). The hollow cup-like mineral deposits seen in figure 4.4 are faintly seen at the surface of the thin-section. The thick carbonation zone is likely due to being submerged in fluid, open to the atmosphere, in which biological activity was taking place. The aggregate appear unaffected; the surrounding paste is intact and there is no distinctive microcracking in any of the aggregate types. The elemental maps (figure 4.12a) and the backscatter images (figure 4.12b) confirm what is seen in thin-section. The elemental maps show that the hollow round mineral deposits contain phosphate and calcite. Figure 4.13 especially shows how thin this apatite layer is on the AcC surface versus the GC surface.

The delicate white precipitate is the one feature that stands out as unusual on the surface of the AcC. A white precipitate also formed on the surface of concrete in a mixture of lactic and acetic acids. X-ray diffraction confirmed it to be calcium acetate, different calcium acetate hydrates and calcium lactate hydrates (De Belie, *et al.*, 1997). Thus, this precipitate is probably not entirely of biological origin. However, apatite deposits on marble have been attributed to biological activity (Urzi et al, 1999). When the formation of patinas on marble surfaces was simulated in a lab, the phosphorous was sequestered from the media and precipitated as apatite. This did not happen in the abiological controls. Rivadeneyra (1985) reports that if the phosphate concentration is above a critical level, its mineral precipitation by certain soil bacteria will interfere with the calcium carbonate deposition. The presence of phosphate is a likely indicator of biological activity on the surface of the concrete.

The acetate thin-sections show very little damage to the cement paste (as compared to the glucose thin-sections). The contact zone between the apatite/calcite crust does not appear leached in calcium, compared to the glucose map. Urzi et al (1999) report visible degradation at the interface of the marble substratum and biologically precipitated calcite in a patina. Spikey calcite crystals (consistent with marble corrosion) were observed together with small micritic crystals, which the authors determined to be the broken remnants of larger, biologically produced crystals. Such a layer is not observed here. However, some of the deposit in figure 4.4 could be biologically produced calcite. Regardless, bacterial respiration could be indirectly contributing to carbonation, if the CO_2 production is greater than the organic acid production. It would be insightful to know what acids can be produced with acetate as the carbon source.

The average pH levels over the course of the approximately 12-week incubation period did not significantly differ between the acetate and glucose medias. In both cases it took approximately the same amount of time to go from the most acidic point to the most basic (approximately 14 days). What is significant to note is the pH measurement 24 hours after the media change; the glucose solutions contained sufficient biological activity to cause a shift in pH. In contrast there was insufficient biological activity with the acetate carbon source to counteract the calcium donation by the concrete. The degradation of glucose does generate organic acids. Organisms from both create EPS molecules. However, since acetate is a much poorer substrate much less EPS could be produced when acetate is the main carbon source. This

is consistent with what it pictured in figures 4.1 and 4.2. The cylinders in the acetate media exhibited small patches of biological material. This film, though, was much thinner, and covered less area than the film on the cylinders in the glucose media.

The metabolic succession that takes place within microbial habitats could also be an important factor controlling the corrosion mechanisms and rates. A richer media could support biological activity over a longer period of time. In the absence of oxygen (or other electron acceptors, e.g., Mn^{4+}, Fe^{3+}, NO_3^-, SO_4^{2-}, fermentation takes place, which also results in acid production. In fact, acid excretion is enhanced in anoxic or organic-rich, nutrient-poor environments. These conditions may exist in micro-environments, even when the macro conditions may be rich in oxygen and nutrients, if fluid movement to a micro-area is somehow impeded. Thus, possibly the initial pH drop was the result of rapid uptake of nutrients by the biofilm, leading to acid excretory metabolism in their absence. Common acids produced by subsurface microorganisms in a nutrient-limited glucose medium are gluconate, lactate, formate, alpha-keto acid, acetate, butyrate (Ullman et al., 1996).

These results do differ with the study by Zherebytaeva et al. (1991) that concluded that the acid by-products of microbial activity, in the absence of an exogenous sulfur source, were dissolved hydrosilicates from cement paste rather than calcium hydroxide.

In addition to succession, synergism between microorganisms could be a corrosion-controlling factor. Concrete exposed to both *T. intermedius* and the fungus *Fusarium* corroded faster than did concrete exposed only to the bacteria. The authors proposed that this increase was due to the syngeristic relationship of the two organisms: high concentrations of carbon substrate can inhibit the growth of autotrophic bacteria, like *Thiobacillus*, but they can promote the growth of a heterotrophic fungus. Thus, the concrete is corroded by the sulfur oxidizing behavior of the *Thiobacillus* and by the metabolism, and hyphea growth of the fungus (Gu et al., 1998). Thus, it was more practical in this initial study not to use a specific culture.

Concrete that has been only exposed to atmospheric conditions, and no aggressive fluids, generally only has a layer of carbonation 1 to 2 mm thick. The untreated concrete in this study exhibited no abnormalities. As shown in figure 4.5, the hydrated cement paste at the fracture surface appears similar in color to the hydrated cement paste further toward the center of the cylinder. Because the cylinders were in molds in a moist curing room prior to being split, only a thin layer of carbonation developed prior to surface stabilization with epoxy.

6.2. ACIDIC FE(II) OXIDATION INCUBATION

There is little apparent difference between the concrete exposed to the Fe(II) oxidizing *A. ferrooxidans* and the abiotic controls. Generally, the results found here agree with the evidence of crown corrosion and other forms of acid attack. The Fe(II)-oxidizing activity made little difference to the cement, and it did not cause increased calcium sulfide oxidation in the slag. The cement surrounding slag particles turns blue when the calcium sulfide oxidizes. Also, ettringite and portlandite appear recrystallized in the voids (Hammerling, 1999). These artifacts are not seen in any of the concrete exposed to the acidic media, the acidic media with Fe(II)

sulfate, or the acidic media with Fe(II0 sulfate and *Acidthiobacillus ferrooxidans* (thin-section micrographs and back scatter images in Chapter 5 and Appendix.E).

Gypsum ($CaSO_4$) accumulation accompanies corrosion by sulfuric acid. Beldeens et al (2000) observed gypsum precipitation whether the sulfuric acid-attack was biological or abiological. This study did note a difference in the texture between the biological and abiological gypsum deposits, but such a difference (large, rough biotic crystals, versus smaller, smoother abiotic crystals) was not seen in this study. If the gypsum layer was brushed off (in the abiotic tests), the rate of calcium hydroxide leaching became greater. The rate of calcium hydroxide leaching was also greater in the biological versus the abiological tests. The gypsum forms from the calcium carbonate, calcium oxide, and calcium hydroxide in the cement, with the sulfur in the acid. Acid producing microorganisms can function deep within this layer, continuing the corrosion behind the gypsum layer (Islander et al., 1991). Possibly, if this study were carried out for a long enough period of time, the biological corrosion rate would petrographically appear significantly greater than the abiotic mechanisms.

The studies cited in this thesis regarding biological sulfuric acid production on concrete did not discuss the petrography of the concrete. It is discussed in other studies of acid attack, though. Similar petrographic features are seen between the AFB concrete and those described in the acid attack on concrete literature. HCl produces three distinctive layers on the surfaces of cement mortar in a study by Chandra (1988). The outer layer was a corrosion zone of siliceous relic, followed by a brown layer of ferric and aluminum hydroxides abutted against an inner undisturbed zone. As HCl attacks the cement minerals, it forms calcium salts, which are soluble and leach out of the cement. This loss of calcium hydroxide to the surrounding solution increases porosity of the cement, as well as increasing the pH of the attacking acid. As hydrolysis resumes, Si, Al, and Fe gels are produced, which can protect the underlying cement. Ceukelaire (1992) noted similar zoning. A similar Fe gel band can be seen in all of the thin-sections of the sulfuric acid attacked concrete in this study.

CHAPTER 7 – CONCLUSIONS AND FUTURE DIRECTIONS

The bullet points below summarize the main findings of the work presented in this study.

- The concrete incubated in the glucose media showed signs of calcium hydroxide leaching from the cement paste in light-micrographs, elemental maps, and backscatter images.
- The appearance of the glucose media incubated concrete is similar to those seen in the literature of acid attack of concrete.
- The concrete incubated in the acetate media did not show signs of calcium hydroxide leaching.
- The pH dropped in the glucose media 24 hours after being refreshed; this same pH drop did not occur in the acetate media. This finding, along with the appearance of abundant organic material in the glucose media and on those cylinders (as well as an unpleasant odor), support the conclusion that more intense biological activity took place in the glucose media.
- The surface of the acetate media incubated concrete was covered in a white, precipitated mineral, which X-ray diffraction confirmed to be hydroxy apatite.
- All three replicates for each aggregate type followed a similar pH trend.
- The concrete of all three of the aggregate types had a similar petrographic appearance.
- Concrete exposed to *A. ferrooxidans* weathered similarly to that exposed only to the acidic media. This corrosion was consistent with the literature on chemical and biological acid attack.
- Of the concrete exposed to the acidic *A. ferrooxidans* media, the blast furnace slag and limestone aggregates appeared to be more susceptible to the acid attack than did the natural gravel. However, the concrete made with these aggregates exhibited no other abnormalities.

The concrete incubated in the glucose media was petrographically similar to concrete weathered by acid. Both have zones leached of calcium hydroxide. It is highly possible that the organic material on the concrete surface concentrated organic acids (and CO_2). Also, the extra-cellular polysaccharide material, as well as other constituents of biological membranes and cell walls, could have contributed to the calcium hydroxide leaching. The fact that similar leaching was not seen in the acetate media incubated concrete points to either the lower levels of biological activity with the poorer carbon source, or some other chemical difference between the two solutions. Likely, both biological and abiological factors were at work.

Damage to concrete microstructure is most often attributed to causes such as sulfate attack, alkali-silica reactivity, and freeze-thaw action. Increased porosity can speed the damage caused by these factors. Thus the corrosive activity of bacteria may speed the concrete's demise by more rapidly increasing the porosity. The leaching seen in the glucose incubation is evidence that such action can occur in the presence of bacteria, by some combination of the mechanisms explained above. It would be site specific as to whether bacteria could turn over enough organic matter to produce a sufficient amount of these substances to be the principle cause of the concrete degradation. Given the ubiquity of concrete in natural environments, evidence of microbiological activity would be seen very often on concrete recovered from the field if it were the principle agent of corrosion. However, microbes must not be overlooked, as biochemical reactions usually occur faster than their purely chemical counterparts. Studies by Hiebert and Behnett (1992) and Callot et al. (1987) found that presence of surface adhering microorganisms increased the rate of dissolution of silicate minerals over abiotic mechanisms. Thus, studies should be done to estimate the rate of corrosion by biological vs. purely chemical means.

The slag coarse aggregate was suspected to contribute to the early deterioration of sections of pavement on US-23 south of Flint Michigan. Study of this concrete in thin section revealed alkali-silica reactive chert particles within the fine aggregate. The concrete also exhibited secondary mineral formation of ettringite, which can form from the dissolution of calcium sulfide. Alkali and sulfate levels in the concrete were both higher in the deteriorated sections of the concrete than the unaffected areas. The authors proposed that the higher alkaline levels in the pore water increased the solubility of the calcium sulfide in the slag. Therefore, the attack on this concrete was due to both ASR and sulfate attack (Peterson et al., 2002). The thin sections from this pavement do not resemble the thin sections of the current study. There is no evidence from this study that microbiological activity will directly lead to early failure in concrete, whether or not blast-furnace slag coarse aggregate was used.

There is no evidence from this study that the acidophilic *A. thiobaciluus* acts on concrete any differently from other *Thiobacillus* microorganisms. Additionally, more highly controlled studies should be done to determine if the rate of slag aggregate weathering is significantly faster than for limestone or natural gravel. The petrographic evidence of this study suggests that slag and limestone are more weathered in the sulfuric acid than the natural gravel. However, the concrete made with slag aggregate exhibits no other apparent abnormalities.

The results detailed here lay groundwork for future study. Studies of the rate of attack should be done. Such studies could be based on weight, analysis of the bulk solution, or careful measurements from thin sections. The rate likely depends on, among other things, where microbial activity is located (i.e., in front of or behind the protective layer) and the type of conditions available for microbial activity (i.e., aerobic, anaerobic, nutrient rich, nutrient poor, etc.). Allison and Sutherland (1984) report on a simple staining technique that, when used in conjunction with a chemical assay, makes the association of polysaccharide material with adhering bacteria visible by light microscope. The bacteria observed in this study had adhered to microscope slides. Cement or concrete could be made into thin sections (without the fluorescent epoxy) and then inoculated with bacteria. After an elapsed period of time, the thin sections could be stained, and the adherence of the polysaccharide observed. Certain heavy metal stains could be similarly used for SEM observation (Fletcher and Floodgate, 1973). Similar staining

techniques were usually successfully by Urzi et al. (1991) to study biodeterioration on thin marble slabs (2mm). This technique could show where biological material is concentrated. Inoculating thin sections could also be a simple method to determine the rate of corrosion. Alternatively, cement mortar samples, of carefully controlled weights, could be used to find the rate at which material is lost due to microbiological activity. It would be most insightful to do these studies in a flow-through reactor.

Future studies on microbe/concrete interactions should also analyze concrete in the field by analyzing the pore water that passes through the concrete, as well as the nutrient content of the surrounding soil. "Clean-microcosms", as described by Bennett (1996) could be set up to measure the rate of attack in the field. Other factors that should be investigated might include the impact that chemical admixtures (e.g. air entrainers, water reducers, etc.) and membrane forming curing compounds might have on the promotion of microbiological activity in concrete. Further, many biodegradable deicers have a very nutrient rich composition that might promote microbiological growth, and should therefore be investigated.

REFERENCES

Aono, R., K. Horikoshi, S. Goto (1984) Composition of the peptidoglycan of alkalophilic Bacillus spp. *Journal of Bacteriology*, 157:688-689.

Aono, R., K. Horikoshi (1983) Chemical composition of cell walls of alkalophilic strains of Bacillus. *Journal of General Microbiology*, 129:1083-1087.

Aono, R., Sanada, K. (1994) Hyper-autolysis of the facultative alkaliphilic *Bacillus* sp. C-125 cells grown at neutral pH: culture-pH dependent cross-linking of the peptide moieties of the peptidoglycan. *Bioscience, Biotechnology, and Biochemistry*, 58:2015-2019.

Aono, R, T. Sanada, K. Horikoshi. (1996) Purification and characterization of cell wall-associated N-acetylmuramyl- L-alanine amidase from alkaliphilic Bacillus lentus C-125. *Bioscience, Biotechnology, and Biochemistry*, 60:1140-5.

Barker, W.W., J.F. Banfield. (1998) Zones of chemical and physical interaction at the interface between microbial communities and minerals: a model. *Geomicrobiology Journal*, 15(3):223-244

Barker, W.W., J.F. Banfield. (1996) Biologically versus inorganically mediated weathering reactions: relationships between minerals and extracellular microbial polymers in lithobiontic communities. *Chemical Geology*, 132:55-69.

Beeldens, A. *et al.* (2001) The influence of biochemical and chemical sulfuric acid corrosion on the micro-structure of polymer modified mortar and concrete. *Proceedings of the 8th Euroseminar on Microscopy Applied to Building Materials*, 61-67.

Bennett, P.C., M.E. Melcer, D.L. Siegel, J.P. Hassett.(1988) The dissolution of quartz in dilute aqueous solutions of organic acids at 25°C. *Geochimica et Cosmochimica Acta*, 52:1521-1530.

Bennett, P.C., F.K. Hiebert, W.J. Choi. (1996) Microbial colonization and weathering of silicates in a petroleum-contaminated groundwater. *Chemical Geology*, 132:45-53.

Callot, G., M. Maurette, L. Pottier, A. Dubois. (1987) Biogenic etching of microfractures in amorphous and crystalline silicates. *Nature*, 328:147-149.

Casanova, I., L. Agullo, A. Aguado. (1996) Aggregate expansivity due to sulfide oxidation –I. Reaction system and rate model. *Cement and Concrete Research*. 26:993-998.

Chandra, S. (1988) Hydrochloric Acid Attack. *Cement and Concrete Research*, 18:193-203.

Coleman, R.N., I.D. Gaudet. (1993) *Thiobacillus neopolitanus* implicated in the degradation of concrete tanks used for potable water storage. *Water Research*, 27:413-418.

Duff, R.B., D.M. Webley, R.O. Scott. (1963) Solubilization of mineral and related materials by 2-ketogluconic acid producing bacteria. *Soil Science*, 95:105-114.

Ehrlich, H.L. (2000) *Geomicrobiology*. New York : Marcel Dekker, Inc, pp 239-245, 184-218, 350-364.

Everett, L.H., W. Gutt. (1967) Steel in concrete with blastfurnace slag. *Magazine of Concrete Research*, 19:83-94.

Grube, H., W. Rechenberg. (1989) Durability of Concrete Structures in Acidic Waters. *Cement and Concrete Research*, 19:738-792.

Gutt, W., W. Kinniburgh, A.J. Newman. (1967) Blastfurnace slag as aggregate in concrete. *Magazine of Concrete Research*, 19:71-82.

Hammerling, D. (1999) *Calcium Sulfide in BlastFurnace Slag Used as Concrete Aggregate.* M.S. Thesis, Michigan Technological University.

Heinen, W., A.M. Lauwers. (1988) Leaching of silica and uranium and other quantitative aspects of the lithobiotic colonization in a radioactive thermal spring. *Microbial Ecology*, 15:135-149.

Horikoshi, K. (1971) production of alkaline enzymes by alkaliphilic microorganisms. Part I. Alkaline protease produced by *Bacillus* No. 221. *Agricultural Biological Chemistry*, 36:1407-1414.

Horikoshi, K., (1998) Alkaliphiles. In Horikoshi, K. (ed): *Extremophiles; Microbial Life in Extreme Environments*. New York: Wiley-Liss, pp. 155-57.

Islander, J., *et al.* (1991) Microbiol ecology of crown corrosion in sewers. *Journal of Environmental Engineering*, 117:751-770.

Ivey, D.M., A.A. Guffanti, T.A. Krulwich. (1993) The Na^+ cycle of alkaliphilic *Bacillus* species. In Bakker, E.P. (ed): *Alkaline Cation Transport Systems*. Boca Raton, FL: CRC Press, pp. 101-124.

Jones, D.W., M.J. Wilson, W.J. McHardy. (1981) Lichen weathering of rock forming- minerals: Applications of scanning-electron microscopy and microprobe analysis. *Journal of Microscopy*, 124:95-104.

Karlsson, S., *et al.* (1988) Identification and characterization of alkali-tolerant clostridia isolated from biodeteriorated casein-containing building materials. *Applied Microbiology and Biotechnology*, 28, p. 305-310.

Kitada, M., M. Hashimoto, T. Kudo, K. Horikoshi. (1994) Properties of two different Na super(+)/H super(+) antiport systems in alkaliphilic Bacillus sp. strain C-125. *Journal of Bacteriology*, 176:6464-6469.

Koelliker, E. 1965. *Cement and Concrete Research*. 15, 100

Krumbein, W.E. (1983) *Microbial Geochemistry*. Oxford: Blackwell Scientific Publications.

Lauwers, A.M., W. Heinen (1974) Bio-degradation and utilization of silica and quartz. *Archives of Microbiology*, 95:67-78.

Lea, F.M. (1970) *The Chemistry of Cement and Concrete, 3rd edition*. London: Edward Arnold (Publishers) LTD, pp. 647-650.

Maeda, T., *et al.* (1999) Isolation of iron-oxidizing bacteria from corroded concretes of sewage treatment plants. *Journal of Bioscience and Bioengineering*, 88:300-305.

Milde, K., *et al.* (1983) *Thiobacilli* of the corroded concrete walls of the Hamburg sewer system. *Journal of General Microbiology*, 129:1327-1333.

Mindess, S., F. Young and D. Darwin. (2003) *Concrete*. Upper Saddle River, NJ: Prentice Hall, 644 pp.

Parker, C.D. (1945) The Corrosion of Concrete. *The Austrailian Journal of Experimental Biology and Medical Science*. 23:81-98.

Parker, T.W. (1960). An unusual form of unsoundness in slag concrete.

Pavlik, V. (1994). Corrosion of Hardened Cement Paste by Acetic and Nitric Acids; Part II: Formation and Chemical Composition of the Corrosion Products Layer. *Cement and Concrete Research*, 24:1495-1508.

Ramakrishnan *et al,* (2002) Performance of bacterial cement mortar. *Proceedings of the 22nd International Conference on Cement Microscopy, San Diego CA.*, pp. 293-305.

Rivadeneyra, M.A., R. Delgado, E. Quesada, A. Ramos-Cormenzana. (1991) Bacterial precipitation of calcium carbonate in presence of phosphate. *Soil Biology and Biochemistry*, 17:171-172.

Rogers, R.D., M.A. Hamilton, J.W. McConnell (1993). Microbial-Influenced Cement Degradation; Literature Review. Prepared for: Division of Regulatory Applications, Office of Nuclear Regulatory Research.

Sand, W. (1987) Importance of hydrogen sulfide, thiosulfate, and methylmercaptan for growth of *Thiobacilli* during simulation of concrete corrosion. *Applied and Environmental Microbiology*, 53:7 p. 1645-1648.

St. John, D.A., A.W. Poole, I. Sims. (1998) *Concrete Petrography: a Handbook of Investigative Techniques*. London: Arnold Publishers, pp. 273.

Staudigel, H., R.A. Chastain, A. Yayanos, W. Bourcier. (1995) Biologically mediated dissolution of glass. *Chemical Geology*, 126:147-154.

Stocks-Fischer, S., K. Galinat, S.S. Bang. (1999) Microbiological precipitation of $CaCO_3$. *Soil Biology and Biochemistry*, 31:1563-1571.

Ullman, W.J., D.L. Kirchman, S.A. Welch, P. Vandevivere. (1996) Laboratory evidence for microbially mediated silicate mineral dissolution in nature. *Chemical Geology*, 132:11-17

Urzi, C., M. Garcia-Valles, M. Vendrell, A. Pernice. (1999) Biomineralization processes on rock and monument surfaces observed in field and in laboratory conditions. *Geomicrobiology Journal*, 16:39-54.

Urzi, C., S. Lisi, G. Criseo, A. Pernice. (1991) Adhesion to and degradation of marble by a *Micrococcus* strain isolated from it. *Geomicrobiology Journal*, 9:81-90.

Vandevivere, P., S.A. Welch, W.J. Ullman, D.L. Kirchman. (1994) Enhanced dissolution of silicate minerals by bacteria at near-neutral pH *Microbial Ecology*, 27:241-251.

Vincke, E., *et al.* (2000) Recent developments in biogenic sulfuric acid attack on concrete, in Lens, P., P. Pol (eds): *Environmental Technologies to Treat Sulfur Pollution*. London: IWA Publishing, pp.515-543.

Walker, H.N., B.F. Marshall (1979) Methods and equipment used in preparing and examining fluorescent ultrathin sections of Portland cement. *ASTM*

Welch, S.A., W.J. Ullman. (1993) The effects of organic acids on on plagioclase dissolution rates and stoichiometry. *Geochmica et Cosmochimia Acta*, 57:2725-2736.

Webley, D.M., M.E.F. Henderson, W.A. Mitchell. (1960) A plate method for studying the breakdown of synthetic and natural silicates by soil bacteria. *Nature*, 188:766-767.

Zherebyateva, T.V., E.V. Lebedeva, G.I. Karavaiko. (1991) Microbiological Corrosion of Concrete Structures of Hydraulic Facilities. *Geomicrobiology Journal*, 9:119-127.

Appendix A: Materials Testing Procedures

A.1: Coarse Aggregate

Summary of ASTM C127

Prior to testing, aggregate stockpile has been stored in 5-gallon buckets topped off with water.

1) Pour aggregate into #8 sieve over sink, and then transfer from sieve to a towel.
2) Stir rocks until saturated surface dry (SSD), with towel
3) Divide the rocks into three piles
4) Weigh the three piles in the submerged weight balance
5) Put rocks back into pans and put them into the oven at 100°C.
6) Remove the aggregate 24 hours later; let sit for an hour and then weigh

Example: Slag (weight in grams)

Trial	1	2	3
(a) SSD Weight	2989.9	2953.7	3289.9
(b) Immersed Weight	1732.1	1711.1	1907.2
(c) Pan + Rocks Weight	3921.6	3473.5	4749.4
(d) Pan Weight	1017.9	590.1	1547.1
(e) Dry Weight (d-c)	2903.7	2883.4	3202.3
(f) Adsorption (a-e)	86.2	70.3	87.6
(g) % Adsorption ((f/e) *100)	2.97	2.44	2.74
(h) Bulk SPG (e/(a-b))	2.31	2.32	2.32
(i) Apparent SPG (e/(e-b))	2.48	2.46	2.47

A.2: Fine Aggregate

Summary of ASTM C128

Prior to testing, sand stockpile has been stored in 5-gallon buckets topped off with water.

1) Put sand into pycnometers (pycs), then rinse the pycs into pan
2) Refill the pycs to line with water and weigh them
3) Get the sand SSD with a heat lamp
4) Get weight for the empty pycs, the pycnometers filled with SSD sand, and then the pycs with the sand and water
5) Agitate the pyc to get all of the air out of the sand, dip a paper towel in to get rid of bubbles.
6) Put the sand in a pan and then put the pan in the oven at 100°C.
7) Remove sand 24 hours later; let sit for an hour and then weigh.

Worksheet for sand (weight in grams)

Trial	1	2	3
(a) Pycnometer (pyc.) weight	208.6	209.3	224.7
(b) Pyc. weight + sand	743.1	710.7	769.8
(c) Pyc. Weight + sand + water	1042.3	1022.0	1065.4
(d) Pyc. Weight + water, no sand	702.9	704.4	718.3
(e) Oven dried sand + pan	1551.0	1086.8	755.4
(f) Pan weight	1020.9	589.9	212.8
(g) Oven dry sand weight (e-f)	530.1	496.9	542.6
(h) SSD weight	534.5	501.4	545.1
(i) Adsorption (h-g)	4.4	4.5	2.5
(j) % Adsorption ((i/g)*100)	0.83	0.91	0.46
(k) Bulk SPG	2.74	2.73	2.75
(l) Apparent SPG	2.78	2.77	2.78

Appendix B: Concrete Mix Procedure

Example of the worksheet used to determine the concrete mix using the carbonate aggregate.

B.1: Coarse Aggregate Worksheet (in preparation for mix day)

1) Thoroughly mix the aggregate stockpile.

2) Fill in the required kg of dry coarse aggregate (from mix design)
(a) 34.13 kg

3) Estimate the moisture in the stockpile (usually between 0.5 to 1.0%, the true moisture value will be determined later).
(b) 0.6%

4) Determine mass of "moist" coarse aggregate needed from stockpile based on estimation (b).
(c) = -a/((b/100)-1) = 34.34

5) Prepare coarse aggregate for mixing the next day: split the value from "c" between two buckets, weigh them, and then top the buckets off with water and cover them securely (with lids in which small holes have been drilled). **The wet weights will be determined the following day**.

	Bucket Weight	kg Moist (including bucket)	kg Wet (including bucket)
Bucket 1	0.825	17.995	17.785
Bucket 2	1.000	18.17	18.990
Sum	**(d)** 1.825	**(e)** 36.165	**(f)** 37.775
		(g) 34.34	**(h)** 35.95
		g = (e-d) = c	**h = (f-d)**

6) Prepare coarse aggregate for a "butter batch" by filling a bucket with half of the value listed for **(c)**. After weighing, top off the bucket with water and cover with a hole-punched top.

kg Bucket Weight	kg Moist (including bucket)
(i) 0.985	**(j)** 5.380
	(k) 4.395
	k = (j-i) = c/2

7) Determine true moisture value by drying a ~3 kg sample of stockpile coarse aggregate in an oven at 100°C overnight. Re-weigh the following day.

Pan Weight (g)	g Moist (including pan)	g Dry (including pan)
(m) 573.4	(n) 2570.4	(o) 2569.7
	(p) 1997	(q) 1996.3
	p = (n-m)	q = (o-m)

Percent Moisture: **(r) = ((p-q)/q)*100 = 0.04%**

B.2: Fine Aggregate Worksheet (in preparation for mix day)

1) Thoroughly mix the stockpile.

2) Fill three to four buckets with sand from the stockpile, and then transfer the buckets into the cement mixer. With the cement mixer mixing, spray sand with water, making it SLIGHTLY damp. Mix for 10 to 20 minutes.

3) Transfer the sand back to the buckets and cover tightly.

4) Determine the moisture in the sand by taking a representative ~1 kg sample from the buckets in step 3, and drying it in a 100°C oven overnight.

Pan Weight (g)	g Moist (including pan)	g Dry (including pan)
(a) 590.5	(b) 1761.6	(c) 1743.0
	(d) 1171.4	(e) 1152.8
	d = (b-a)	e = (c-a)

Percent Moisture: **(f) = ((d-e)/e)*100 = 1.61%**

B.3: Mix Day

1) Fill in the required weight of the dry fine aggregate from the mix design:
(g) = 34.12

2) Determine the weight of moist sand required for the concrete batch, and fill several buckets with exactly that amount (h) (tightly seal buckets to prevent moisture loss):
(h) = -g/((f/100)-1) = 34.68

3) Determine the weight of the moist sand required for a butter batch. Prepare a bucket to contain that exact weight of sand (i):
(i) = h/2 = 4.46

4) Determine the SSD weight of the sand (use the %absorption value for the sand).
(j) 0.73% (from previous tests)
(k) = g + ((g*j)/100) = 34.37

6) Determine the amount of free water from the moist sand:
(m) = h-k = 0.31

7) Overturn the two buckets containing the coarse aggregate, and the butter bucket containing the coarse aggregate, and allow the water to drain through the small holes drilled in the lids. Allow for about ½ hour of draining, agitating the bucket periodically.

8) After draining, weight the buckets, and finish filling out the tables from steps 5 and 6.

9) Determine the dry weight of the aggregate (the value should be +/- 1 kg of (a)).
(s) = g – (g*r)/100 = a = 34.33

10) Determine the SSD weight of the aggregate (using the %absorption value previously determined):
(t) = 2.31% (absorption value for aggregate, previously determined)
(u) SSD weight u = ((t*s)/100) + s = 35.12

11) Determine the amount of water absorbed by the aggregate
(v) = u-g = 0.78

12) Determine the amount of free water from the wet coarse aggregate
(w) = h-u-v = 0.78

13) Put the lids back on the buckets.

15) Calculate the amount of water needed to make the concrete batch

(a) kg of free water from the mix design = 6.58

(b) kg of water needed for the concrete batch, after correcting for free water from the sand & rock

b = a – w – m = 6.58- 1.05- 0.24

w is from the coarse aggregate worksheet

m is from the fine aggregate worksheet

16) Calculate the amount of water you will need to make the butter batch

c = b/2

17) Dampen the interiors of containers that will be used to weigh the mix water, and tare the containers in their dampened state. Then weigh out the amount of water needed.

18) Weigh out the amount of cement powder needed from the mix design

(d)= 11.96

19) Weigh out the amount of cement powder needed for the butter batch

(e) = 1.54 = 11.96/7.77; (11.96*0.162)

20) Determine the amount of air-entrainer needed for the concrete batch, and add this amount to the mix water:

(f) = (25*d)/45 = 6.64

21) Determine the amount of air-entrainer needed for the butter batch, and add this amount to the mix water

(g) = f/2 = 0.86 = 6.64/7.77

22) Make the butter batch first. Start the mixer, add the coarse aggregate to the mixer first, then the fine aggregate, then the cement, and finally the water. Mix for 2 minutes. Allow the mixer to rest for 3 minutes, and then mix again for another 3 minutes.

23) Make the cylinders.

Appendix C. Acetate and Glucose Media Incubations

Concrete subjected to the same treatment had a similar appearance post-incubation regardless of the aggregate type. This appendix contains the images of the other two aggregate types that were not highlighted in chapter 4.

a.

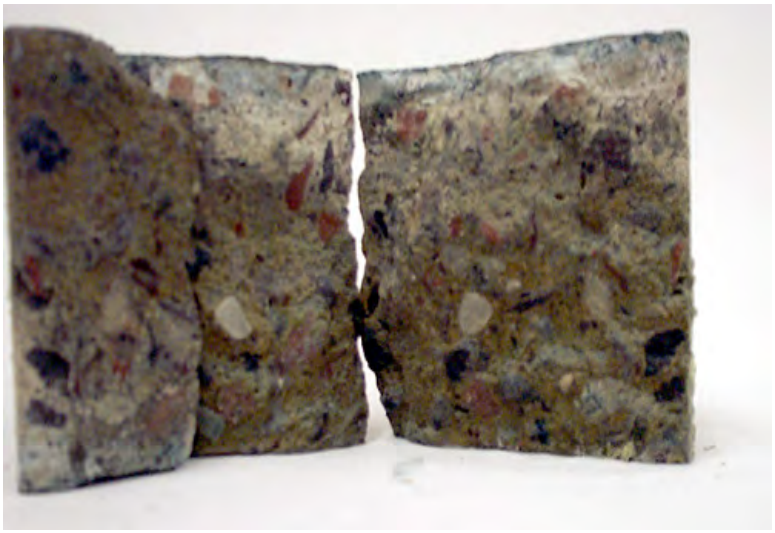

b.

Figure C.1. GC Cylinders. Corresponds to figure 4.1a. a) carbonate aggregate, b) natural gravel aggregate.

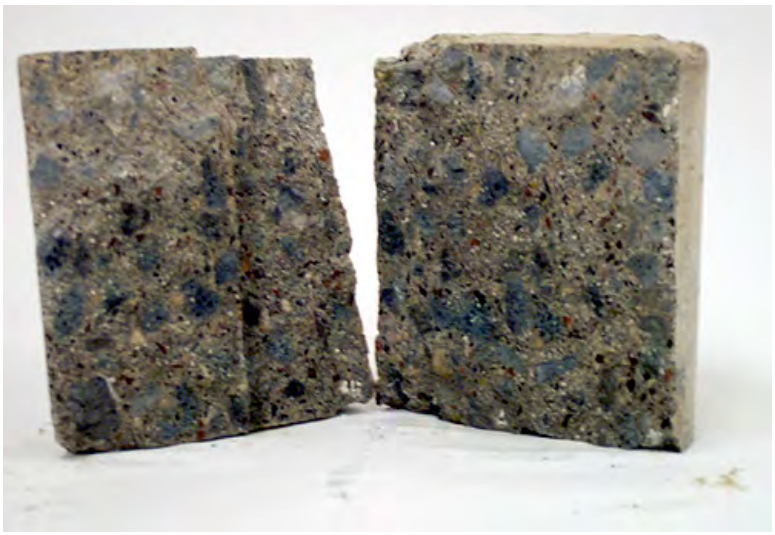

a.

b.

Figure C.2. AcC Cylinders. Corresponds to figure 4.1b. a) slag aggregate, b) natural gravel aggregate.

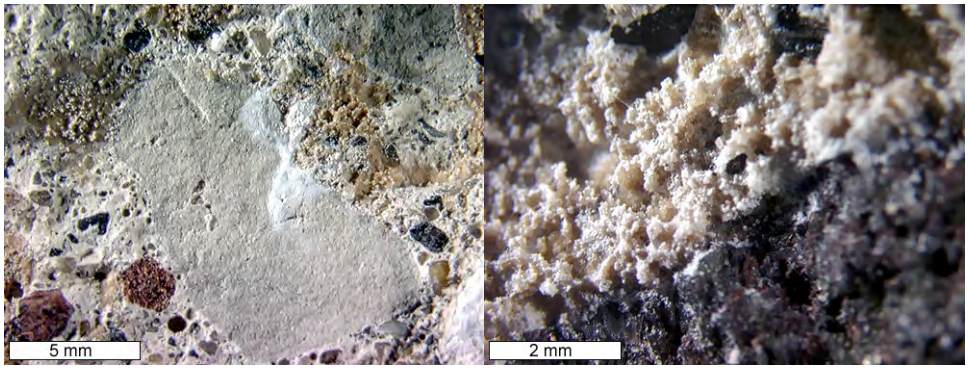

a.

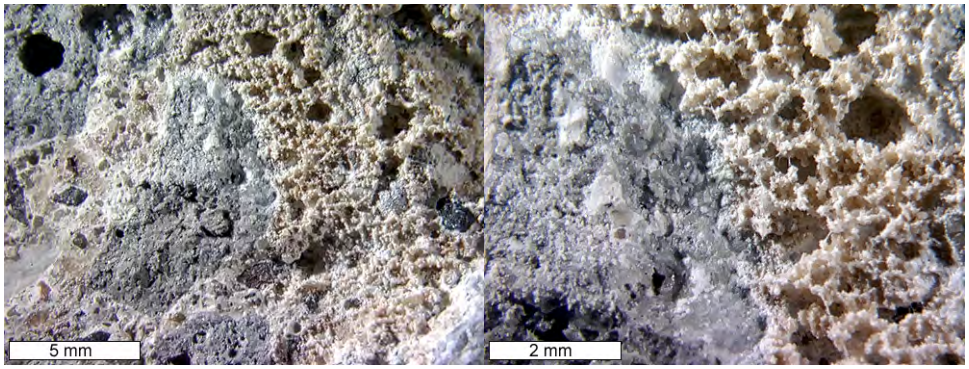

b.

Figure C.3. Magnified Images of the Surface of the GC. Corresponds to figure 4.2a, a) carbonate aggregate, b) slag aggregate.

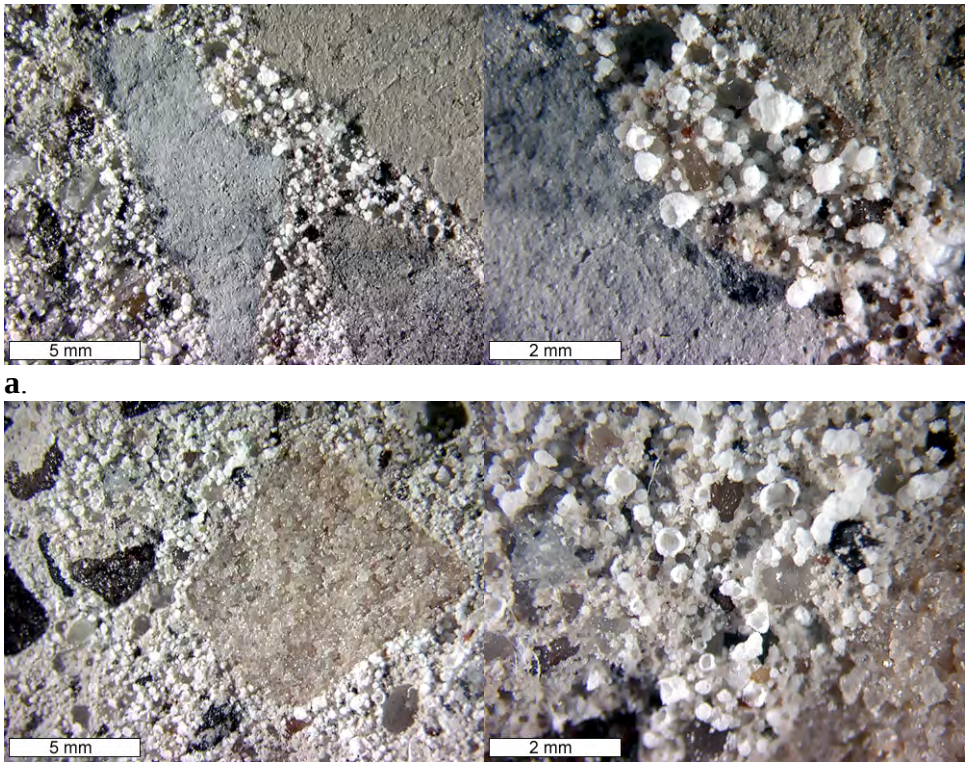

a.

b.

Figure C.4. Magnified Images of the Surface of the AcC. Corresponds to figure 4.2b, a) carbonate aggregate, b) natural gravel aggregate.

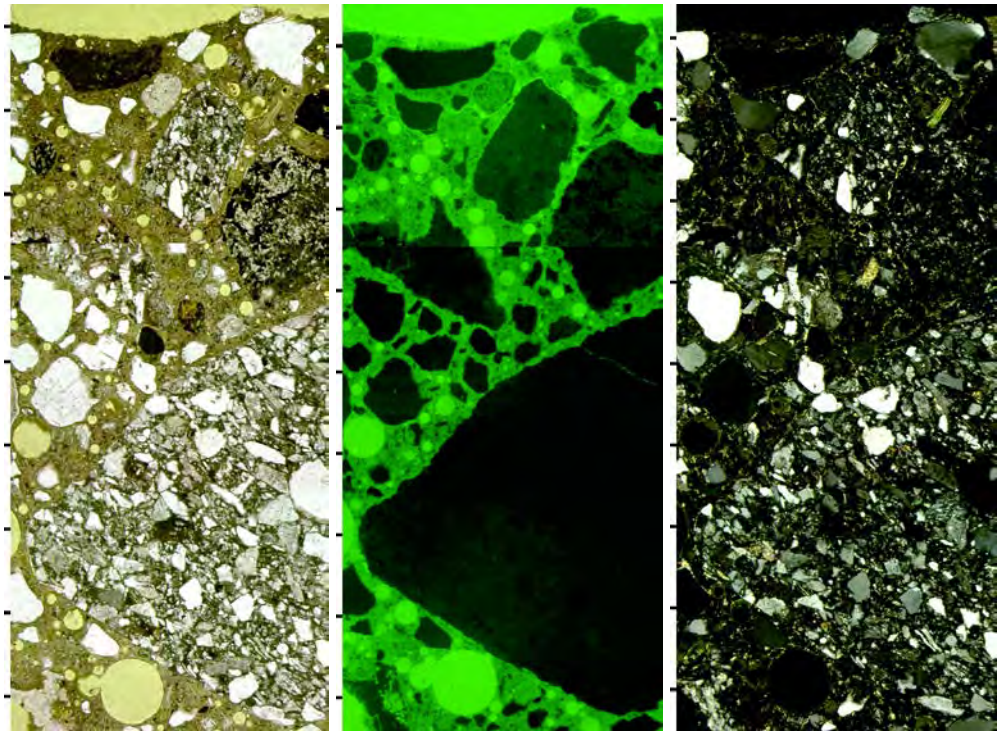

a.

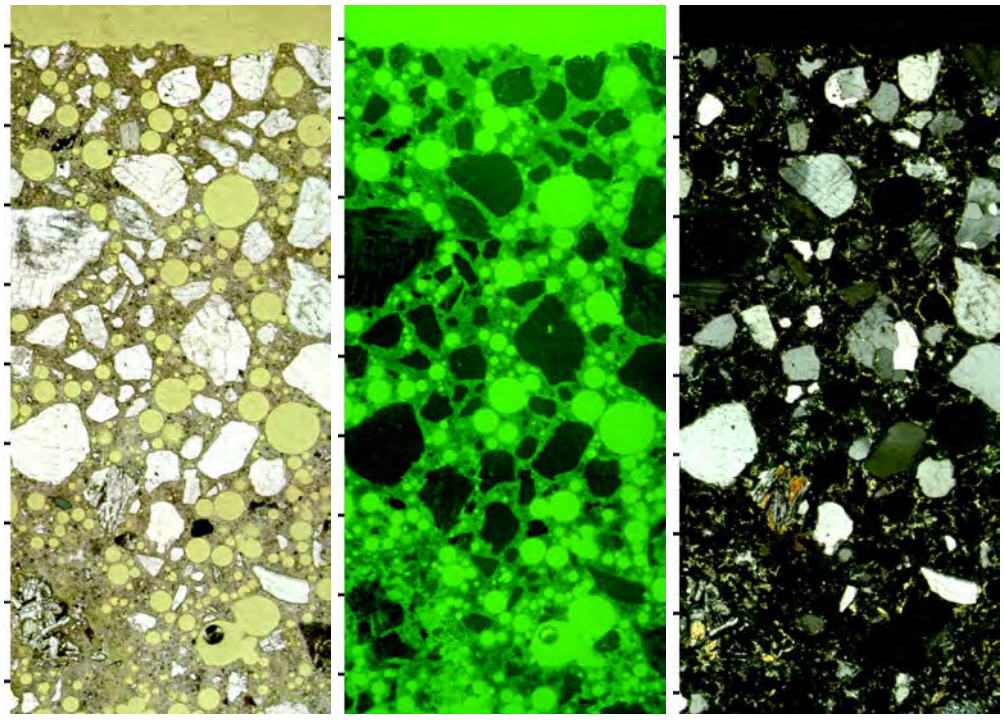

b.

Figure C.5. Thin-sections of the Control Cylinders. Corresponds to figure 4.5, a) carbonate aggregate, b) natural gravel aggregate.

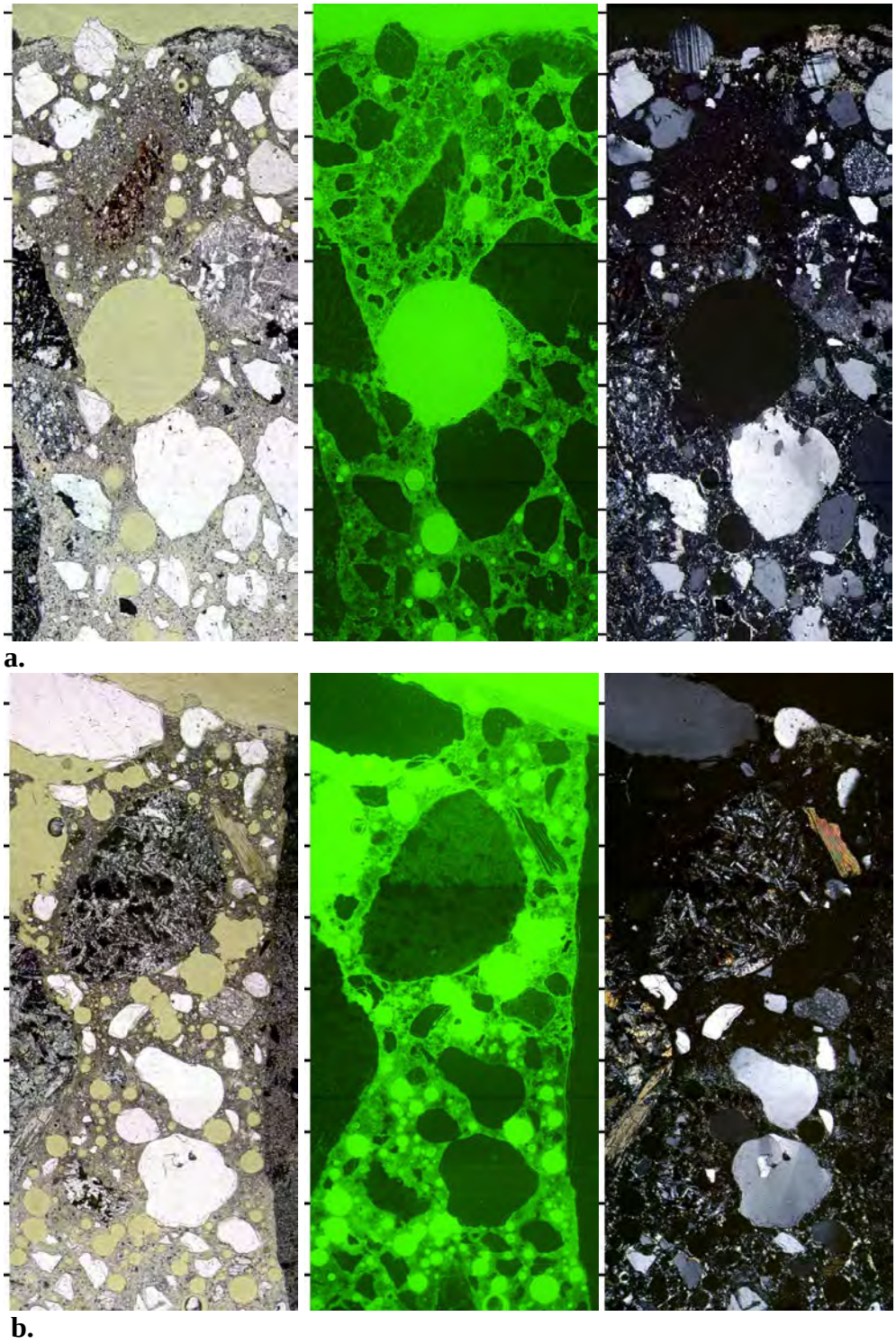

a.

b.

Figure C.6. Petrographic Thin-Sections of the GC Fracture Surface. Corresponds to figure 4.6, a) slag aggregate, b) natural gravel aggregate.

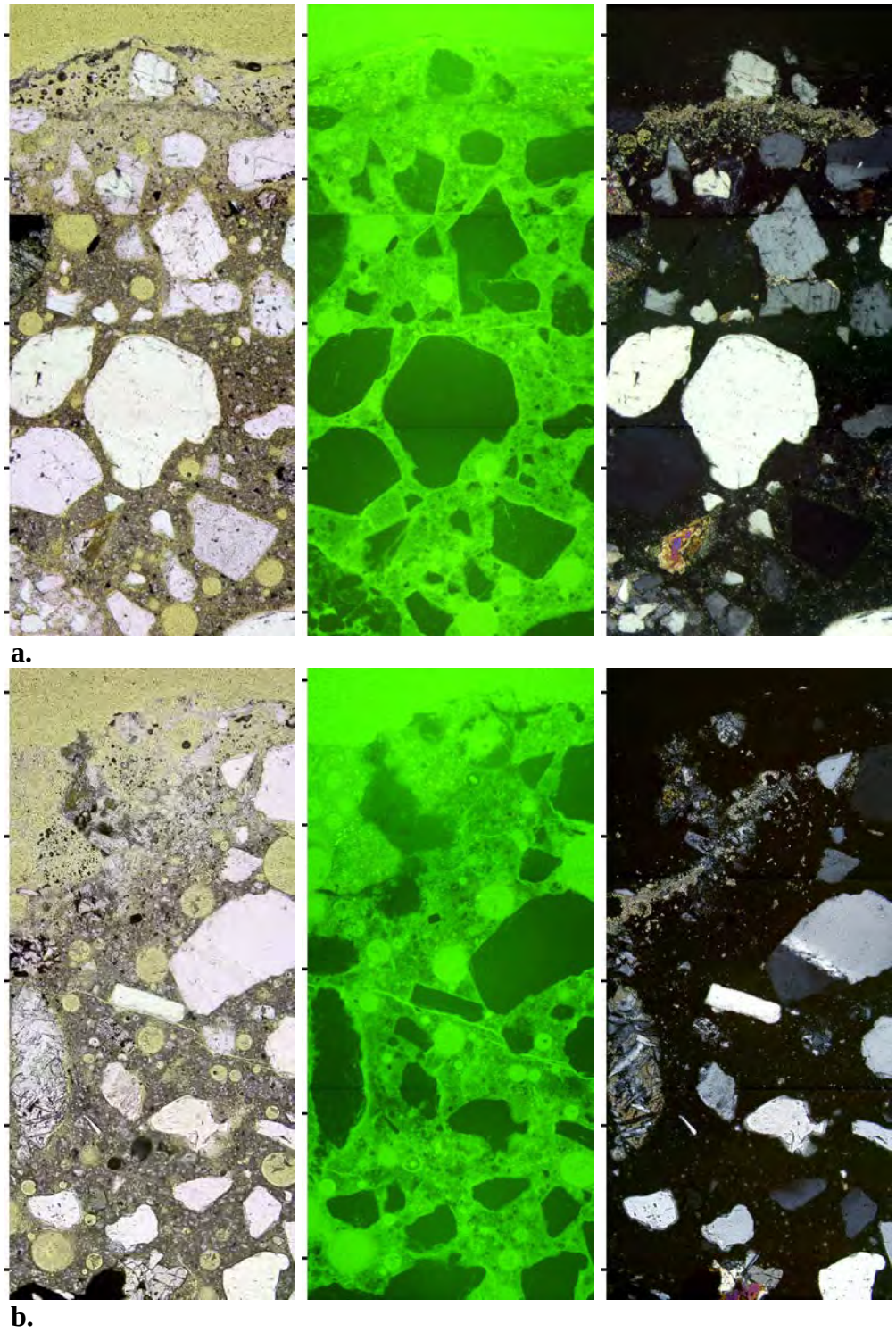

Figure C.7. Detailed Image of the GC. Corresponds to figure 4.7, a) carbonate aggregate, b) natural gravel aggregate.

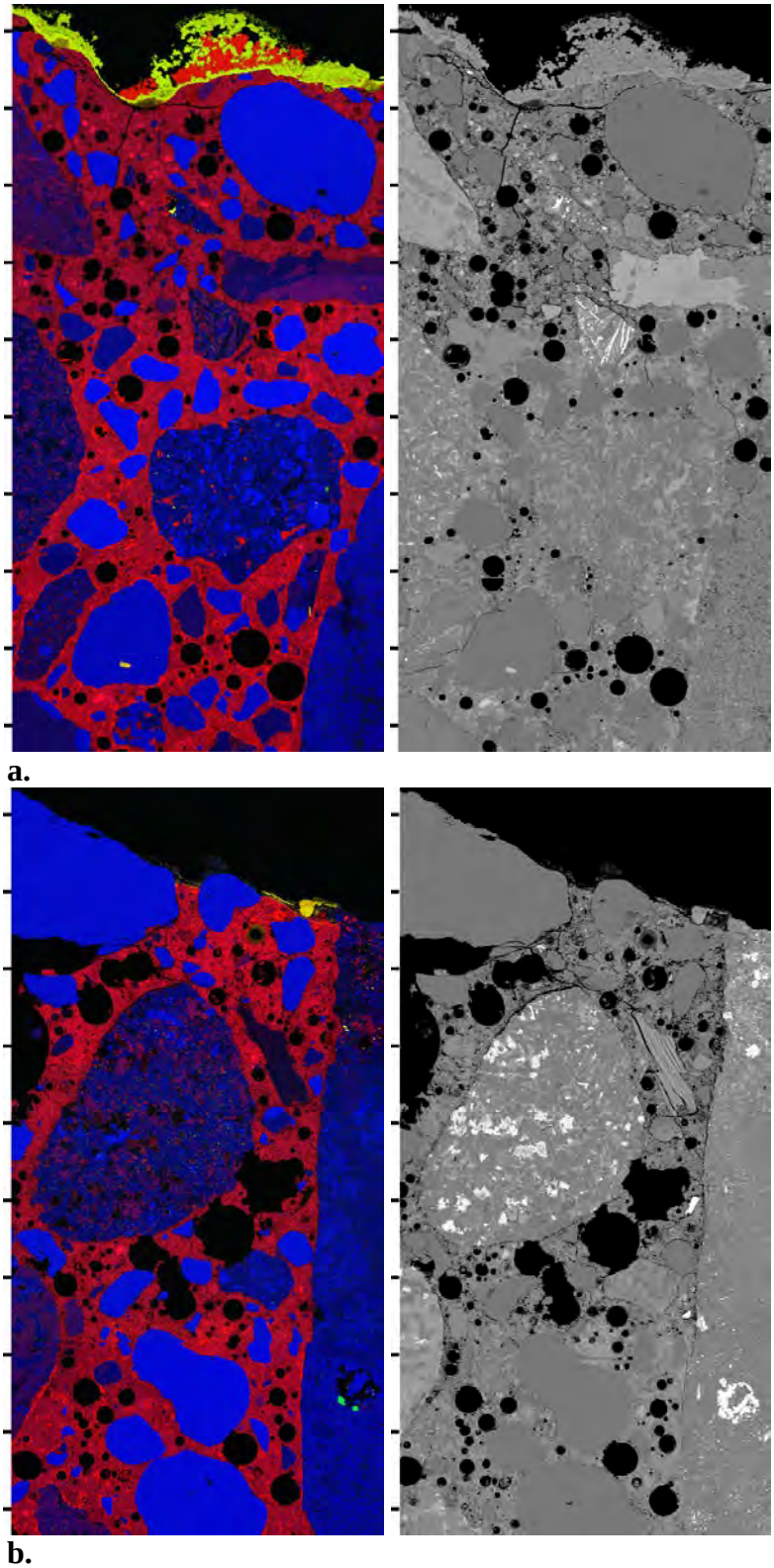

a.

b.

Figure C.8. X-Ray Energy Maps of the GC. Corresponds to figure 4.8, a) carbonate aggregate, b) natural gravel aggregate.

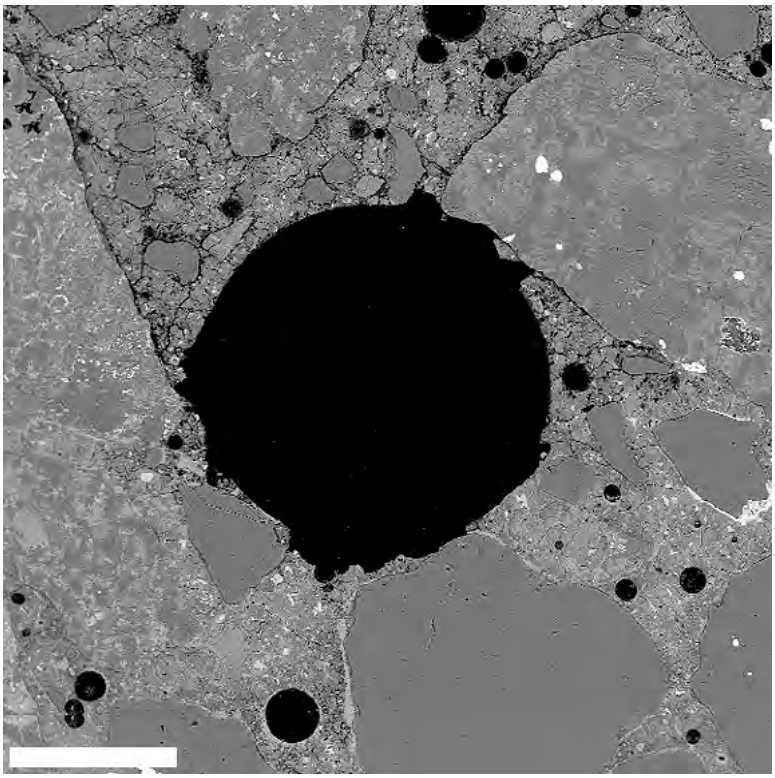

a.

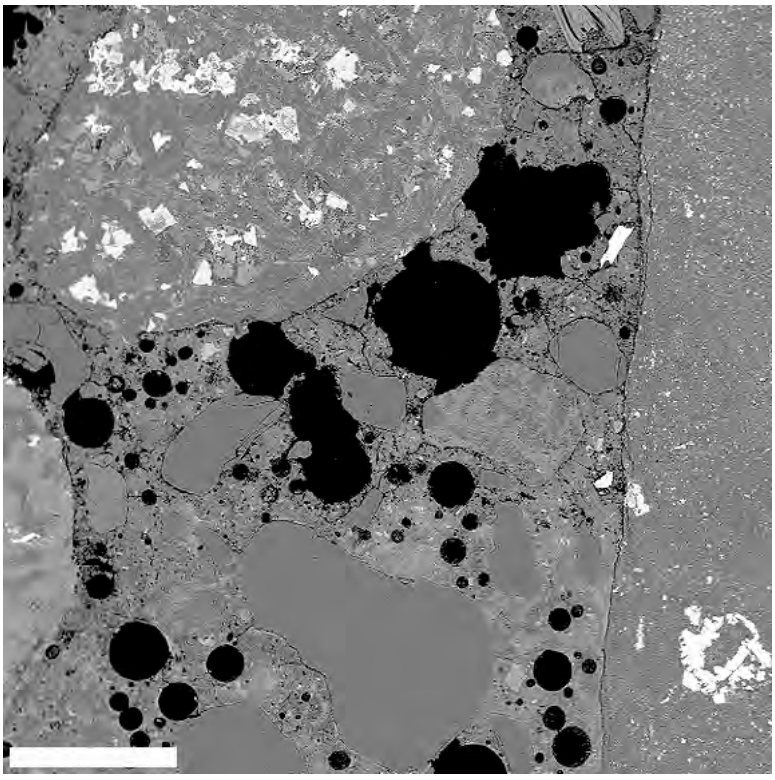

b.

Figure C.9. Back Scatter Images of GC. Corresponds to figure 4.9, a) slag aggregate, b) natural gravel aggregate.

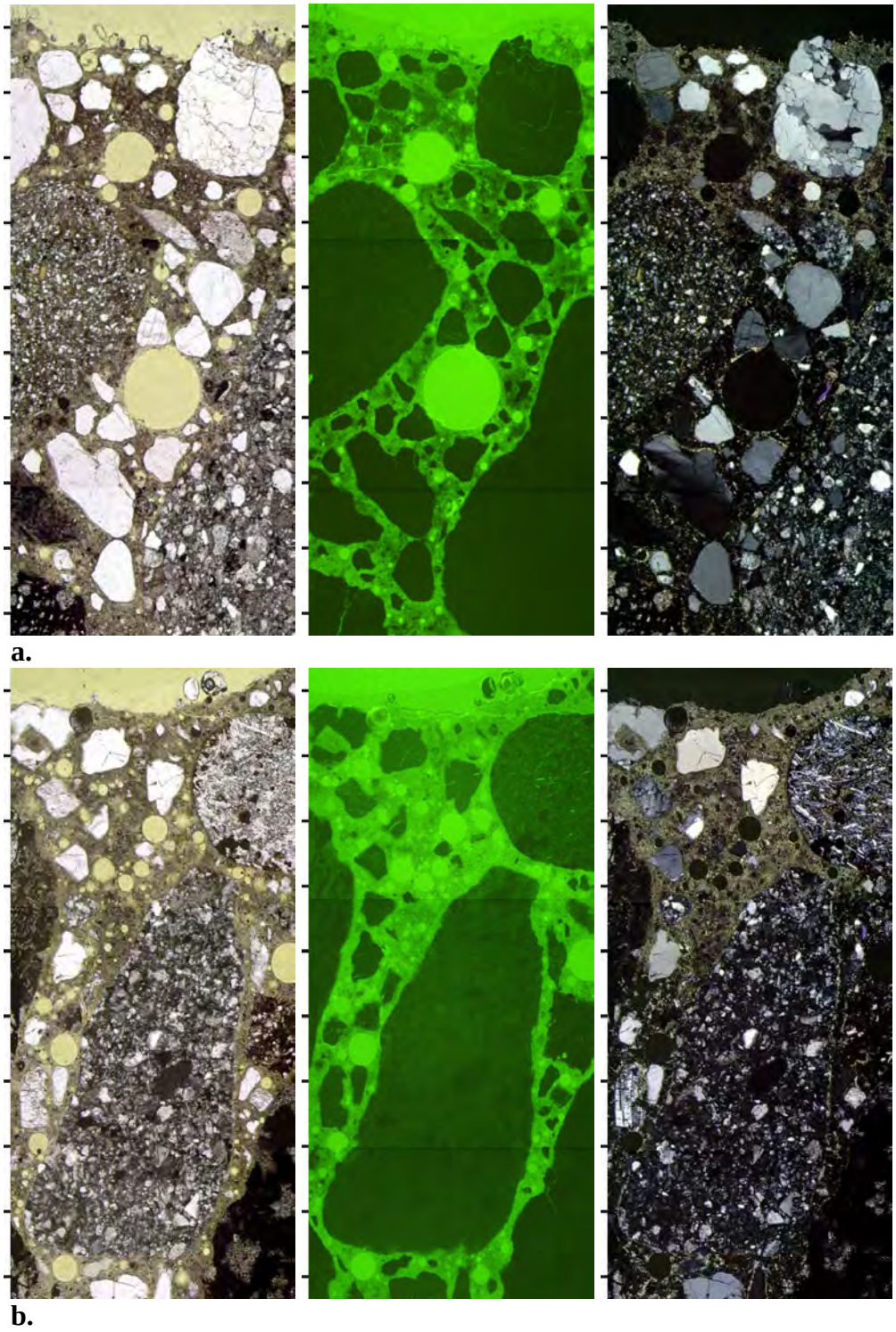

Figure C.10. Thin-sections of the AcC. Corresponds to Figure 4.11, a) carbonate aggregate, b) natural gravel aggregate.

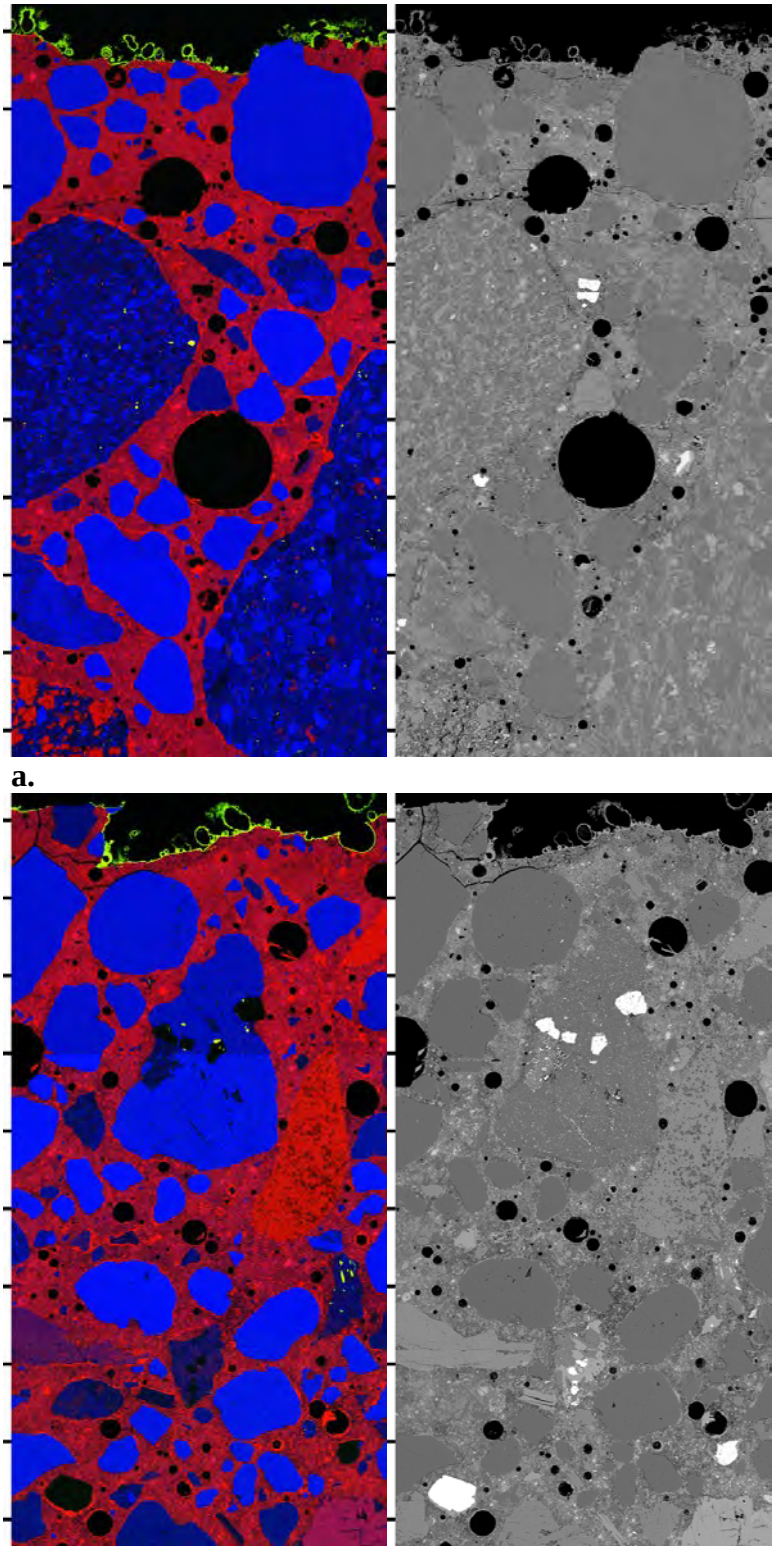

a.

b.

Figure C.11. X-Ray Energy Maps of the AcC. Corresponds to figure 4.12, a) carbonate aggregate, b) slag aggregate.

Appendix D: Data

The following section contains the raw data for the weights of the cylinders, as well as the pH of the GC and AcC systems during their incubations.

Table D.1. Mean Mass Difference of GC and AcC Before and After Treatment. As indicated by the range, this data is highly variable. According to the averages the GC cylinders lost less weight than their AcC counterparts. Because some of the ranges overlap, it is unknown if this difference is significant. The surface area on the specimens differed, which is the likely origin of the large disparity between values.

	Mean Difference (kg)	+/- Range From Mean (kg)
NG GC	63.83	3.77/3.63
LS GC	52.83	7.37/14.63
SL GC	65.87	51.73/37.77
NG AcC	124.57	128.23/67.27
LS AcC	81.77	61.33/38.47
SL AcC	92.97	45.83/81.57

Table D.2. Mean Mass Difference of A, AF, and AFB concrete before and after treatment. The range of this data is quite small. The surface areas were more consistent in this case.

	NG	range (+)	range (-)	LS	range(+)	range(-)	S	range(+)	range(-)
A	3.7	0.3	0.3	3.67	0.33	0.37	2.17	0.33	0.37
AF	4.63	0.57	0.43	3.93	0.57	0.33	2.23	0.07	0.03
AFB	3.5	0.3	0.4	4.17	0.73	0.87	2.33	0.27	0.43

The following tables and figures show the pH data from these experiments. Figure D.1 shows the range for all of the pH measurements taken from each replicate. Tables C.2-C.4 show the z-scores of the five data points at each time point for all three replicates of a given aggregate type. The raw pH data is given in the tables following the z-scores. The time is given in days. Between the five measurements, the standard deviation is relatively low. Generally, the values lie between 1 to 1.5 standard deviations from the mean. In many cases the readings were identical for a given system. For the first couple of weeks for both medias the pH was taken with pH paper when the system appeared biologically inactive and inclined toward high pH. Thus, those values indicated with an (*) in the tables following the z-scores were taken with pH paper. Although accurate, the precision is subjective and thus the actual value of the pH could be ~+/- 0.5 pH units. For figure 3.20, the pH values were rounded up; and the alkalinity threshold is at 10 for the glucose media and 9 for the acetate.

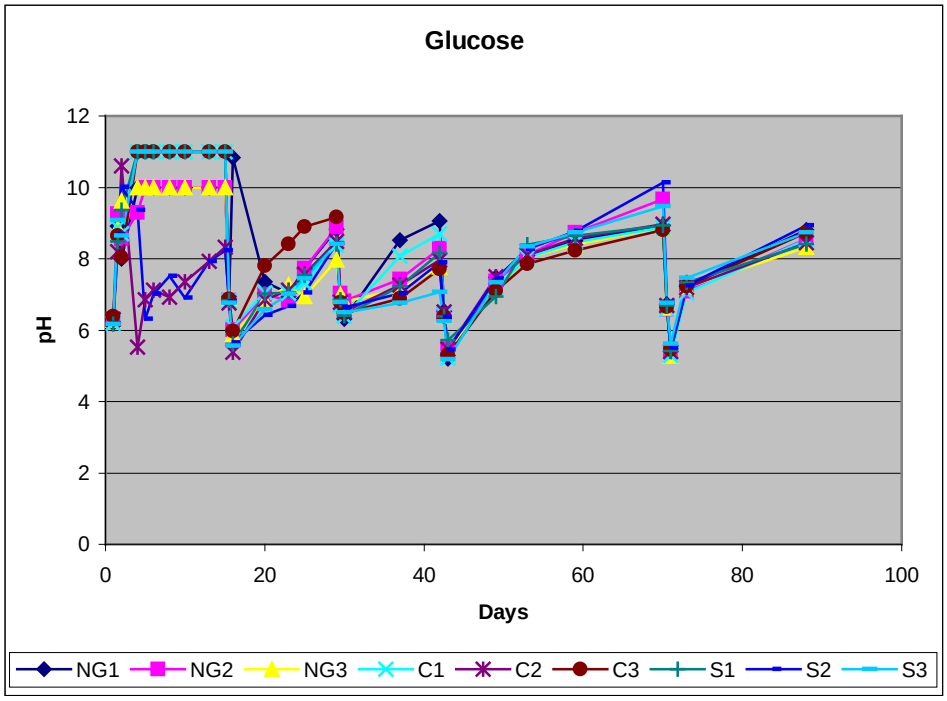

a.

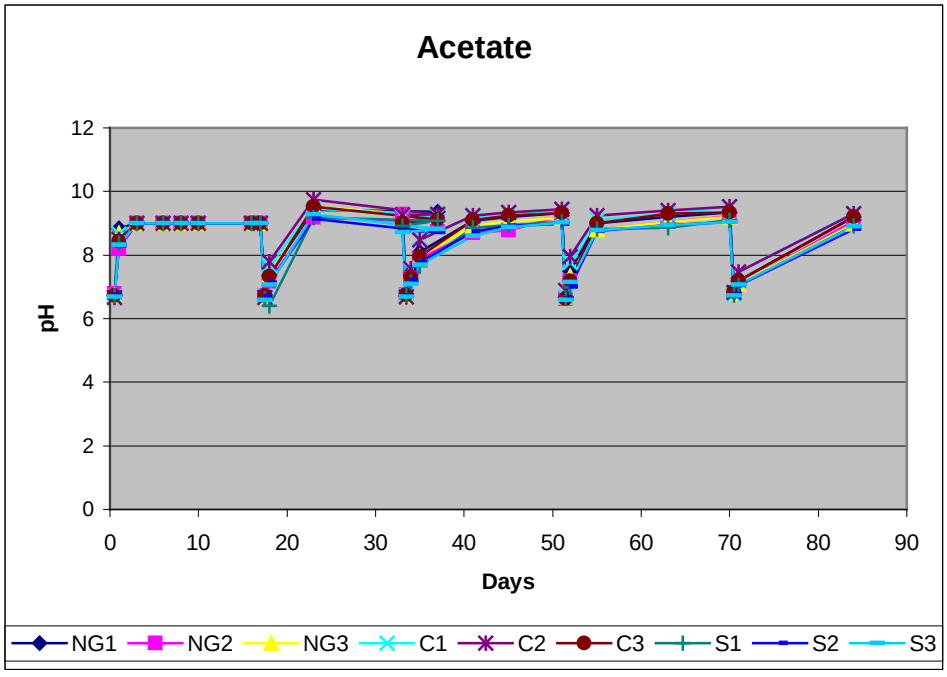

b.

Figure D.1. a) Range of pH measurements for all nine of the concrete cylinders in the glucose media. b) range of the pH measurements for all nine of the concrete cylinders in the acetate media.

Table D.3. Z-Scores NG GC

1	2	3	4	5	1	2	3	4	5	1	2	3	4	5
-0.82	1.63	-0.82			-1.41	1.41	0.00			-0.48	1.59	-1.11		
-1.44	1.39	0.05			1.08	0.53	-1.60			0.37	1.19	-1.56		
1.17	0.72	-1.41	-0.29	-0.18	-0.55	1.59	0.20	-0.19	-1.05	0.89	0.63	0.67	-1.07	-1.11
n/a	n/a	n/a	n/a	n/a	1.04	1.04	-0.45	-1.19	-0.45	n/a	n/a	n/a	n/a	n/a
n/a	n/a	n/a	n/a	n/a	n/a	n/a	n/a	n/a	n/a	n/a	n/a	n/a	n/a	n/a
n/a	n/a	n/a	n/a	n/a	n/a	n/a	n/a	n/a	n/a	n/a	n/a	n/a	n/a	n/a
n/a	n/a	n/a	n/a	n/a	n/a	n/a	n/a	n/a	n/a	n/a	n/a	n/a	n/a	n/a
n/a	n/a	n/a	n/a	n/a	n/a	n/a	n/a	n/a	n/a	n/a	n/a	n/a	n/a	n/a
n/a	n/a	n/a	n/a	n/a	n/a	n/a	n/a	n/a	n/a	n/a	n/a	n/a	n/a	n/a
n/a	n/a	n/a	n/a	n/a	n/a	n/a	n/a	n/a	n/a	n/a	n/a	n/a	n/a	n/a
0.73	0.73	-1.10	0.73	-1.10	-1.57	-0.45	0.67	0.67	0.67	0.18	0.18	-1.64	1.10	0.18
0.00	0.00	-0.53	1.60	-1.07	-1.19	1.09	-0.18	0.96	-0.68	1.27	-1.00	-0.32	0.82	-0.77
-1.08	0.58	1.00	0.58	-1.08	-0.90	0.30	1.51	0.00	-0.90	-1.00	-0.58	1.08	-0.58	1.08
-1.77	0.37	0.37	0.67	0.37	-0.55	-0.71	1.60	0.37	-0.71	-0.96	-0.96	1.23	0.79	-0.09
-0.73	-0.73	-0.73	1.10	1.10	0.00	0.00	-0.82	1.63	-0.82	0.73	0.73	-1.10	0.73	-1.10
0.73	-1.10	0.73	0.73	-1.10	1.10	-0.73	-0.73	1.10	-0.73	0.73	-1.10	0.73	-1.10	0.73
1	1	-8.9E-14	-1	-1	1.74	-0.19	-0.19	-0.68	-0.68	1	-1	0	-1	1
-0.96	1.43	0.24	0.24	-0.96	1.43	0.24	-0.96	0.24	-0.96	-0.96	0.24	1.43	0.24	-0.96
-1.10	0.73	0.73	0.73	-1.10	-1	1	8.9E-14	-1	1	-0.67	1.57	0.45	-0.67	-0.67
n/a	n/a	n/a	n/a	n/a	n/a	n/a	n/a	n/a	n/a	-0.45	-0.45	-0.45	1.79	-0.45
-1.71	0.26	0.26	0.26	0.92	-1.34	-0.76	0.41	0.70	0.99	0.00	0.00	-1.41	1.41	0.00
-1.41	0.00	0.00	1.41	0.00	-1.69	0.61	-0.15	0.61	0.61	-0.73	1.10	-0.73	-0.73	1.10
1.48	-0.54	0.13	-1.21	0.13	n/a	n/a	n/a	n/a	n/a	-1.40	-0.53	0.35	0.35	1.23
0.45	0.45	0.45	0.45	-1.79	1.40	0.53	-0.35	-0.35	-1.23	n/a	n/a	n/a	n/a	n/a
n/a	n/a	n/a	n/a	n/a	1.41	0.00	0.00	0.00	-1.41	-0.67	-0.67	-0.67	1.57	0.45
0.45	-1.79	0.45	0.45	0.45	1.10	-0.73	-0.73	-0.73	1.10	-1.79	0.45	0.45	0.45	0.45
1.5	0.5	-0.5	-0.5	-1	0.00	1.63	-0.82	-0.82	0.00	-1.01	-0.38	-0.59	1.51	0.46
-1.79	0.45	0.45	0.45	0.45	n/a	n/a	n/a	n/a	n/a	-0.73	-0.73	-0.73	1.10	1.10
-0.73	1.10	-0.73	1.10	-0.73	1.41	0.00	-1.41	0.00	0.00	0.00	1.41	-1.41	0.00	0.00
1.79	-0.45	-0.45	-0.45	-0.45	-0.45	-0.45	-0.45	-0.45	1.79	0.45	0.45	-1.79	0.45	0.45

Table D.4. Z-Scores C GC

1	2	3	4	5	1	2	3	4	5	1	2	3	4	5
-1.31	-0.19	1.50			0.31	1.23	-1.54			0.74	-1.63	0.89		
-1.07	1.60	-0.54			0.25	1.27	-1.52			1.59	-1.11	-0.48		
0.19	0.14	1.43			-1.36	-0.33	-0.16	0.52	1.32	1.78	-0.43	-0.64	-0.31	-0.40
n/a	n/a	n/a	n/a	n/a	0.83	1.24	-0.62	-0.31	-1.14	n/a	n/a	n/a	n/a	n/a
n/a	n/a	n/a	n/a	n/a	1.16	-0.11	-1.56	0.07	0.44	n/a	n/a	n/a	n/a	n/a
n/a	n/a	n/a	n/a	n/a	-0.50	0.74	-0.96	-0.65	1.36	n/a	n/a	n/a	n/a	n/a
n/a	n/a	n/a	n/a	n/a	-1	0	-1	1	1	n/a	n/a	n/a	n/a	n/a
n/a	n/a	n/a	n/a	n/a	1.41	0.71	-0.71	-0.71	-0.71	n/a	n/a	n/a	n/a	n/a
n/a	n/a	n/a	n/a	n/a	0.45	0.45	0.45	-1.79	0.45	n/a	n/a	n/a	n/a	n/a
n/a	n/a	n/a	n/a	n/a	0.24	-0.96	1.43	0.24	-0.96	n/a	n/a	n/a	n/a	n/a
-1.69	0.61	-0.15	0.61	0.61	-1.10	0.73	0.73	0.73	-1.10	-1.41	-0.71	0.71	0.71	0.71
0.86	-1.66	0.35	-0.15	0.60	1.74	-0.64	-0.64	-0.40	-0.05	1.77	-0.49	-0.23	-0.53	-0.53
-0.24	0.96	-1.43	-0.24	0.96	-1.19	-0.45	1.04	-0.45	1.04	-1.06	0.92	0.26	0.92	-1.06
-0.90	-0.90	1.51	0.30	0.00	-1	1	-1	0	1	1.43	-0.96	0.24	-0.96	0.24
-0.73	-0.73	1.10	-0.73	1.10	1.41	0.00	-1.41	0.00	0.00	1.10	-0.73	-0.73	1.10	-0.73
1.43	0.24	0.24	-0.96	-0.96	0.96	-0.24	0.96	-1.43	-0.24	1.40	-0.35	0.53	-1.23	-0.35
-1.45	-0.16	-0.16	0.49	1.27	0.24	-0.96	-0.96	0.24	1.43	1.43	0.24	0.24	-0.96	-0.96
0.45	-1.79	0.45	0.45	0.45	-0.73	1.10	-0.73	-0.73	1.10	-1.10	0.73	-1.10	0.73	0.73
-1.10	0.73	-1.10	0.73	0.73	0.89	0.89	0.89	0.89	0.89	n/a	n/a	n/a	n/a	n/a
0.73	-1.10	0.73	-1.10	0.73	1.79	-0.45	-0.45	-0.45	-0.45	-1.10	0.73	0.73	0.73	-1.10
-1.23	-0.79	0.96	0.96	0.09	-0.96	1.43	0.24	0.24	-0.96	-1.43	-0.24	-0.24	0.96	0.96
n/a	n/a	n/a	n/a	n/a	0.24	-0.96	-0.96	0.24	1.43	-1.08	-0.86	1.40	0.27	0.27
-1.70	0.73	0.12	0.12	0.73	1.40	0.53	-0.35	-1.23	-0.35	-1.63	0.00	0.82	0.82	0.00
1.41	0.00	0.00	0.00	-1.41	n/a	n/a	n/a	n/a	n/a	1.79	-0.45	-0.45	-0.45	-0.45
n/a	n/a	n/a	n/a	n/a	n/a	n/a	n/a	n/a	n/a	1.79	-0.45	-0.45	-0.45	-0.45
n/a	n/a	n/a	n/a	n/a	n/a	n/a	n/a	n/a	n/a	n/a	n/a	n/a	n/a	n/a
-0.33	-0.88	1.32	0.77	-0.88	-0.96	-0.96	-0.16	1.04	1.04	-1.76	0.27	0.27	0.61	0.61
-1.10	-1.10	0.73	0.73	0.73	-1.10	-1.10	0.73	0.73	0.73	1.43	-0.96	0.24	-0.96	0.24
1.19	0.45	0.45	-1.04	-1.04	1.10	-0.73	-0.73	1.10	-0.73	1.41	0.00	-1.41	0.00	0.00
1.10	-0.73	-0.73	1.10	-0.73	0.96	-0.24	0.96	-0.24	-1.43	1.79	-0.45	-0.45	-0.45	-0.45

Table D.5. Z-Score S GC

1	2	3	4	5	1	2	3	4	5	1	2	3	4	5
-1.13	1.59	-0.45			-1.59	0.45	1.13			-0.45	-1.13	1.59		
1.29	0.22	-1.51			0.34	1.22	-1.55			0.91	0.72	-1.63		
-0.37	-1.00	-0.50	0.28	1.59	-0.73	-0.75	-0.71	1.18	1.00	-0.96	-1.07	0.11	0.78	1.14
n/a	n/a	n/a	n/a	n/a	0.89	0.69	0.40	-0.45	-1.54	n/a	n/a	n/a	n/a	n/a
n/a	n/a	n/a	n/a	n/a	-1.44	1.29	-0.25	-0.04	0.45	n/a	n/a	n/a	n/a	n/a
n/a	n/a	n/a	n/a	n/a	-1.09	-0.18	-0.36	1.63	0.00	n/a	n/a	n/a	n/a	n/a
n/a	n/a	n/a	n/a	n/a	-0.47	-0.46	-0.39	-0.46	1.79	n/a	n/a	n/a	n/a	n/a
n/a	n/a	n/a	n/a	n/a	1.38	-0.15	0.61	-0.92	-0.92	n/a	n/a	n/a	n/a	n/a
n/a	n/a	n/a	n/a	n/a	1.34	0.27	0.27	-0.53	-1.34	n/a	n/a	n/a	n/a	n/a
n/a	n/a	n/a	n/a	n/a	1.43	0.24	0.24	-0.96	-0.96	n/a	n/a	n/a	n/a	n/a
0.96	0.96	-0.24	-1.43	-0.24	-0.24	-1.43	0.96	0.96	-0.24	-0.45	-1.57	0.67	0.67	0.67
-1.41	1.41	0.00	0.00	0.00	-0.17	-1.50	0.02	1.25	0.40	-0.77	-1.04	-0.13	1.43	0.51
0.82	0.00	0.82	-1.63	0.00	-0.24	-1.43	0.96	-0.24	0.96	n/a	n/a	n/a	n/a	n/a
-1.70	0.73	0.12	0.12	0.73	0.58	-1.08	1.00	-1.08	0.58	-0.44	-0.27	1.78	-0.61	-0.44
0.73	-1.10	0.73	-1.10	0.73	n/a	n/a	n/a	n/a	n/a	n/a	n/a	n/a	n/a	n/a
1.23	0.35	0.35	-0.53	-1.40	1.38	0.61	-0.92	-0.15	-0.92	1.43	0.24	-0.96	0.24	-0.96
-1.29	0.55	-0.83	1.01	0.55	-0.58	-0.58	0.00	1.73	-0.58	-1.00	-1.00	0.00	1.00	1.00
-0.24	-1.43	-0.24	0.96	0.96	-1.41	0.00	0.00	1.41	0.00	-1.40	-0.53	0.35	1.23	0.35
0.73	-1.10	0.73	-1.10	0.73	-1.26	-0.63	0.00	0.63	1.26	0.89	0.89	0.89	0.89	0.89
0.18	0.18	-1.64	0.18	1.10	n/a	n/a	n/a	n/a	n/a	-1.10	0.73	0.73	0.73	-1.10
0.45	0.45	-1.79	0.45	0.45	-1.77	0.59	0.29	0.59	0.29	1.10	-0.73	1.10	-0.73	-0.73
-1.43	0.96	-0.24	0.96	-0.24	-1.10	0.73	-1.10	0.73	0.73	-1.71	0.26	0.26	0.26	0.92
-1.41	0.00	1.41	0.00	0.00	1.62	0.32	-0.65	-0.65	-0.65	1.79	-0.45	-0.45	-0.45	-0.45
0.73	-1.10	0.73	-1.10	0.73	-0.96	0.24	-0.96	0.24	1.43	-1.79	0.45	0.45	0.45	0.45
n/a	n/a	n/a	n/a	n/a	0.73	-1.10	0.73	-1.10	0.73	n/a	n/a	n/a	n/a	n/a
-1.10	-1.10	0.73	0.73	0.73	-1.43	-0.24	-0.24	0.96	0.96	-0.45	-0.45	-0.45	-0.45	1.79
0.24	-0.96	-0.96	0.24	1.43	0.73	-1.10	0.73	-1.10	0.73	-1.29	-0.83	1.01	0.55	0.55
-0.89	-1.26	0.96	0.59	0.59	-1.57	-0.45	0.67	0.67	0.67	0.73	-1.10	0.73	0.73	-1.10
-1.79	0.45	0.45	0.45	0.45	n/a	n/a	n/a	n/a	n/a	0.89	0.89	0.89	0.89	0.89
n/a	n/a	n/a	n/a	n/a	-1.79	0.45	0.45	0.45	0.45	n/a	n/a	n/a	n/a	n/a

Table D.6. Z-Scores NG AcC

1	2	3	4	5	1	2	3	4	5	1	2	3	4	5
0.73	0.73	-1.10	-1.10	0.73	-0.73	-0.73	1.10	1.10	-0.73	1.79	-0.45	-0.45	-0.45	-0.45
-0.61	1.08	1.08	-0.61	-0.95	-0.73	1.10	1.10	-0.73	-0.73	-1.66	0.42	0.94	0.42	-0.10
n/a	n/a	n/a	n/a	n/a	n/a	n/a	n/a	n/a	n/a	n/a	n/a	n/a	n/a	n/a
n/a	n/a	n/a	n/a	n/a	n/a	n/a	n/a	n/a	n/a	n/a	n/a	n/a	n/a	n/a
n/a	n/a	n/a	n/a	n/a	n/a	n/a	n/a	n/a	n/a	n/a	n/a	n/a	n/a	n/a
n/a	n/a	n/a	n/a	n/a	n/a	n/a	n/a	n/a	n/a	n/a	n/a	n/a	n/a	n/a
n/a	n/a	n/a	n/a	n/a	n/a	n/a	n/a	n/a	n/a	n/a	n/a	n/a	n/a	n/a
n/a	n/a	n/a	n/a	n/a	n/a	n/a	n/a	n/a	n/a	n/a	n/a	n/a	n/a	n/a
-1.74	0.68	0.19	0.19	0.68	-0.73	1.10	1.10	-0.73	-0.73	0.96	-0.24	-0.24	0.96	-1.43
1.34	0.73	-0.49	-1.10	-0.49	-1.26	-0.63	0.00	0.63	1.26	-0.79	1.54	-0.43	-0.79	0.46
-1.41	0.00	0.00	1.41	0.00	-1.38	-0.61	0.92	0.15	0.92	-1.79	0.45	0.45	0.45	0.45
-0.73	-0.73	1.10	-0.73	1.10	0.24	1.43	-0.96	0.24	-0.96	-0.73	1.10	-0.73	1.10	-0.73
-1.40	-0.53	0.35	0.35	1.23	0.73	-1.10	0.73	0.73	-1.10	-0.45	-0.45	-0.45	-0.45	1.79
-1.33	-0.82	0.72	0.72	0.72	-1.57	-0.45	0.67	0.67	0.67	-0.73	1.10	1.10	-0.73	-0.73
-0.73	-0.73	1.10	1.10	-0.73	-0.73	1.10	-0.73	1.10	-0.73	-1.51	0.00	0.90	-0.30	0.90
0.73	-1.10	0.73	-1.10	0.73	-1.10	0.73	-1.10	0.73	0.73	0.45	-1.79	0.45	0.45	0.45
-0.73	-0.73	-0.73	1.10	1.10	-1.43	-0.24	0.96	-0.24	0.96	-0.73	-0.73	-0.73	1.10	1.10
-1.64	0.18	0.18	1.10	0.18	0.42	-1.79	0.49	0.45	0.42	n/a	n/a	n/a	n/a	n/a
-1.43	-0.24	0.96	0.96	-0.24	-1.43	-0.24	0.96	-0.24	0.96	-1.63	0.00	0.00	0.82	0.82
-0.45	-0.45	-0.45	-0.45	1.79	-1.23	-0.35	-0.35	0.53	1.40	1.10	-0.73	-0.73	1.10	-0.73
-1.41	0.00	0.00	0.00	1.41	-1.79	0.45	0.45	0.45	0.45	-1.10	-1.10	0.73	0.73	0.73
-1.57	-0.45	0.67	0.67	0.67	-1.29	-0.88	0.72	0.72	0.72	-0.73	-0.73	1.10	-0.73	1.10
-1.79	0.45	0.45	0.45	0.45	-1.38	-0.61	0.15	0.92	0.92	-1.57	-0.45	0.67	0.67	0.67
-0.73	-0.73	1.10	-0.73	1.10	-1.10	0.73	0.73	0.73	-1.10	-0.73	-0.73	1.10	-0.73	1.10
0.67	-1.57	-0.45	0.67	0.67	-0.73	1.10	-0.73	1.10	-0.73	-1.10	-1.10	0.73	0.73	0.73
-0.01	0.00	0.00	0.00	0.00	0.00	0.00	-0.01	0.00	0.00	-0.01	0.00	0.00	0.00	0.00
-1.79	0.45	0.45	0.45	0.45	-1.79	0.45	0.45	0.45	0.45	-1.38	-0.61	0.15	0.92	0.92

Table D.7. Z-Scores C AcC

1	2	3	4	5	1	2	3	4	5	1	2	3	4	5
1.43	-0.96	-0.96	0.24	0.24	1.63	0.00	0.00	-0.82	-0.82	0.73	0.73	-1.10	-1.10	0.73
-1.43	0.96	-0.24	0.96	-0.24	-0.73	1.10	1.10	-0.73	-0.73	n/a	n/a	n/a	n/a	n/a
n/a	n/a	n/a	n/a	n/a	n/a	n/a	n/a	n/a	n/a	n/a	n/a	n/a	n/a	n/a
n/a	n/a	n/a	n/a	n/a	n/a	n/a	n/a	n/a	n/a	n/a	n/a	n/a	n/a	n/a
n/a	n/a	n/a	n/a	n/a	n/a	n/a	n/a	n/a	n/a	n/a	n/a	n/a	n/a	n/a
n/a	n/a	n/a	n/a	n/a	n/a	n/a	n/a	n/a	n/a	n/a	n/a	n/a	n/a	n/a
n/a	n/a	n/a	n/a	n/a	n/a	n/a	n/a	n/a	n/a	n/a	n/a	n/a	n/a	n/a
n/a	n/a	n/a	n/a	n/a	n/a	n/a	n/a	n/a	n/a	0.92	0.92	0.15	-0.61	-1.38
-0.96	-0.96	0.24	1.43	0.24	-0.67	0.45	-0.67	1.57	-0.67	-1.43	0.96	-0.24	0.96	-0.24
-1.10	-1.10	0.73	0.73	0.73	-1.44	-0.58	0.29	0.87	0.87	-0.94	-0.42	-0.42	0.10	1.66
-1	-1	1.8E-13	1	1	-1.40	-0.53	0.35	0.35	1.23	-1.79	0.45	0.45	0.45	0.45
n/a	n/a	n/a	n/a	n/a	n/a	n/a	n/a	n/a	n/a	-1.57	-0.45	0.67	0.67	0.67
-1.10	-1.10	0.73	0.73	0.73	-0.73	-0.73	-0.73	1.10	1.10	-0.92	-0.92	1.38	0.61	-0.15
-1.26	-0.63	0.00	0.63	1.26	-1.10	-1.10	0.73	0.73	0.73	0.00	0.00	-1.41	1.41	0.00
-0.82	0.00	0.00	-0.82	1.63	n/a	n/a	n/a	n/a	n/a	-1.10	-1.10	0.73	0.73	0.73
-0.73	1.10	-0.73	1.10	-0.73	-1.10	0.73	0.73	-1.10	0.73	-0.92	-0.92	-0.15	0.61	1.38
-0.73	-0.73	-0.73	1.10	1.10	-1.57	-0.45	0.67	0.67	0.67	-1.79	0.45	0.45	0.45	0.45
-1.33	-0.82	0.72	0.72	0.72	-1.10	-1.10	0.73	0.73	0.73	-1.43	-0.24	-0.24	0.96	0.96
-0.45	-0.45	-0.45	-0.45	1.79	-1.10	0.73	0.73	0.73	-1.10	0.73	0.73	-1.10	0.73	-1.10
-0.45	-0.45	-0.45	-0.45	1.79	1.04	-1.19	-0.45	1.04	-0.45	-0.73	1.10	-0.73	-0.73	1.10
-1.63	0.00	0.00	0.82	0.82	-1.43	-0.24	-0.24	0.96	0.96	-1.57	-0.45	0.67	0.67	0.67
-0.73	1.10	-0.73	-0.73	1.10	-1.79	0.45	0.45	0.45	0.45	n/a	n/a	n/a	n/a	n/a
-1.79	0.45	0.45	0.45	0.45	-1.10	0.73	0.73	-1.10	0.73	-1.43	-0.24	0.96	-0.24	0.96
-1.79	0.45	0.45	0.45	0.45	n/a	n/a	n/a	n/a	n/a	-1.41	-0.71	0.71	0.71	0.71
0.45	-1.79	0.45	0.45	0.45	-1.57	-0.45	0.67	0.67	0.67	0.67	-1.57	0.67	-0.45	0.67
0.73	-1.10	-1.10	0.73	0.73	1.01	1.01	-1.23	-0.67	-0.11	n/a	n/a	n/a	n/a	n/a
-1.10	0.73	0.73	-1.10	0.73	-0.73	-0.73	1.10	-0.73	1.10	n/a	n/a	n/a	n/a	n/a

Table D.8. Z-Scores S AcC

1	2	3	4	5	1	2	3	4	5	1	2	3	4	5
0.73	-1.10	0.73	-1.10	0.73	-1.10	0.73	-1.10	0.73	0.73	-0.67	0.45	1.57	-0.67	-0.67
1.10	-0.73	1.10	-0.73	-0.73	1.43	0.24	-0.96	0.24	-0.96	0.73	-1.10	-1.10	0.73	0.73
n/a	n/a	n/a	n/a	n/a	n/a	n/a	n/a	n/a	n/a	n/a	n/a	n/a	n/a	n/a
n/a	n/a	n/a	n/a	n/a	n/a	n/a	n/a	n/a	n/a	n/a	n/a	n/a	n/a	n/a
n/a	n/a	n/a	n/a	n/a	n/a	n/a	n/a	n/a	n/a	n/a	n/a	n/a	n/a	n/a
n/a	n/a	n/a	n/a	n/a	n/a	n/a	n/a	n/a	n/a	n/a	n/a	n/a	n/a	n/a
n/a	n/a	n/a	n/a	n/a	n/a	n/a	n/a	n/a	n/a	n/a	n/a	n/a	n/a	n/a
n/a	n/a	n/a	n/a	n/a	n/a	n/a	n/a	n/a	n/a	n/a	n/a	n/a	n/a	n/a
-1.40	0.35	0.35	-0.53	1.23	-1.10	-0.49	-0.49	0.73	1.34	-0.45	1.79	-0.45	-0.45	-0.45
0.42	0.43	0.47	0.47	-1.79	-1.43	-0.24	-0.24	0.96	0.96	-1.71	0.85	0.00	0.43	0.43
-0.67	-0.67	0.45	1.57	-0.67	-1.43	-0.24	0.96	0.96	-0.24	-1.10	0.73	0.73	-1.10	0.73
n/a	n/a	n/a	n/a	n/a	n/a	n/a	n/a	n/a	n/a	-1.10	0.73	0.73	-1.10	0.73
-1.10	0.73	0.73	-1.10	0.73	-0.73	1.10	-0.73	1.10	-0.73	-1.41	0.00	0.00	0.00	1.41
-1.10	-0.18	-0.18	-0.18	1.64	-1.79	0.45	0.45	0.45	0.45	-1.43	-0.24	-0.24	0.96	0.96
0.89	0.89	0.89	0.89	0.89	-0.73	-0.73	-0.73	1.10	1.10	-0.89	-0.89	-0.89	-0.89	-0.89
-1.79	0.45	0.45	0.45	0.45	-0.73	1.10	-0.73	1.10	-0.73	-1.79	0.45	0.45	0.45	0.45
n/a	n/a	n/a	n/a	n/a	-1.79	0.45	0.45	0.45	0.45	0.00	-1.41	0.00	0.00	1.41
-1.38	-0.61	0.15	0.92	0.92	n/a	n/a	n/a	n/a	n/a	-0.73	1.10	-0.73	1.10	-0.73
-1.79	0.45	0.45	0.45	0.45	n/a	n/a	n/a	n/a	n/a	-0.72	0.82	-0.72	-0.72	1.33
-0.73	-0.73	-0.12	-0.12	1.70	-1.41	0.00	1.41	0.00	0.00	-1.10	0.73	-1.10	0.73	0.73
-0.73	-0.73	-0.73	1.10	1.10	-0.73	-0.73	1.10	1.10	-0.73	-1.79	0.45	0.45	0.45	0.45
0.00	-1.41	0.00	0.00	1.41	0.73	-1.10	0.73	-1.10	0.73	-1.19	-0.45	-0.45	1.04	1.04
-1.41	0.00	0.00	1.41	0.00	-1.10	-1.10	0.73	0.73	0.73	-1.26	0.00	-0.63	1.26	0.63
-1.00	-1.00	0.00	1.00	1.00	-1.00	0.00	1.00	-1.00	1.00	-0.73	1.10	-0.73	1.10	-0.73
-1.57	-0.45	0.67	0.67	0.67	1.10	-0.73	1.10	-0.73	-0.73	-1.57	0.67	-0.45	0.67	0.67
-1.10	0.73	0.73	-1.10	0.73	-0.89	-0.89	-0.89	-0.89	-0.89	-1.32	-0.77	0.88	0.88	0.33
-0.73	-0.73	-0.73	1.10	1.10	-1.79	0.45	0.45	0.45	0.45	n/a	n/a	n/a	n/a	n/a

Table D.9. NGAc, 1

Time	1	2	3	4	5	Mean
0.5	6.75	6.75	6.74	6.74	6.75	6.75
1	8.82	8.87	8.87	8.82	8.81	8.84
3	9*	9*	9*	9*	9*	9
6	9*	9*	9*	9*	9*	9
8	9*	9*	9*	9*	9*	9
10	9*	9*	9*	9*	9*	9
16	9*	9*	9*	9*	9*	9
17	9*	9*	9*	9*	9*	9
17.5	6.6	6.65	6.64	6.64	6.65	6.64
18	7.39	7.38	7.36	7.35	7.36	7.37
23	9.41	9.42	9.42	9.43	9.42	9.42
37	9.35	9.35	9.36	9.35	9.36	9.35
33	8.91	8.92	8.93	8.93	8.94	8.93
33.5	6.67	6.68	6.71	6.71	6.71	6.70
34	7.44	7.44	7.45	7.45	7.44	7.44
35	8.1	8.09	8.1	8.09	8.1	8.10
41	9.08	9.08	9.08	9.09	9.09	9.08
45	9.18	9.2	9.2	9.21	9.2	9.20
51	9.31	9.32	9.33	9.33	9.32	9.32
51.5	6.67	6.67	6.67	6.67	6.68	6.67
52	7.48	7.49	7.49	7.49	7.5	7.49
55	8.98	8.99	9	9	9	8.99
63	9.19	9.2	9.2	9.2	9.2	9.20
70	9.33	9.33	9.34	9.33	9.34	9.33
70.5	6.83	6.81	6.82	6.83	6.83	6.82
71	7.16	7.17	7.19	7.19	7.19	7.18
84	9.19	9.2	9.2	9.2	9.2	9.20

Table D.10. NGAc, 2

Time	1	2	3	4	5	Mean
0.5	6.73	6.72	6.72	6.72	6.72	6.72
1	8.65	8.69	8.7	8.69	8.68	8.68
3	9*	9*	9*	9*	9*	9.00
6	9*	9*	9*	9*	9*	9.00
8	9*	9*	9*	9*	9*	9.00
10	9*	9*	9*	9*	9*	9.00
16	9*	9*	9*	9*	9*	9.00
17	9*	9*	9*	9*	9*	9.00
17.5	6.69	6.68	6.68	6.69	6.67	6.68
18	7.33	7.46	7.35	7.33	7.4	7.37
23	9.5	9.53	9.53	9.53	9.53	9.52
37	9.22	9.23	9.22	9.23	9.22	9.22
33	9.19	9.19	9.19	9.19	9.2	9.19
33.5	6.72	6.73	6.73	6.72	6.72	6.72
34	7.43	7.44	7.45	7.44	7.45	7.44
35	7.96	7.95	7.96	7.96	7.96	7.96
41	8.91	8.91	8.91	8.92	8.92	8.91
45	9.06	9.06	9.06	9.06	9.06	9.06
51	9.14	9.16	9.16	9.17	9.17	9.16
51.5	6.69	6.68	6.68	6.69	6.68	6.68
52	7.32	7.32	7.33	7.33	7.33	7.33
55	8.8	8.8	8.81	8.8	8.81	8.80
63	9.02	9.03	9.04	9.04	9.04	9.03
70	9.19	9.19	9.2	9.19	9.2	9.19
70.5	6.8	6.8	6.81	6.81	6.81	6.81
71	7.07	7.08	7.09	7.09	7.09	7.08
84	8.97	8.98	8.99	9	9	8.99

Table D.11. NGAc, 3

Time	1	2	3	4	5	Mean
0.5	6.78	6.78	6.79	6.79	6.78	6.78
1	8.2	8.21	8.21	8.2	8.2	8.20
3	9*	9*	9*	9*	9*	9.00
6	9*	9*	9*	9*	9*	9.00
8	9*	9*	9*	9*	9*	9.00
10	9*	9*	9*	9*	9*	9.00
16	9*	9*	9*	9*	9*	9.00
17	9*	9*	9*	9*	9*	9.00
17.5	6.73	6.74	6.74	6.73	6.73	6.73
18	7.15	7.16	7.17	7.18	7.19	7.17
23	9.17	9.18	9.2	9.19	9.2	9.19
37	9.05	9.06	9.04	9.05	9.04	9.05
33	9.29	9.28	9.29	9.29	9.28	9.29
33.5	6.74	6.75	6.76	6.76	6.76	6.75
34	7.26	7.27	7.26	7.27	7.26	7.26
35	7.89	7.9	7.89	7.9	7.9	7.90
41	8.68	8.69	8.7	8.69	8.7	8.69
45	8.97	8.01	9	8.98	8.97	8.79
51	9.21	9.22	9.23	9.22	9.23	9.22
51.5	6.61	6.62	6.62	6.63	6.64	6.62
52	7.17	7.18	7.18	7.18	7.18	7.18
55	8.76	8.77	8.81	8.81	8.81	8.79
63	9.03	9.04	9.05	9.06	9.06	9.05
70	9.22	9.23	9.23	9.23	9.22	9.23
70.5	6.81	6.82	6.81	6.82	6.81	6.81
71	7.07	7.08	7.06	7.07	7.08	7.07
84	9.06	9.07	9.07	9.07	9.07	9.07

Table D.12. CacC, 1

Time	1	2	3	4	5	Mean
0.5	6.72	6.7	6.7	6.71	6.71	6.71
1	8.64	8.68	8.66	8.68	8.66	8.66
3	9*	9*	9*	9*	9*	9
6	9*	9*	9*	9*	9*	9
8	9*	9*	9*	9*	9*	9
10	9*	9*	9*	9*	9*	9
16	9*	9*	9*	9*	9*	9
17	9*	9*	9*	9*	9*	9
17.5	6.71	6.71	6.72	6.73	6.72	6.72
18	7.67	7.67	7.68	7.68	7.68	7.68
23	9.45	9.45	9.46	9.47	9.47	9.46
37	9.25	9.25	9.25	9.25	9.25	9.25
33	9.22	9.22	9.23	9.23	9.23	9.23
33.5	6.71	6.72	6.73	6.74	6.75	6.73
34	7.55	7.56	7.56	7.55	7.58	7.56
35	8.51	8.52	8.51	8.52	8.51	8.51
41	9.2	9.2	9.2	9.21	9.21	9.20
45	9.3	9.31	9.34	9.34	9.34	9.33
51	9.4	9.4	9.4	9.4	9.41	9.40
51.5	6.69	6.69	6.69	6.69	6.7	6.69
52	7.76	7.78	7.78	7.79	7.79	7.78
55	9.1	9.11	9.1	9.1	9.11	9.10
63	9.29	9.3	9.3	9.3	9.3	9.30
70	9.5	9.51	9.51	9.51	9.51	9.51
70.5	6.77	6.76	6.77	6.77	6.77	6.77
71	7.47	7.46	7.46	7.47	7.47	7.47
84	9.32	9.33	9.33	9.32	9.33	9.33

Table D.13. CacC, 2

Time	1	2	3	4	5	Mean
0.5	6.68	6.66	6.66	6.65	6.65	6.66
1	8.5	8.51	8.51	8.5	8.5	8.50
3	9*	9*	9*	9*	9*	9
6	9*	9*	9*	9*	9*	9
8	9*	9*	9*	9*	9*	9
10	9*	9*	9*	9*	9*	9
16	9*	9*	9*	9*	9*	9
17	9*	9*	9*	9*	9*	9
17.5	6.65	6.66	6.65	6.67	6.65	6.66
18	7.75	7.78	7.81	7.83	7.83	7.8
23	9.72	9.73	9.74	9.74	9.75	9.74
37	9.29	9.29	9.29	9.29	9.29	9.29
33	9.26	9.26	9.26	9.27	9.27	9.26
33.5	6.68	6.68	6.69	6.69	6.69	6.69
34	7.57	7.57	7.57	7.57	7.57	7.57
35	8.47	8.48	8.48	8.47	8.48	8.48
41	9.22	9.23	9.24	9.24	9.24	9.23
45	9.33	9.33	9.34	9.34	9.34	9.34
51	9.44	9.45	9.45	9.45	9.44	9.45
51.5	6.9	6.87	6.88	6.9	6.88	6.89
52	7.94	7.95	7.95	7.96	7.96	7.95
55	9.23	9.24	9.24	9.24	9.24	9.24
63	9.4	9.41	9.41	9.4	9.41	9.41
70	9.53	9.53	9.53	9.53	9.53	9.53
70.5	6.81	6.82	6.83	6.83	6.83	6.82
71	7.49	7.49	7.45	7.46	7.47	7.47
84	9.29	9.29	9.3	9.29	9.3	9.30

Table D.14. CacC, 3

Time	1	2	3	4	5	Mean
0.5	6.72	8.44	8.43	8.43	8.44	8.44
1	9*	9*	9*	9*	9*	9
3	9*	9*	9*	9*	9*	9
6	9*	9*	9*	9*	9*	9
8	9*	9*	9*	9*	9*	9
10	9*	9*	9*	9*	9*	9
16	9*	9*	9*	9*	9*	9
17	6.73	6.73	6.72	6.71	6.7	6.72
17.5	7.32	7.34	7.33	7.34	7.33	7.33
18	9.5	9.51	9.51	9.52	9.55	9.52
23	9.12	9.13	9.13	9.13	9.13	9.13
37	9	9.01	9.02	9.02	9.02	9.01
33	6.73	6.73	6.76	6.75	6.74	6.74
33.5	7.29	7.29	7.28	7.3	7.29	7.29
34	7.94	7.94	7.95	7.95	7.95	7.95
35	9.09	9.09	9.1	9.11	9.12	9.10
41	9.23	9.24	9.24	9.24	9.24	9.24
45	9.32	9.33	9.33	9.34	9.34	9.33
51	6.63	6.63	6.62	6.63	6.62	6.63
51.5	7.18	7.19	7.18	7.18	7.19	7.18
52	8.98	8.99	9	9	9	8.99
55	9.3	9.3	9.3	9.3	9.3	9.3
63	9.34	9.35	9.36	9.35	9.36	9.35
70	6.82	6.83	6.85	6.85	6.85	6.84
70.5	7.2	7.18	7.2	7.19	7.2	7.20
71	9.2	9.2	9.2	9.2	9.2	9.2
84	9.2	9.2	9.2	9.2	9.2	9.2

Table D.15. Sac, 1

Time	1	2	3	4	5	Mean
0.5	6.67	6.68	6.69	6.67	6.67	6.67
1	8.31	8.3	8.3	8.31	8.31	8.31
3	9*	9*	9*	9*	9*	9*
6	9*	9*	9*	9*	9*	9*
8	9*	9*	9*	9*	9*	9*
10	9*	9*	9*	9*	9*	9*
16	9*	9*	9*	9*	9*	9*
17	9*	9*	9*	9*	9*	9*
17.5	6.58	6.59	6.58	6.58	6.58	6.58
18	7.02	7.08	7.06	7.07	7.07	7.02
23	9.27	9.28	9.28	9.27	9.28	9.27
37	8.81	8.82	8.82	8.81	8.82	8.81
33	8.71	8.72	8.72	8.72	8.73	8.71
33.5	6.67	6.68	6.68	6.69	6.69	6.67
34	7.09	7.09	7.09	7.09	7.09	7.09
35	7.68	7.69	7.69	7.69	7.69	7.68
41	8.59	8.58	8.59	8.59	8.6	8.59
45	8.88	8.89	8.88	8.89	8.88	8.88
51	9	9.03	9	9	9.04	9
51.5	6.57	6.58	6.57	6.58	6.58	6.57
52	7.13	7.14	7.14	7.14	7.14	7.13
55	8.76	8.77	8.77	8.79	8.79	8.76
63	8.91	8.93	8.92	8.95	8.94	8.91
70	9.03	9.04	9.03	9.04	9.03	9.03
70.5	6.71	6.73	6.72	6.73	6.73	6.71
71	7.05	7.06	7.09	7.09	7.08	7.05
84	8.9	8.9	8.9	8.9	8.9	8.9

Table D.16. Sac, 2

Time	1	2	3	4	5	Mean
0.5	6.74	6.75	6.74	6.75	6.75	6.75
1	8.3	8.29	8.28	8.29	8.28	8.29
3	9*	9*	9*	9*	9*	9.00
6	9*	9*	9*	9*	9*	9.00
8	9*	9*	9*	9*	9*	9.00
10	9*	9*	9*	9*	9*	9.00
16	9*	9*	9*	9*	9*	9.00
17	9*	9*	9*	9*	9*	9.00
17.5	6.69	6.7	6.7	6.72	6.73	6.71
18	7.12	7.13	7.13	7.14	7.14	7.13
23	9.12	9.13	9.14	9.14	9.13	9.13
37	8.72	8.72	8.72	8.72	8.72	8.72
33	8.78	8.79	8.78	8.79	8.78	8.78
33.5	6.71	6.72	6.72	6.72	6.72	6.72
34	7.21	7.21	7.21	7.22	7.22	7.21
35	7.76	7.77	7.76	7.77	7.76	7.76
41	8.74	8.75	8.75	8.75	8.75	8.75
45	8.92	8.92	8.92	8.92	8.92	8.92
51	8.98	8.98	8.98	8.98	8.98	8.98
51.5	6.61	6.62	6.63	6.62	6.62	6.62
52	7	7	7.01	7.01	7	7.00
55	8.77	8.76	8.77	8.76	8.77	8.77
63	8.94	8.94	8.95	8.95	8.95	8.95
70	9.03	9.04	9.05	9.03	9.05	9.04
70.5	6.78	6.77	6.78	6.77	6.77	6.77
71	7.04	7.04	7.04	7.04	7.04	7.04
84	8.81	8.82	8.82	8.82	8.82	8.82

Table D.17. Sac, 3

Time	1	2	3	4	5	Mean
0.5	6.72	6.71	6.72	6.71	6.72	6.72
1	8.39	8.38	8.39	8.38	8.38	8.38
3	9*	9*	9*	9*	9*	9.00
6	9*	9*	9*	9*	9*	9.00
8	9*	9*	9*	9*	9*	9.00
10	9*	9*	9*	9*	9*	9.00
16	9*	9*	9*	9*	9*	9.00
17	9*	9*	9*	9*	9*	9.00
17.5	6.6	6.62	6.62	6.61	6.63	6.62
18	6.97	6.98	7.03	7.04	4.04	6.41
23	9.18	9.18	9.19	9.2	9.18	9.19
37	9.08	9.08	9.08	9.08	9.08	9.08
33	8.92	8.93	8.93	8.92	8.93	8.93
33.5	6.71	6.72	6.72	6.72	6.74	6.72
34	7.14	7.14	7.14	7.14	7.14	7.14
35	7.65	7.66	7.66	7.66	7.66	7.66
41	8.85	8.85	8.85	8.85	8.85	8.85
45	8.92	8.93	8.94	8.95	8.95	8.94
51	9.03	9.04	9.04	9.04	9.04	9.04
51.5	6.63	6.63	6.64	6.64	6.67	6.64
52	6.98	6.98	6.98	6.99	6.99	6.98
55	8.82	8.81	8.82	8.82	8.83	8.82
63	8.85	8.86	8.86	8.87	8.86	8.86
70	9.1	9.1	9.11	9.12	9.12	9.11
70.5	6.74	6.75	6.76	6.76	6.76	6.75
71	7.04	7.05	7.05	7.04	7.05	7.05
84	8.91	8.91	8.91	8.92	8.92	8.91

Table D.18. GCNG, 1

Time	1	2	3	4	5	Mean
1	6.18	6.25	6.18			6.20
1.5	8.54	9.07	8.82			8.81
2	8.11	8.07	7.88	7.98	7.99	8.01
4	11*	11*	11*	11*	11*	11.00
5	11*	11*	11*	11*	11*	11.00
6	11*	11*	11*	11*	11*	11.00
8	11*	11*	11*	11*	11*	11.00
10	11*	11*	11*	11*	11*	11.00
13	11*	11*	11*	11*	11*	11.00
15	11*	11*	11*	11*	11*	11.00
15.5	6.88	6.88	6.87	6.88	6.87	6.88
16	10.83	10.83	10.82	10.86	10.81	10.83
20	7.32	7.36	7.37	7.36	7.32	7.35
23	6.97	7.04	7.04	7.05	7.04	7.03
25	7.71	7.71	7.71	7.73	7.73	7.72
29	8.83	8.82	8.83	8.83	8.82	8.83
29.5	6.98	6.98	6.97	6.96	6.96	6.97
30	6.31	6.33	6.32	6.32	6.31	6.32
37	8.51	8.53	8.53	8.53	8.51	8.52
42	9.06	9.06	9.06	9.06	9.06	9.06
42.5	6.51	6.54	6.54	6.54	6.55	6.54
43	5.19	5.2	5.2	5.21	5.2	5.20
49	7.5	7.47	7.48	7.46	7.48	7.48
53	8.09	8.09	8.09	8.09	8.08	8.09
59	8.5	8.5	8.5	8.5	8.5	8.50
70	8.94	8.93	8.94	8.94	8.94	8.94
70.5	6.75	6.73	6.71	6.71	6.7	6.72
71	5.39	5.4	5.4	5.4	5.4	5.40
73	7.23	7.24	7.23	7.24	7.23	7.23
88	8.81	8.8	8.8	8.8	8.8	8.80

Table D.19. GCNG, 2.

Time	1	2	3	4	5	Mean
1	6.31	6.35	6.33			6.33
1.5	9.69	9.47	8.62			9.26
2	8.39	9.04	8.62	8.5	8.24	8.56
4	9.34	9.34	9.26	9.22	9.26	9.28
5	11*	11*	11*	11*	11*	10.00
6	11*	11*	11*	11*	11*	10.00
8	11*	11*	11*	11*	11*	10.00
10	11*	11*	11*	11*	11*	10.00
13	11*	11*	11*	11*	11*	10.00
15	11*	11*	11*	11*	11*	10.00
15.5	6.82	6.83	6.84	6.84	6.84	6.83
16	5.91	6.09	5.99	6.08	5.95	6.00
20	6.97	7.01	7.05	7	6.97	7.00
23	6.79	6.78	6.93	6.85	6.78	6.83
25	7.73	7.73	7.72	7.75	7.72	7.73
29	8.88	8.87	8.87	8.88	8.87	8.87
29.5	7.1	7.02	7.02	7	7	7.03
30	6.83	6.82	6.81	6.82	6.81	6.82
37	7.41	7.43	7.42	7.41	7.43	7.42
42	8.29	8.29	8.29	8.29	8.29	8.29
42.5	6.38	6.4	6.44	6.45	6.46	6.43
43	5.44	5.47	5.46	5.47	5.47	5.46
49	7.37	7.37	7.37	7.37	7.37	7.37
53	8.12	8.11	8.1	8.1	8.09	8.10
59	8.74	8.73	8.73	8.73	8.72	8.73
70	9.67	9.66	9.66	9.66	9.67	9.66
70.5	6.58	6.6	6.57	6.57	6.58	6.58
71	5.43	5.43	5.43	5.43	5.43	5.43
73	7.09	7.08	7.07	7.08	7.08	7.08
88	8.56	8.56	8.56	8.56	8.57	8.56

Table D.20. GCNG, 3.

Time	1	2	3	4	5	Mean
1	6.28	6.38	6.25			6.30
1.5	9	9.3	8.29			8.86
2	10.03	9.91	9.93	9.13	9.11	9.62
4	11*	11*	11*	11*	11*	10.00
5	11*	11*	11*	11*	11*	10.00
6	11*	11*	11*	11*	11*	10.00
8	11*	11*	11*	11*	11*	10.00
10	11*	11*	11*	11*	11*	10.00
13	11*	11*	11*	11*	11*	10.00
15	11*	11*	11*	11*	11*	10.00
15.5	6.87	6.87	6.85	6.88	6.87	6.87
16	5.94	5.84	5.87	5.92	5.85	5.88
20	6.79	6.8	6.84	6.8	6.84	6.81
23	7.24	7.24	7.29	7.28	7.26	7.26
25	6.95	6.95	6.93	6.95	6.93	6.94
29	7.96	7.95	7.96	7.95	7.96	7.96
29.5	7	6.98	6.99	6.98	7	6.99
30	6.79	6.8	6.81	6.8	6.79	6.80
37	7.13	7.15	7.14	7.13	7.13	7.14
42	7.77	7.77	7.77	7.78	7.77	7.77
42.5	6.39	6.39	6.38	6.4	6.39	6.39
43	5.37	5.38	5.37	5.37	5.38	5.37
49	7.12	7.13	7.14	7.14	7.15	7.14
53	8.03	8.03	8.03	8.03	8.03	8.03
59	8.39	8.39	8.39	8.41	8.4	8.40
70	8.86	8.88	8.88	8.88	8.88	8.88
70.5	6.57	6.6	6.59	6.69	6.64	6.62
71	5.27	5.27	5.27	5.28	5.28	5.27
73	7.2	7.21	7.19	7.2	7.2	7.20
88	8.32	8.32	8.31	8.32	8.32	8.32

Table D.21. CGC, 1

Time	1	2	3	4	5	Mean
1	6.14	6.16	6.19			6.16
1.5	8.47	9.48	8.67			8.87
2	8.74	8.73	8.97	8.46	8.62	8.704
4	11*	11*	11*	11*	11*	11
5	11*	11*	11*	11*	11*	11
6	11*	11*	11*	11*	11*	11
8	11*	11*	11*	11*	11*	11
10	11*	11*	11*	11*	11*	11
13	11*	11*	11*	11*	11*	11
15	11*	11*	11*	11*	11*	11
15.5	6.8	6.83	6.82	6.83	6.83	6.82
16	6.13	6.03	6.11	6.09	6.12	6.10
20	7.04	7.05	7.03	7.04	7.05	7.04
23	7.01	7.01	7.09	7.05	7.04	7.04
25	7.31	7.31	7.32	7.31	7.32	7.31
29	8.39	8.38	8.38	8.37	8.37	8.38
29.5	6.68	6.7	6.7	6.71	6.722	6.70
30	6.38	6.37	6.38	6.38	6.38	6.38
37	8.07	8.08	8.07	8.08	8.08	8.08
42	8.7	8.69	8.7	8.69	8.7	8.70
42.5	6.4	6.41	6.45	6.45	6.43	6.43
43	5.22	5.22	5.22	5.22	5.22	5.22
49	7.15	7.19	7.18	7.18	7.19	7.18
53	8.05	8.04	8.04	8.04	8.03	8.04
59	8.46	8.46	8.46	8.46	8.46	8.46
70	8.88	8.88	8.88	8.88	8.88	8.88
70.5	6.59	6.58	6.62	6.61	6.58	6.60
71	5.29	5.29	5.3	5.3	5.3	5.30
73	7.06	7.05	7.05	7.03	7.03	7.04
88	8.55	8.53	8.53	8.55	8.53	8.54

Table D.22. CGC, 2

Time	1	2	3	4	5	Mean
1	6.25	6.27	6.21			6.24
1.5	8.29	8.64	7.68			8.20
2	10.37	10.55	10.58	10.7	10.84	10.61
4	5.61	5.65	5.47	5.5	5.42	5.53
5	6.91	6.84	6.76	6.85	6.87	6.85
6	7.09	7.17	7.06	7.08	7.21	7.12
8	6.91	6.92	6.91	6.93	6.93	6.92
10	7.38	7.37	7.35	7.35	7.35	7.36
13	7.93	7.93	7.93	7.92	7.93	7.93
15	8.33	8.32	8.34	8.33	8.32	8.33
15.5	6.75	6.76	6.76	6.76	6.75	6.76
16	5.53	5.33	5.33	5.35	5.38	5.38
20	6.84	6.85	6.87	6.85	6.87	6.86
23	7.12	7.14	7.12	7.13	7.14	7.13
25	7.58	7.57	7.56	7.57	7.57	7.57
29	8.5	8.49	8.5	8.48	8.49	8.49
29.5	6.78	6.77	6.77	6.78	6.79	6.78
30	6.5	6.51	6.5	6.5	6.51	6.50
37	7.27	7.27	7.27	7.27	7.27	7.27
42	7.97	7.96	7.96	7.96	7.96	7.96
42.5	6.5	6.52	6.51	6.51	6.5	6.51
43	5.47	5.46	5.46	5.47	5.48	5.47
49	7.51	7.5	7.49	7.48	7.49	7.49
53	8.1	8.1	8.1	8.1	8.1	8.10
59	8.58	8.58	8.58	8.58	8.58	8.58
70	8.97	8.97	8.97	8.97	8.97	8.97
70.5	6.67	6.67	6.69	6.72	6.72	6.69
71	5.39	5.39	5.4	5.4	5.4	5.40
73	7.2	7.19	7.19	7.2	7.19	7.19
88	8.45	8.44	8.45	8.44	8.43	8.44

Table D.23. CGC, 3

Time	1	2	3	4	5	Mean
1	6.38	6.23	6.39			6.33
1.5	9	8.4	8.54			8.65
2	8.78	7.85	7.76	7.9	7.86	8.03
4	11*	11*	11*	11*	11*	11
5	11*	11*	11*	11*	11*	11
6	11*	11*	11*	11*	11*	11
8	11*	11*	11*	11*	11*	11
10	11*	11*	11*	11*	11*	11
13	11*	11*	11*	11*	11*	11
15	11*	11*	11*	11*	11*	11
15.5	6.85	6.86	6.88	6.88	6.88	6.87
16	6.38	5.86	5.92	5.85	5.85	5.97
20	7.79	7.82	7.81	7.82	7.79	7.81
23	8.42	8.4	8.41	8.4	8.41	8.41
25	8.91	8.9	8.9	8.91	8.9	8.90
29	9.18	9.16	9.17	9.15	9.16	9.16
29.5	6.8	6.79	6.79	6.78	6.78	6.79
30	6.47	6.48	6.47	6.48	6.48	6.48
37	6.88	6.88	6.88	6.88	6.88	6.88
42	7.7	7.71	7.71	7.71	7.7	7.71
42.5	6.38	6.39	6.39	6.4	6.4	6.39
43	5.26	5.27	5.37	5.32	5.32	5.31
49	7.09	7.11	7.12	7.12	7.11	7.11
53	7.86	7.85	7.85	7.85	7.85	7.85
59	8.25	8.24	8.24	8.24	8.24	8.24
70	8.81	8.81	8.81	8.81	8.81	8.81
70.5	6.61	6.67	6.67	6.68	6.68	6.66
71	5.47	5.45	5.46	5.45	5.46	5.46
73	7.24	7.23	7.22	7.23	7.23	7.23
88	8.74	8.73	8.73	8.73	8.73	8.73

Table D.24. SGC, 1

Time	1	2	3	4	5	Mean
1	6.11	6.19	6.13			6.14
1.5	9	8.7	8.22			8.64
2	9.1	8.66	9.01	9.56	10.49	9.36
4	11*	11*	11*	11*	11*	11.00
5	11*	11*	11*	11*	11*	11.00
6	11*	11*	11*	11*	11*	11.00
8	11*	11*	11*	11*	11*	11.00
10	11*	11*	11*	11*	11*	11.00
13	11*	11*	11*	11*	11*	11.00
15	11*	11*	11*	11*	11*	11.00
15.5	6.85	6.85	6.84	6.83	6.84	6.84
16	5.51	5.71	5.61	5.61	5.61	5.61
20	7.03	7.02	7.03	7	7.02	7.02
23	7.04	7.08	7.07	7.07	7.08	7.07
25	7.53	7.52	7.53	7.52	7.53	7.53
29	8.42	8.41	8.41	8.4	8.39	8.41
29.5	6.8	6.88	6.82	6.9	6.88	6.86
30	6.41	6.4	6.41	6.42	6.42	6.41
37	7.24	7.23	7.24	7.23	7.24	7.24
42	8.17	8.17	8.15	8.17	8.18	8.17
42.5	6.38	6.38	6.37	6.38	6.38	6.38
43	5.71	5.73	5.72	5.73	5.72	5.72
49	6.93	6.94	6.95	6.94	6.94	6.94
53	8.39	8.38	8.39	8.38	8.39	8.39
59	8.65	8.65	8.65	8.65	8.65	8.65
70	8.92	8.92	8.93	8.93	8.93	8.93
70.5	6.69	6.68	6.68	6.69	6.7	6.69
71	5.4	5.39	5.45	5.44	5.44	5.42
73	7.33	7.34	7.34	7.34	7.34	7.34
88	8.42	8.42	8.42	8.42	8.42	8.42

Table D.25. SGC, 2

Time	1	2	3	4	5	Mean
1	6.1	6.19	6.22			6.17
1.5	8.74	8.81	8.59			8.71
2	9.68	9.67	9.69	10.54	10.46	10.01
4	9.55	9.51	9.45	9.28	9.06	9.37
5	6.11	6.5	6.28	6.31	6.38	6.32
6	6.95	7	6.99	7.1	7.01	7.01
8	6.9	6.91	7	6.91	9.9	7.52
10	6.93	6.91	6.92	6.9	6.9	6.91
13	7.97	7.93	7.93	7.9	7.87	7.92
15	8.25	8.24	8.24	8.23	8.23	8.24
15.5	6.79	6.78	6.8	6.8	6.79	6.79
16	5.63	5.49	5.65	5.78	5.69	5.65
20	6.42	6.41	6.43	6.42	6.43	6.42
23	6.69	6.65	6.7	6.65	6.69	6.68
25	7.05	7.05	7.05	7.05	7.05	7.05
29	8.45	8.44	8.42	8.43	8.42	8.43
29.5	6.75	6.75	6.76	6.79	6.75	6.76
30	6.62	6.63	6.63	6.64	6.63	6.63
37	7.02	7.03	7.04	7.05	7.06	7.04
42	7.9	7.9	7.9	7.9	7.9	7.90
42.5	6.31	6.39	6.38	6.39	6.38	6.37
43	5.44	5.45	5.44	5.45	5.45	5.45
49	7.5	7.46	7.43	7.43	7.43	7.45
53	8.26	8.27	8.26	8.27	8.28	8.27
59	8.78	8.77	8.78	8.77	8.78	8.78
70	10.13	10.14	10.14	10.15	10.15	10.14
70.5	6.79	6.78	6.79	6.78	6.79	6.79
71	5.5	5.51	5.52	5.52	5.52	5.51
73	7.24	7.24	7.24	7.24	7.24	7.24
88	8.93	8.94	8.94	8.94	8.94	8.94

Table D.26. SGC, 3

Time	1	2	3	4	5	Mean
1	6.15	6.14	6.18			6.16
1.5	9.17	9.15	8.9			9.07
2	8.3	8.26	8.68	8.92	9.05	8.64
4	11*	11*	11*	11*	11*	11
5	11*	11*	11*	11*	11*	11
6	11*	11*	11*	11*	11*	11
8	11*	11*	11*	11*	11*	11
10	11*	11*	11*	11*	11*	11
13	11*	11*	11*	11*	11*	11
15	11*	11*	11*	11*	11*	11
15.5	6.75	6.74	6.76	6.76	6.76	6.75
16	5.48	5.45	5.55	5.72	5.62	5.56
20	6.58	6.58	6.58	6.58	6.58	6.58
23	6.99	7	7.12	6.98	6.99	7.02
25	7.45	7.45	7.45	7.45	7.45	7.45
29	8.42	8.41	8.4	8.41	8.4	8.41
29.5	6.77	6.77	6.78	6.79	6.79	6.78
30	6.48	6.49	6.5	6.51	6.5	6.50
37	6.77	6.77	6.77	6.77	6.77	6.77
42	7.07	7.08	7.08	7.08	7.07	7.08
42.5	6.25	6.24	6.25	6.24	6.24	6.24
43	5.16	5.19	5.19	5.19	5.2	5.19
49	7.35	7.34	7.34	7.34	7.34	7.34
53	8.34	8.35	8.35	8.35	8.35	8.35
59	8.74	8.74	8.74	8.74	8.74	8.74
70	9.46	9.46	9.46	9.46	9.47	9.46
70.5	6.73	6.74	6.78	6.77	6.77	6.76
71	5.61	5.6	5.61	5.61	5.6	5.61
73	7.46	7.46	7.46	7.46	7.46	7.46
88	8.73	8.73	8.73	8.73	8.73	8.73

Appendix E: Concrete Exposed to Acidic Media and Fe(II) Solution

The petrographic thin sections of the A and AF concrete are similar in appearance to the AFB concrete shown in chapter 5. There is a layer of corrosion product at the surface of each thin-section, presumably gypsum. This layer varies in thickness. Figure E.1a shows a very thin layer for the carbonate aggregate concrete, however it does appear thicker in other locations. The decision of where to take a photograph was often based on securing an unobstructed view of the cement paste. The rust colored band visible in the AFB concrete is also seen in figure E.1b and Figure E.2b and E.2C. The carbonate aggregate A concrete did not exhibit the rust-colored band in thin-section (figure E.1a and E.2a). Figure E.3 and E.4 show the same features as E.1 and E.2. The red-colored bands in these figures is more developed, though, likely due to the higher concentration of Fe in the solution containing the concrete. A calcium hydroxide leach zone is visible in all of the thin-sections. These zones vary in thickness within a given thin-section, and thus it is not possible to characterize whether a given treatment was leached to a greater degree. Figures E.5 and E.6 correspond to those of the AFB concrete in chapter 5.

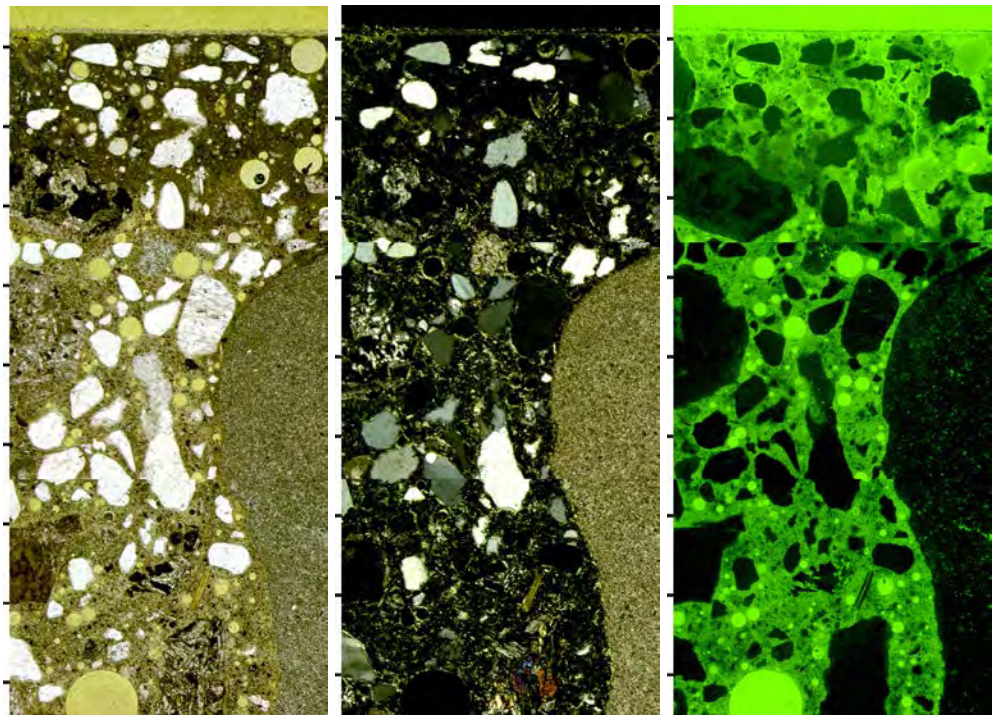

a.

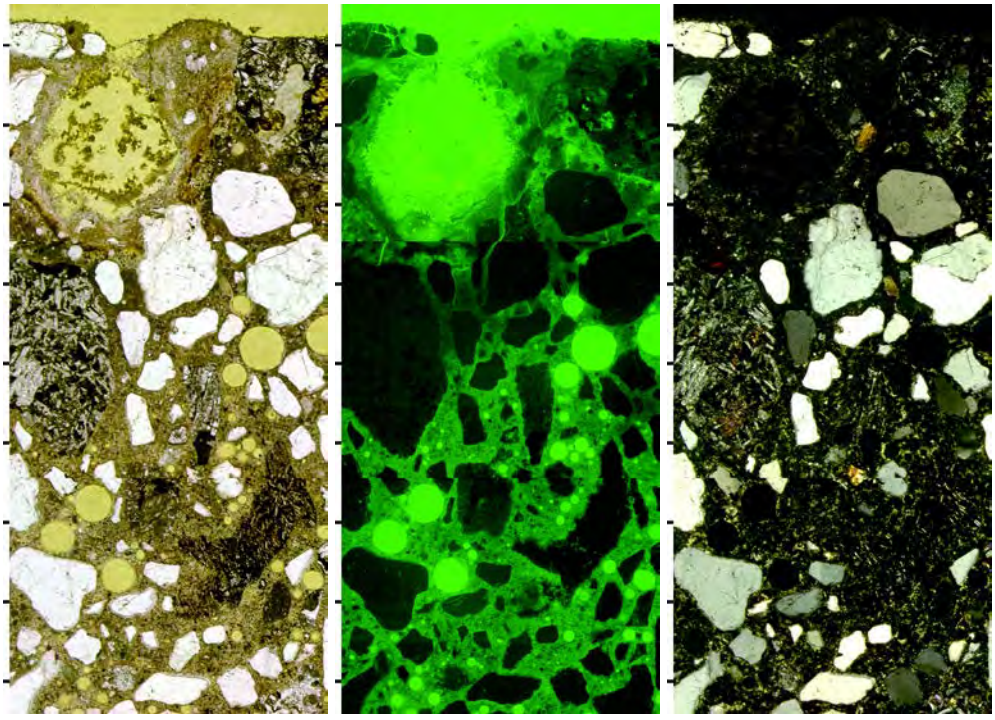

b.

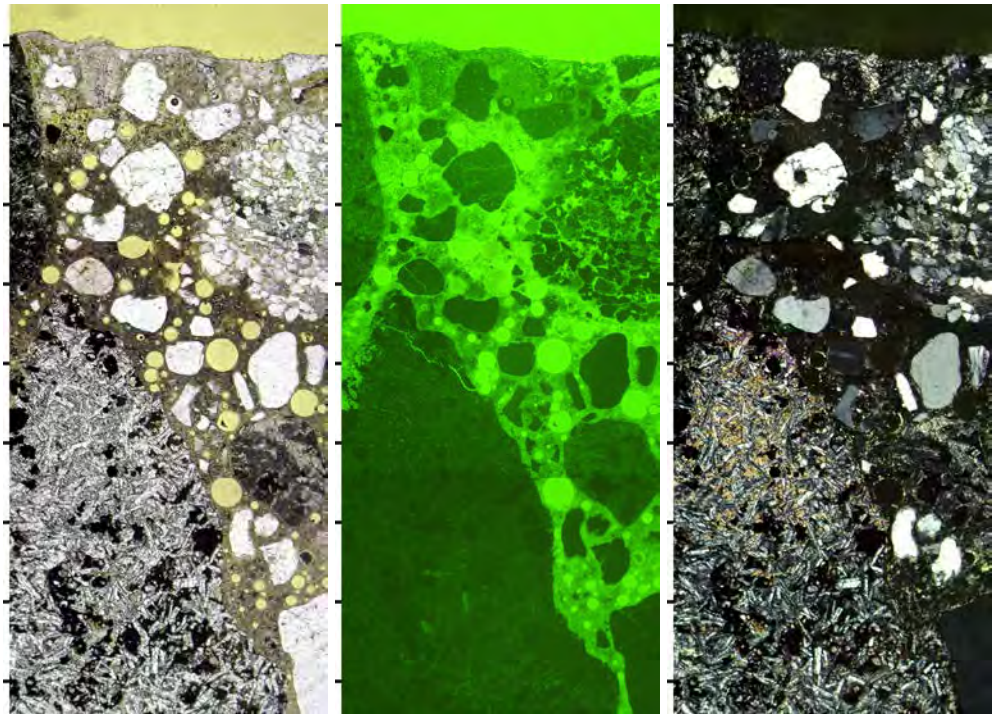

c.

Figure E.1: Thin-Sections of the Concrete Exposed to the Acidic Media.
The above micrographs are as follows: a) carbonate, b) slag, c) natural gravel. All of the surfaces bear a corrosion layer, presumably gypsum, with a leached zone behind this layer. The carbonate aggregate (a) does not have this band and its corrosion zone is much thinner. The reason for this difference is unknown. The tick marks on the side are 0.5 mm apart.

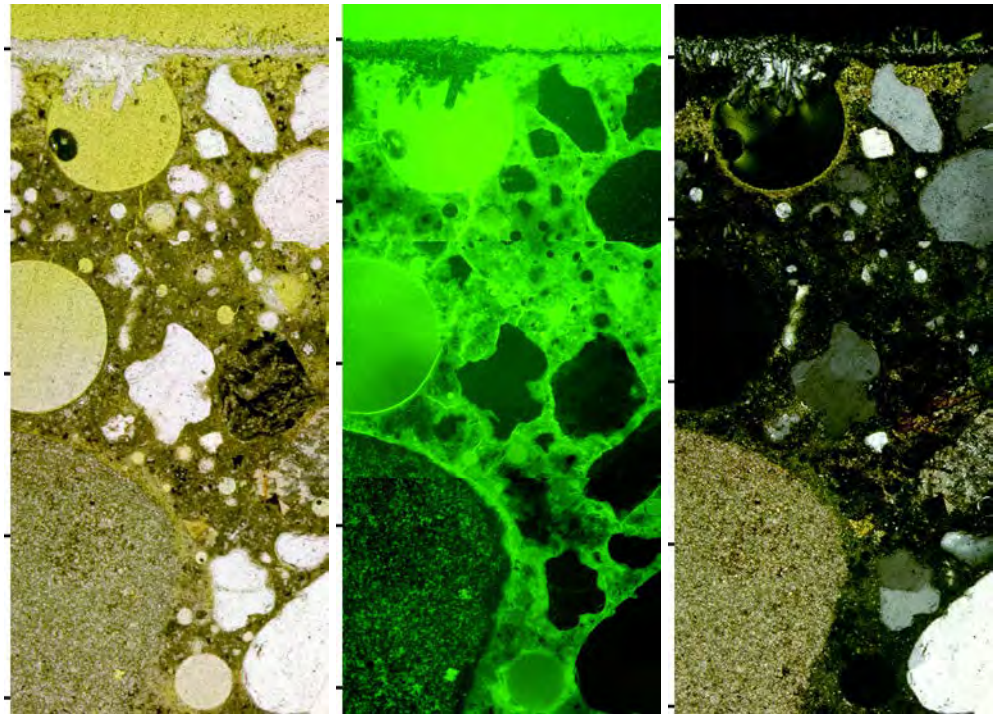

a.

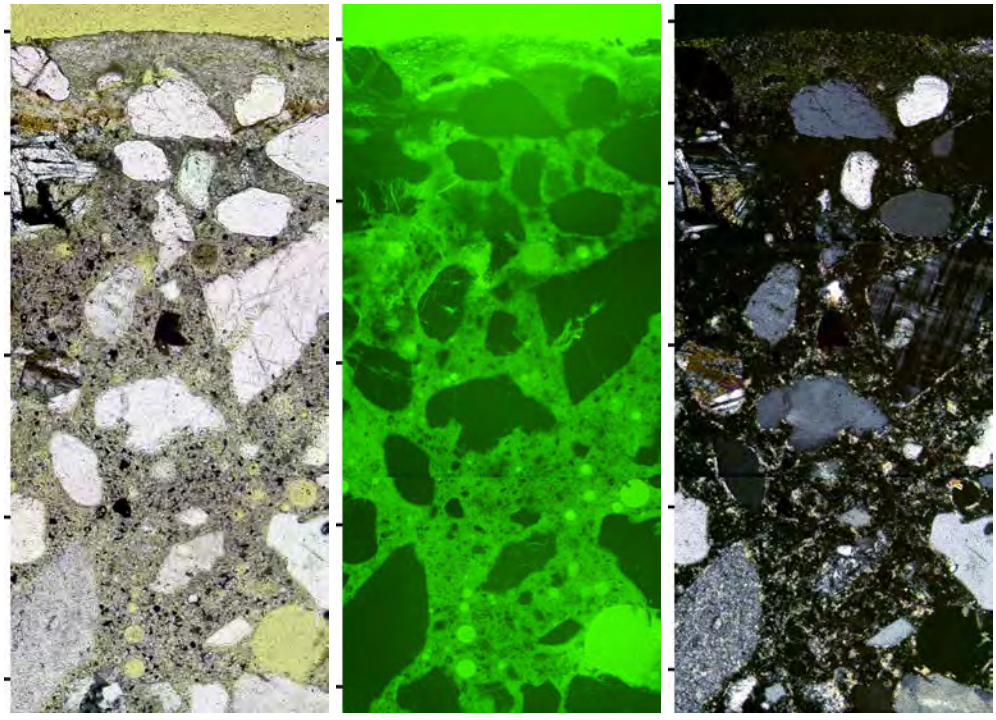

b.

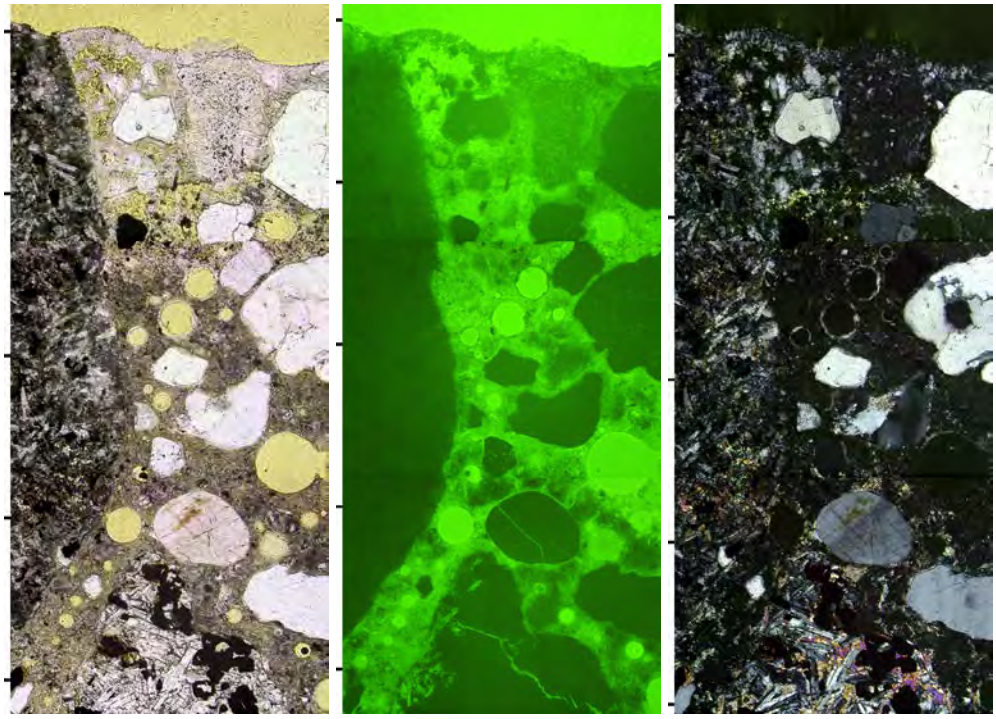

c.

Figure E.2: Thin-Sections of the Concrete Exposed to the Acidic Media, 10x. The above micrographs are as follows: a) carbonate, b) slag, c) natural gravel. These show further detail of the features described in Figure D.1. The tick marks are 0.5-mm apart.

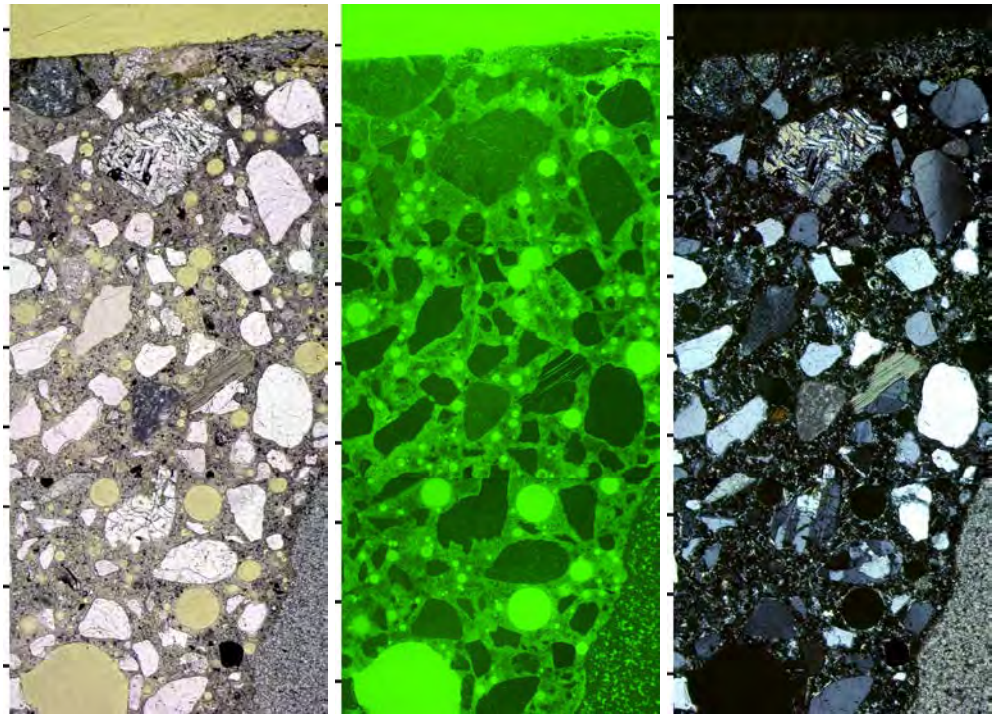

a.

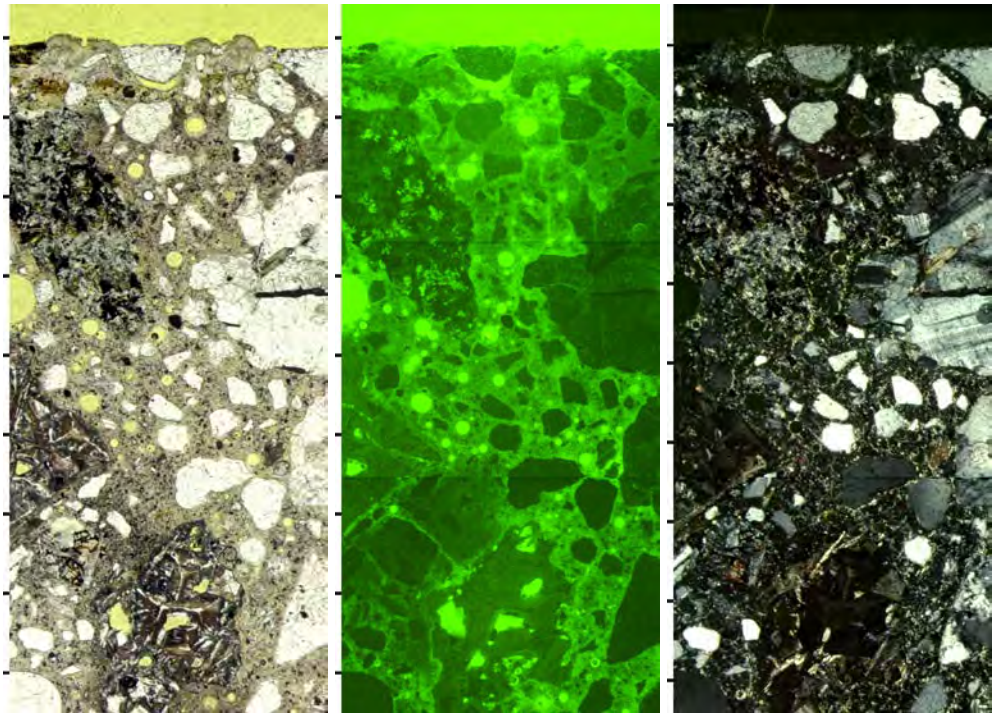

b.

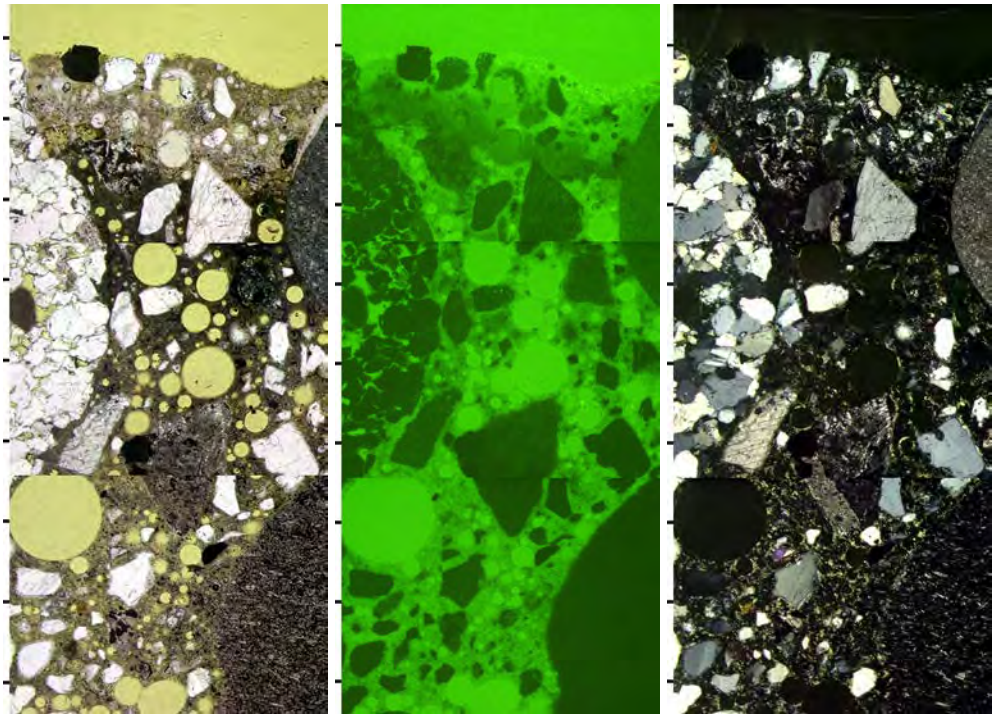

c.

Figure E.3: Thin-Sections of the Concrete Exposed to the Acidic Media, and Fe(II) solution. The above micrographs are as follows: a) carbonate, b) slag, c) natural gravel. These thin-sections show the features common to the other sulfuric acid treatments. The tick marks are 0.5-mm apart.

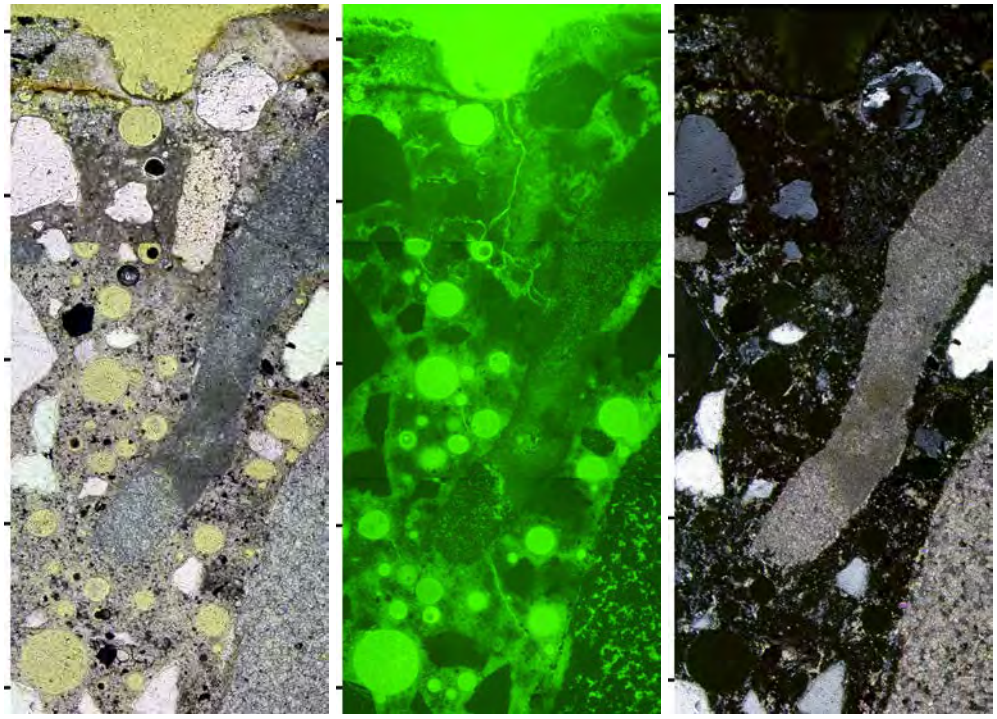

a.

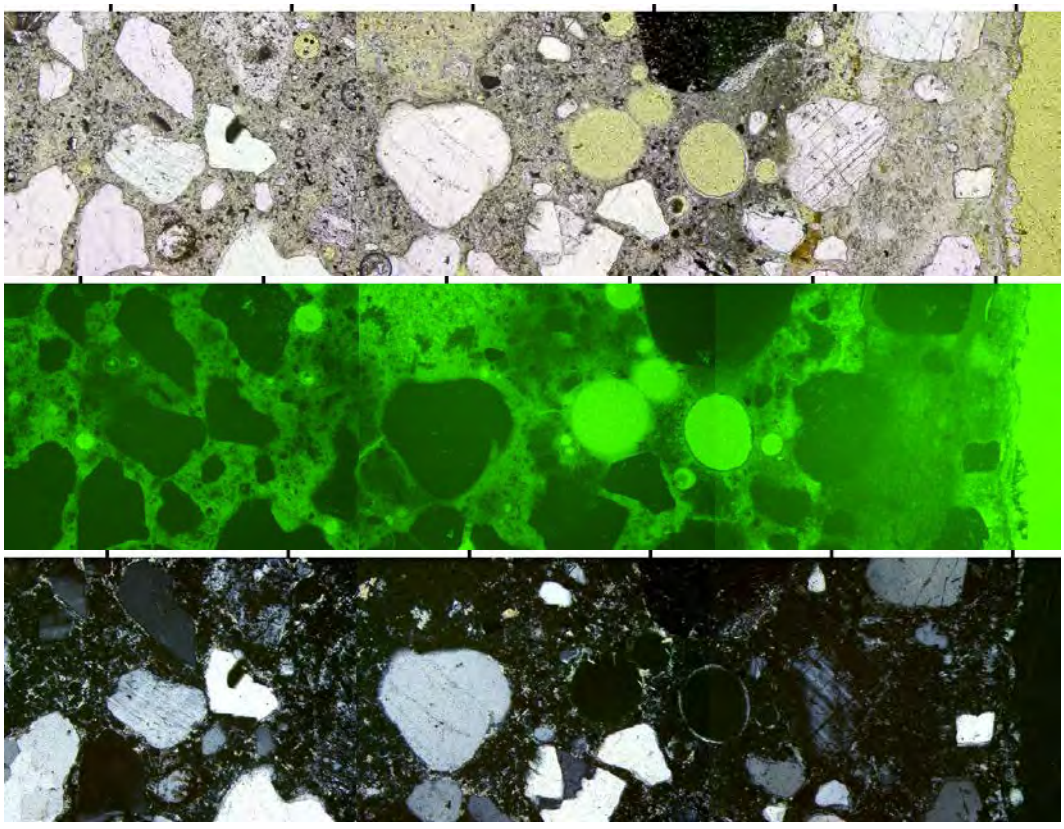

b.

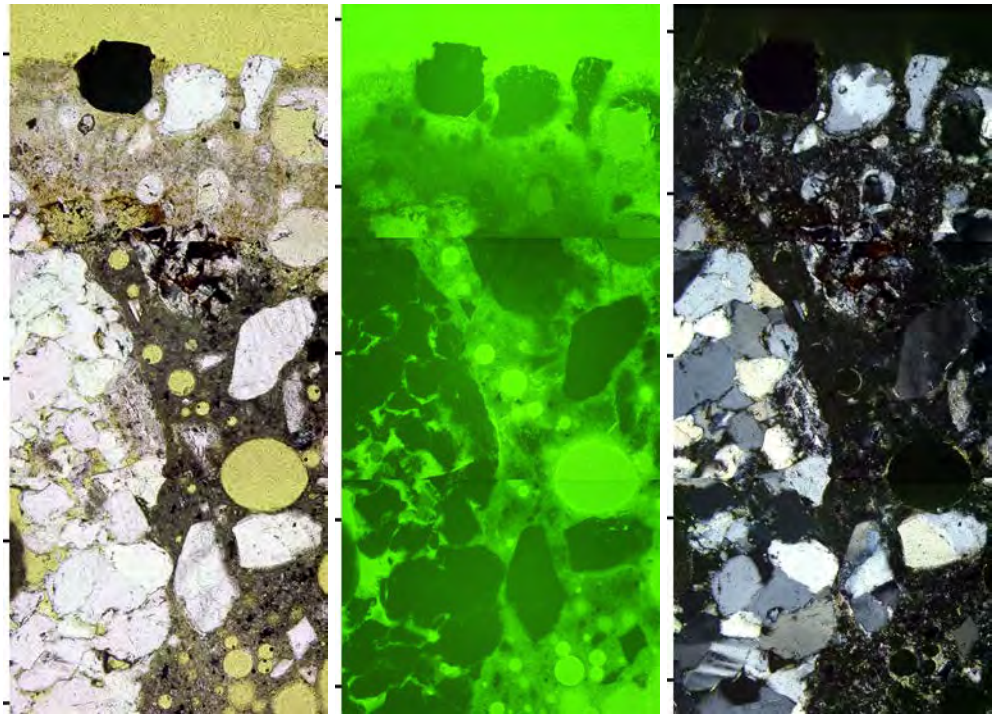

c

Figure E.4: Thin-Sections of the Concrete Exposed to the Acidic Media, and Fe(II) solution, 10x. The above micrographs are as follows: a) carbonate, b) slag, c) natural gravel. These thin-sections show the features common to the other sulfuric acid treatments in more detail. The tick marks are 0.5-mm apart.

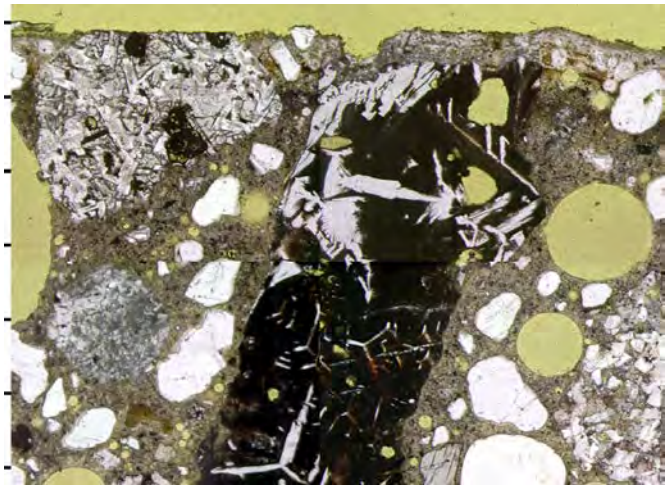

a.

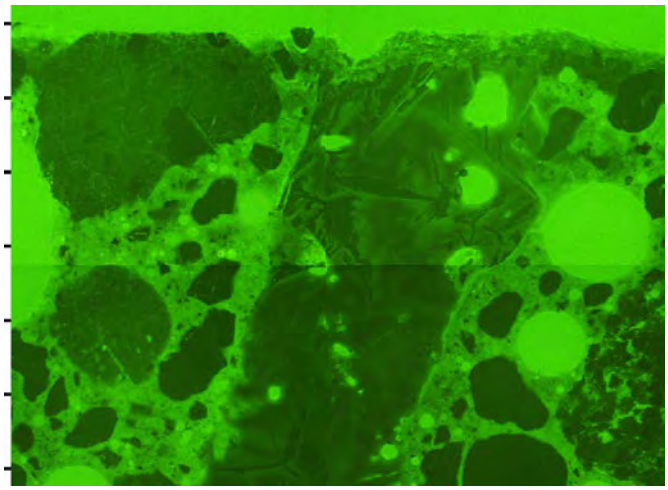

b.

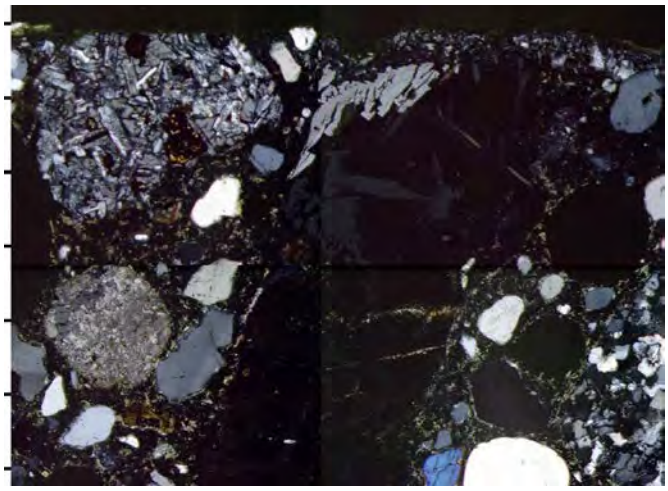

c.

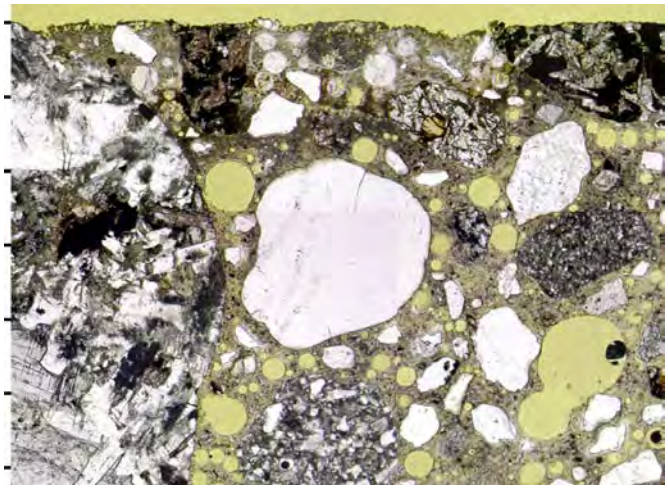

d.

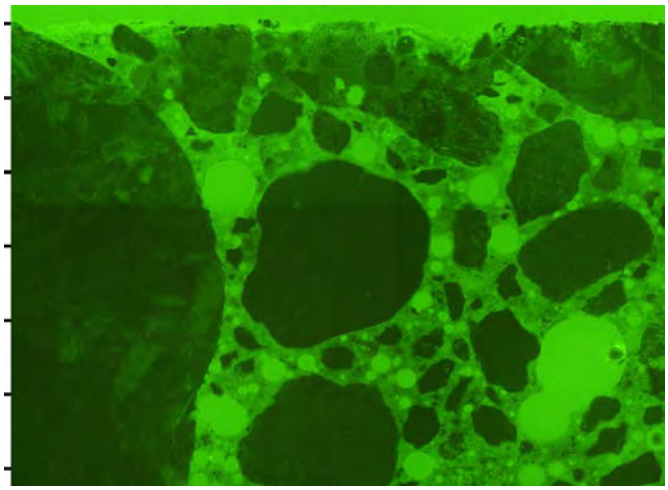

e.

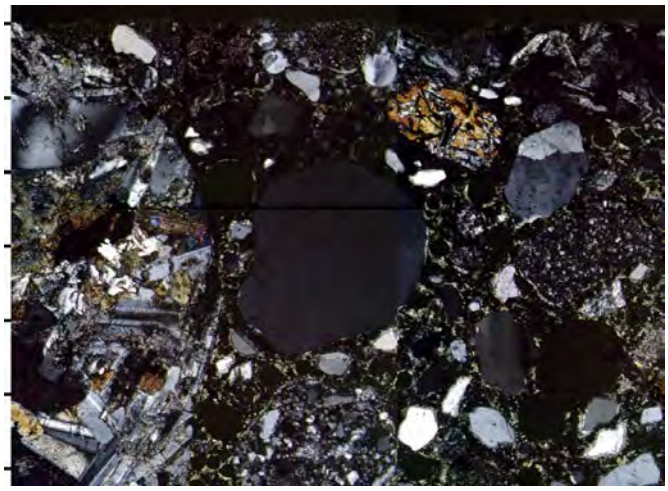

f.

Figure E.5: Petrographic Thin-section of AFB. These figures correspond to figure 5.3. These petrographic thin-sections, at the surface of the slag AFB, are as follows: a) slag plane-polarized light, b) slag epifluorescents, c) slag cross-polarized, d) natural gravel plane-polarized light, e) natural gravel epifluorescents, f) natural gravel cross-polarized. The tick marks are 0.5-mm apart.

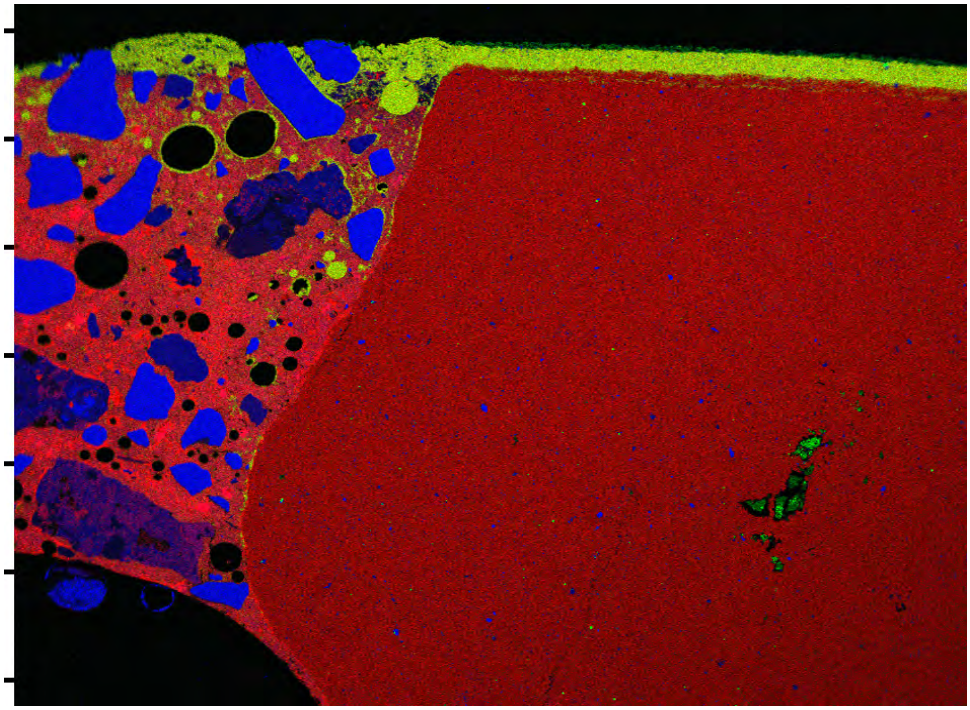

a.

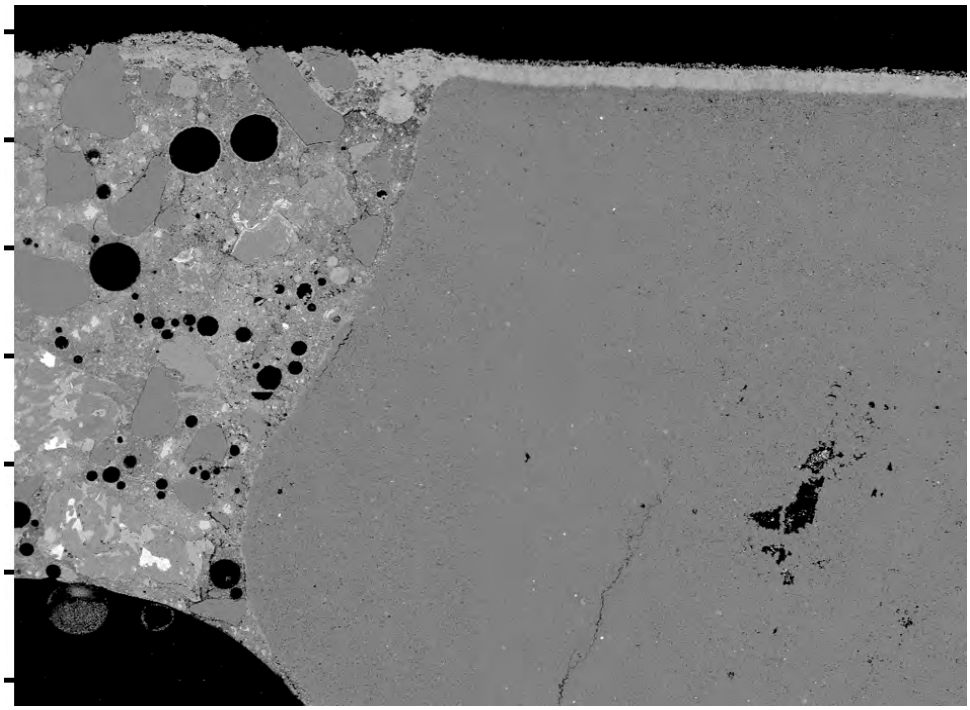

b.

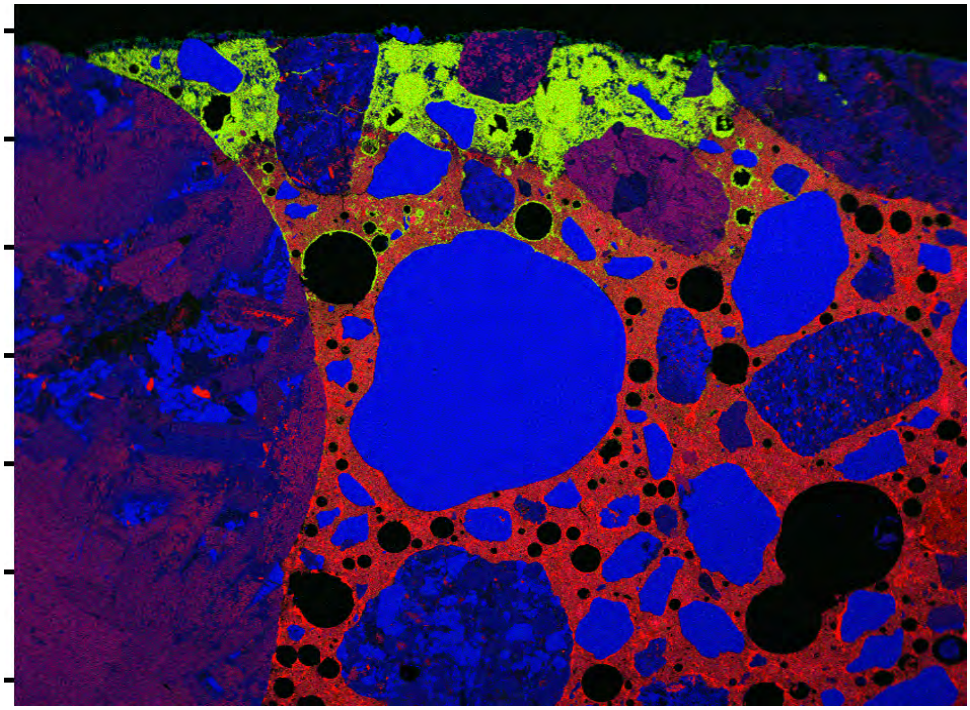

c.

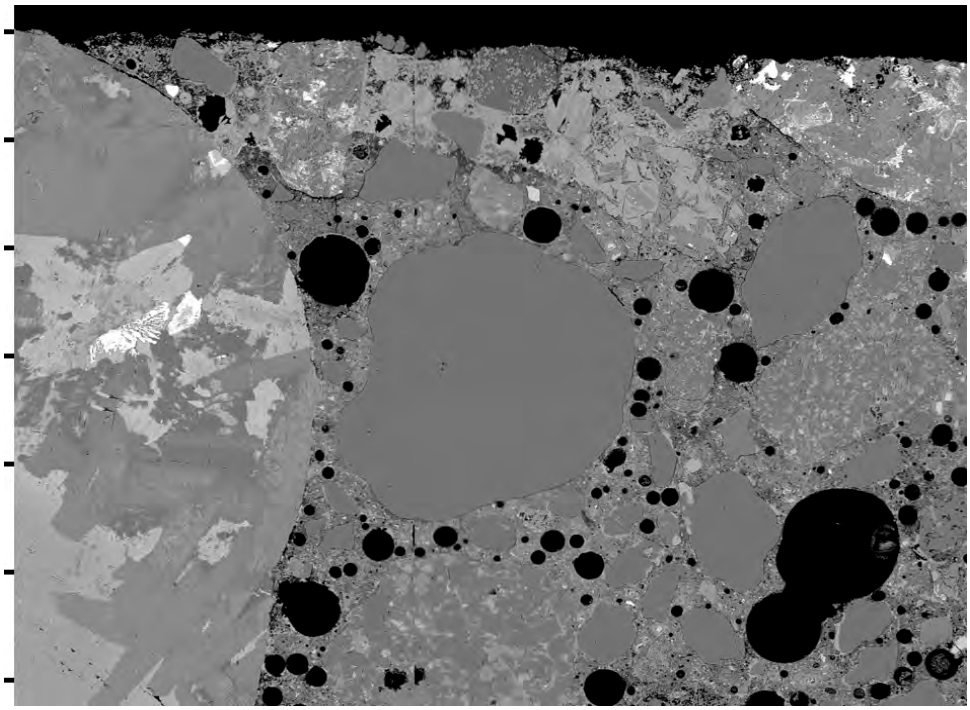

d.

Figure E.6. X-ray Energy Maps and Back Scatter Images of Concrete.
The images above are as follows a) energy map, carbonate, b) back scatter, carbonate, c) energy map, natural gravel, d) back scatter, natural gravel. In the maps, yellow = S, blue = Si, red = Ca. The maps show that the acid has worn the carbonate aggregate, as it is flush with the cement paste (a). In contrast a corrosive gypsum layer surrounds the silicate minerals (c). The paste here appears relatively dense in the back scatter images.